





This is to certify that the

dissertation entitled

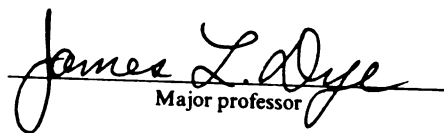
Single-Crystal X-Ray Diffraction and Alkali Metal  
NMR Studies of Alkalides, Electrides  
and Model Compounds

presented by

Songzhan Huang

has been accepted towards fulfillment  
of the requirements for

Ph.D. degree in Chemistry

  
Major professor

Date 17 August 1994

# LIBRARY

## Michigan State University

**PLACE IN RETURN BOX** to remove this checkout from your record.  
**TO AVOID FINES** return on or before date due.

DATE DUE	DATE DUE	DATE DUE
_____	_____	_____
_____	_____	_____
_____	_____	_____
_____	_____	_____
_____	_____	_____
_____	_____	_____
_____	_____	_____

**SINGLE-CRYSTAL X-RAY DIFFRACTION AND ALKALI METAL NMR  
STUDIES OF ALKALIDES, ELECTRIDES AND MODEL COMPOUNDS**

By

Songzhan Huang

A DISSERTATION

Submitted to  
Michigan State University  
in partial fulfillment of the requirements  
for the degree of

DOCTOR OF PHILOSOPHY

Department of Chemistry

1994

## ABSTRACT

### SINGLE-CRYSTAL X-RAY DIFFRACTION AND ALKALI METAL NMR STUDIES OF ALKALIDES, ELECTRIDES AND MODEL COMPOUNDS

By

Songzhan Huang

Three new alkalides that contain 21-crown-7 or dicyclohexano-24-crown-8 were synthesized and their unusual crystal structures were determined.  $(\text{Cs}^+)_2(21\text{C}7)_2(\text{Na}^-)_2$  has twin cation-anion ion pairs in which the  $\text{Cs}^+-\text{Na}^-$  distances are only 4.44(2)Å and 4.52(3)Å respectively, although optical absorption spectroscopy and  $^{23}\text{Na}$  NMR show no charge transfer between  $\text{Na}^-$  and  $\text{Cs}^+$ . In  $(\text{K}^+)_2(21\text{C}7)_3(\text{MeNH}_2)(\text{Na}^-)_2$ , a third 21-crown-7 serves as a bridge connecting the two  $\text{K}^+$  cations, while  $\text{MeNH}_2$  forms a bond to one of them. In  $\text{K}^+(\text{dicyclohexano-24C}8)\text{Na}^-$ , the complexant twists around the  $\text{K}^+$  cation so that all eight oxygen atoms are coordinated to the cation. These alkalides are relatively stable, which is attributed to their unusual structural features in which the cations can be fully coordinated in different ways. The structures of two mixed sandwich complexes,  $\text{Rb}^+(18\text{C}6)(12\text{C}4)\text{Na}^-$  and  $\text{Rb}^+(18\text{C}6)(12\text{C}4)\text{Rb}^-$ , were also determined. These two compounds show multiple optical peaks in contrast to the single peak of other alkalides.

The  $^{133}\text{Cs}$  chemical shifts in nitromethane, versus the  $[\text{L}]/[\text{Cs}^+]$  mole ratio ( $\text{L}$  = crown ether) were determined and showed the formation of the stable 2:1 sandwich complexes,  $\text{Cs}^+(\text{18C6})_2$ ,  $\text{Cs}^+(\text{15C5})_2$ , and  $\text{Cs}^+(\text{HMHCY})_2$ . The formation of an intermediate,  $(\text{Cs}^+)_2(\text{18C6})_3$ , in nitromethane was indicated. By contrast,  $\text{Cs}^+-\text{12C4}$  showed only a single step complexation. The formation of the mixed sandwich complexes,  $\text{Cs}^+(\text{18C6})(\text{15C5})$ ,  $\text{Cs}^+(\text{18C6})(\text{12C4})$ ,  $\text{Cs}^+(\text{HMHCY})(\text{15C5})$ , and  $\text{Cs}^+(\text{HMHCY})(\text{12C4})$  in nitromethane was also demonstrated.

The first single-crystal  $^{133}\text{Cs}$  NMR study of an electride,  $\text{Cs}^+(\text{18C6})_2\text{e}^-$ , was carried out and the quadrupole coupling constants and asymmetry parameters were obtained for the two  $\text{Cs}^+$  ion sites. The original crystalline orientation was preserved rather than the formation of a random powder, even though a transition from a low-temperature phase to a high-temperature phase had occurred.

## **To My Parents**

## ACKNOWLEDGMENTS

I wish to express my sincere gratitude to Professor James L. Dye for his guidance and support throughout this work.

I would like to thank Dr. John McCracken, Dr. Kim Dunbar and Dr. William Reusch for their helpful advice.

I would also like to thank Dr. Rui Huang, Dr. Jineun Kim, and Dr. Evy Jackson for their help and suggestions.

Thank also extended to all of the members of Dr. Dye research with whom I have worked, in particular Kerry Reidy-Cedergren, Kuo-Lih Tsai, Mike Wagner, Erik Hendrickson, and Ching-Tung Kou.

I would like to thank Dr. Long Le and Kermit Johnson for their help with the NMR instruments. I would also like to thank the glassblowers Scott Bancroft, Manfred Langer and Keki mistry and instrument makers Russ Geyer and Dick Menke for their excellent service.

I am grateful for financial support from the Chemistry Department, Michigan State University, the National Science foundation(Grant DMR 90-17292, Grant DMR 84-08088, and Grant DMR 84-03823) and the Michigan state University Center for Fundamental Materials Research.

Special thanks go to my family and my friends for their constant encouragement and assistance.

## TABLE OF CONTENTS

	PAGE
LIST OF TABLES. ....	viii
LIST OF FIGURES. ....	xi
CHAPTER 1. INTRODUCTION. ....	1
CHAPTER 2. SYNTHESIS, STRUCTURE DETERMINATION AND CHARACTERIZATION OF ALKALIDES. ....	7
I. Introduction. ....	7
II. Experimental. ....	10
III. Results and Discussion. ....	13
III.A. $(\text{Cs}^+)_2(21\text{C}7)_2(\text{Na}^-)_2$ . ....	13
III.B. $(\text{K}^+)_2(21\text{C}7)_3(\text{MeNH}_2)(\text{Na}^-)_2$ . ....	27
III.C. $\text{K}^+(\text{dicyclohexano-}24\text{C}8)\text{Na}^-$ . ....	37
III.D. $\text{Rb}^+(21\text{C}7)\text{Na}^-$ and Five Other Sodides. ....	45
III.E. $\text{Rb}^+(18\text{C}6)(12\text{C}4)\text{Na}^-$ and $\text{Rb}^+(18\text{C}6)(12\text{C}4)\text{Rb}^-$	50
CHAPTER 3. SOLUTION NMR STUDIES OF COMPLEXED $\text{Cs}^+$ IONS WITH MIXED CROWN ETHERS. ....	71
I. Introduction. ....	71
II. Experimental. ....	72
III. Results and Discussion. ....	74
III.A. The Ion-Pairing Formation Constants of $\text{Cs}^+$ Ion in Nitromethane Solvent. ....	74

III.B.	Formation Constants of Cesium Thiocynate Complexes with Crown Ethers in Nitromethane. ....	84
III.C.	Formation Constants of Mixed Sandwich Complexes. ....	94
CHAPTER 4.	SINGLE-CRYSTAL $^{133}\text{Cs}$ NMR STUDY OF $\text{Cs}^+(\text{18C6})_2\text{e}^-$ . ....	103
I.	Introduction. ....	103
II.	Experimental. ....	112
III.	Results and Discussion. ....	113
CHAPTER 5.	CONCLUSIONS. ....	122
APPENDIX A.	Crystal Structure Data of $(\text{Cs}^+)_2(\text{21C7})_2(\text{Na}^-)_2$ , $(\text{K}^+)_2(\text{21C7})_3(\text{MeNH}_2)(\text{Na}^-)_2$ , $\text{K}^+(\text{dicyclohexano-24C8})\text{Na}^-$ , $\text{Rb}^+(\text{18C6(12C4)})\text{Na}^-$ and $\text{Rb}^+(\text{18C6(12C4)})\text{Rb}^-$ . ....	125
APPENDIX B.	The Subroutine Program for the Multiple Data Set Fitting. ....	159
APPENDIX C.	The Subroutine Program for the KINFIT Fitting. ....	160
REFERENCES.	.....	162

T

2

2

2

2

3

3

3

## LIST OF TABLES

TABLE		PAGE
2-1.	Summary of Crystallographic Data for (Cs <sup>+</sup> ) <sub>2</sub> (21C7) <sub>2</sub> (Na <sup>-</sup> ) <sub>2</sub> . . . . .	15
2-2.	selected bond distances and bond angles for (Cs <sup>+</sup> ) <sub>2</sub> (21C7) <sub>2</sub> (Na <sup>-</sup> ) <sub>2</sub> . . . . .	18
2-3.	Summary of Crystallographic Data for (K <sup>+</sup> ) <sub>2</sub> (21C7) <sub>3</sub> (MeNH <sub>2</sub> )(Na <sup>-</sup> ) <sub>2</sub> . . . . .	29
2-4.	Summary of Crystallographic Data for K <sup>+</sup> (dicyclohexano-24C8)Na <sup>-</sup> . . . . .	38
2-5.	Summary of thermal processes that occur in the DSC traces with a heating rate of 5°C/min. in °C. . . .	48
2-6.	<sup>133</sup> Cs NMR chemical shifts of the complexed cations in three sodides. . . . .	48
2-7.	Summary of Crystallographic Data for Rb <sup>+</sup> (18C6)(12C4)Na <sup>-</sup> (I) and Rb <sup>+</sup> (18C6)(12C4)Rb <sup>-</sup> (II). . . . .	55
3-1.	<sup>133</sup> Cs Chemical Shifts of Cesium Salt Solution of MeNO <sub>2</sub> at 25°C. . . . .	75
3-2.	Ion Pair and Complexation Formation Constants of Cesium Compounds in Nitromethane at 25°C. . . . .	84
3-3.	Mole Ratio Studies of Crown Ether Complexes	

	with CsSCN in MeNO <sub>2</sub> Solvent by <sup>133</sup> Cs NMR at 25°C. [CsSCN] <sub>T</sub> =0.005M. ....	87
3-4.	Formation Constants for Cs <sup>+</sup> -Crown Ether Complexes in Nitromethane Solvent at 25°C. ....	94
3-5.	Mole Ratio Studies of Mixed Sandwich Complexes with CsSCN in MeNO <sub>2</sub> Solvent by <sup>133</sup> Cs NMR at 25°C. [CsSCN] <sub>T</sub> =0.005M. ....	95
3-6.	Formation Constants for Cs <sup>+</sup> Ion Complexes with Mixed Crown Ethers in Nitromethane Solvent at 25°C. ....	97
3-7.	Mole Ratio Studies of Mixed Sandwich Complexes with CsSCN in MeNO <sub>2</sub> Solvent by <sup>133</sup> Cs NMR at 25°C. [CsSCN] <sub>T</sub> =0.005M. ....	98
4-1.	Results Obtained from Single-Crystal <sup>133</sup> Cs NMR Study of Cs <sup>+</sup> (18C6) <sub>2</sub> e <sup>-</sup> at -50°C. ....	120
A-1.	Positional Parameters and Their Estimated Standard Deviations for (Cs <sup>+</sup> ) <sub>2</sub> (21C7) <sub>2</sub> (Na <sup>-</sup> ) <sub>2</sub> . ....	127
A-2.	Bond Distances (in Angstroms) for (Cs <sup>+</sup> ) <sub>2</sub> (21C7) <sub>2</sub> (Na <sup>-</sup> ) <sub>2</sub> . ....	129
A-3.	Bond Angles (in Degrees) for (Cs <sup>+</sup> ) <sub>2</sub> (21C7) <sub>2</sub> (Na <sup>-</sup> ) <sub>2</sub> . ...	131
A-4.	Positional Parameters and Their Estimated Standard Deviations for (K <sup>+</sup> ) <sub>2</sub> (21C7) <sub>3</sub> (MeNH <sub>2</sub> )(Na <sup>-</sup> ) <sub>2</sub> . ....	136
A-5.	Bond Distances (in Angstroms) for (K <sup>+</sup> ) <sub>2</sub> (21C7) <sub>3</sub> (MeNH <sub>2</sub> )(Na <sup>-</sup> ) <sub>2</sub> . ....	139
A-6.	Bond Angles (in Degrees) for (K <sup>+</sup> ) <sub>2</sub> (21C7) <sub>3</sub> (MeNH <sub>2</sub> )(Na <sup>-</sup> ) <sub>2</sub> . ....	142
A-7.	Positional Parameters and Their Estimated Standard Deviations for K <sup>+</sup> (dicyclohexano-24C8)Na <sup>-</sup> . ....	147

A-8.	Bond Distances (in Angstroms) for K <sup>+</sup> (dicyclohexano-24C8)Na <sup>-</sup> .....	149
A-9.	Bond Angles (in Degrees) for K <sup>+</sup> (dicyclohexano-24C8)Na <sup>-</sup> .....	151
A-10.	Positional Parameters and Their Estimated Standard Deviations for Rb <sup>+</sup> (18C6)(12C4)Na <sup>-</sup> .....	154
A-11.	Bond Distances (in Angstroms) for Rb <sup>+</sup> (18C6(12C4)Na <sup>-</sup> (I) and Rb <sup>+</sup> (18C6(12C4)Rb <sup>-</sup> (II). ....	155
A-12.	Bond Angles (in Degrees) for Rb <sup>+</sup> (18C6(12C4)Na <sup>-</sup> (I) and Rb <sup>+</sup> (18C6(12C4)Rb <sup>-</sup> (II). ....	156
A-13.	Positional Parameters and Their Estimated Standard Deviations for Rb <sup>+</sup> (18C6)(12C4)Rb <sup>-</sup> .....	158

## LIST OF FIGURES

FIGURE		PAGE
2-1.	Representative complexants for alkali metal cations. . . . .	2
2-1.	Vacuum apparatus for the synthesis of alkalides and electrides [3-chamber K-Cell]. . . . .	9
2-2.	Large crown ethers used for the synthesis of alkalides. . . . .	11
2-3.	The molecular structure and the numbering of atoms in $(Cs^+)_2(21C7)_2(Na^-)_2$ . . . . .	16
2-4.	Stereo packing diagram of $(Cs^+)_2(21C7)_2(Na^-)_2$ . . . . .	17
2-5.	ORTEP plot of selected atoms in $(Cs^+)_2(21C7)_2(Na^-)_2$ . . . . .	19
2-6.	$^{133}Cs$ static and MAS NMR spectra of $(Cs^+)_2(21C7)_2(Na^-)_2$ at $-60^\circ C$ ; A) Static; B) MAS, $f=3.6kHz$ ; and C) MAS, $f=5.0kHz$ . . . . .	22
2-7.	Optical absorption spectrum of a thin film of $(Cs^+)_2(21C7)_2(Na^-)_2$ at $-60^\circ C$ , prepared by rapid evaporation of the methylamine solvent. . . . .	24
2-8.	$^{23}Na$ static NMR spectrum of $(Cs^+)_2(21C7)_2(Na^-)_2$ at $-60^\circ C$ . . . . .	25
2-9.	Differential Scanning Calorimetry trace of	

	$(\text{Cs}^+)_2(21\text{C}7)_2(\text{Na}^-)_2$ at a ramping rate of $5^\circ\text{C}/\text{min}$ . .	26
2-10.	The molecular structure and the numbering of atoms in $(\text{K}^+)_2(21\text{C}7)_3(\text{MeNH}_2)(\text{Na}^-)_2$ . . . . .	30
2-11.	Stereo packing diagram of $(\text{K}^+)_2(21\text{C}7)_3(\text{MeNH}_2)(\text{Na}^-)_2$ . . . . .	31
2-12.	Optical absorption spectrum of a thin film of $(\text{K}^+)_2(21\text{C}7)_3(\text{MeNH}_2)(\text{Na}^-)_2$ at $-60^\circ\text{C}$ , prepared by rapid evaporation of the methylamine solvent. . . . .	34
2-13.	$^{23}\text{Na}$ static NMR spectrum of $(\text{K}^+)_2(21\text{C}7)_3(\text{MeNH}_2)(\text{Na}^-)_2$ at $-60^\circ\text{C}$ . . . . .	35
2-14.	Differential Scanning Calorimetry trace of $(\text{K}^+)_2(21\text{C}7)_3(\text{MeNH}_2)(\text{Na}^-)_2$ at a ramping rate of $5^\circ\text{C}/\text{min}$ . . . . .	36
2-15.	The molecular structure and the numbering of atoms in $\text{K}^+(\text{dicyclohexano-}24\text{C}8)\text{Na}^-$ . . . . .	40
2-16.	Stereo packing diagram of $\text{K}^+(\text{dicyclohexano-}24\text{C}8)\text{Na}^-$ . . . . .	41
2-17.	Optical absorption spectrum of a thin film of $\text{K}^+(\text{dicyclohexano-}24\text{C}8)\text{Na}^-$ at $-60^\circ\text{C}$ , prepared by rapid evaporation of the methylamine solvent. . . . .	42
2-18.	$^{23}\text{Na}$ static NMR spectrum of $\text{K}^+(\text{dicyclohexano-}24\text{C}8)\text{Na}^-$ at $-60^\circ\text{C}$ . . . . .	43
2-19.	Differential Scanning Calorimetry trace of $\text{K}^+(\text{dicyclohexano-}24\text{C}8)\text{Na}^-$ at a ramping rate of $5^\circ\text{C}/\text{min}$ . . . . .	44
2-20.	$^{133}\text{Cs}$ static NMR spectra of three alkalides. . . . .	49
2-21.	The molecular structure and the numbering of	

	atoms in $\text{Rb}^+(18\text{C}6)(12\text{C}4)\text{Na}^-$ . . . . .	53
2-22.	Stereo packing diagram of $\text{Rb}^+(18\text{C}6)(12\text{C}4)\text{Na}^-$ . . . .	54
2-23.	The molecular structure and the numbering of atoms in $\text{Rb}^+(18\text{C}6)(12\text{C}4)\text{Rb}^-$ . . . . .	58
2-24.	Stereo packing diagram of $\text{Rb}^+(18\text{C}6)(12\text{C}4)\text{Rb}^-$ . . . .	59
2-25.	$^{23}\text{Na}$ static NMR spectrum of $\text{Rb}^+(18\text{C}6)(12\text{C}4)\text{Na}^-$ at $-60^\circ\text{C}$ . . . . .	62
2-26.	$^{87}\text{Rb}$ NMR spectra of A) $\text{Rb}^+(18\text{C}6)(12\text{C}4)\text{Rb}^-$ and B) $\text{Rb}^+(18\text{C}6)(12\text{C}4)\text{Na}^-$ , obtained with a solid state spin-echo pulse sequence. Note that NMR peaks for both $\text{Rb}^+$ and $\text{Rb}^-$ in $\text{Rb}^+(18\text{C}6)(12\text{C}4)\text{Rb}^-$ were observed. . . . .	63
2-27.	Temperature dependence of the NMR line shapes of the $\text{Rb}^+$ ions in $\text{Rb}^+(18\text{C}6)(12\text{C}4)\text{Na}^-$ . A) $-100^\circ\text{C}$ ; B) $-80^\circ\text{C}$ ; C) $-60^\circ\text{C}$ ; D) $-40^\circ\text{C}$ ; and E) $-20^\circ\text{C}$ . . . . .	65
2-28.	Temperature dependence of the NMR line shapes of the $\text{Rb}^+$ ions in $\text{Rb}^+(18\text{C}6)(12\text{C}4)\text{Rb}^-$ . A) $-100^\circ\text{C}$ ; B) $-80^\circ\text{C}$ ; C) $-60^\circ\text{C}$ ; D) $-40^\circ\text{C}$ ; and E) $-20^\circ\text{C}$ . . . . .	66
2-29.	Computer simulated static second order quadrupolar line shapes for the central transition of a quadrupolar nucleus. . . . .	67
2-30.	Optical absorption spectrum of a thin film of $\text{Rb}^+(18\text{C}6)(12\text{C}4)\text{Na}^-$ at $-60^\circ\text{C}$ , prepared by rapid evaporation of the methylamine solvent. . . . .	68
2-31.	Optical absorption spectrum of a thin film of $\text{Rb}^+(18\text{C}6)(12\text{C}4)\text{Rb}^-$ at $-60^\circ\text{C}$ , prepared by rapid evaporation of the methylamine solvent. . . . .	69

3-1.	Concentration dependence of the $^{133}\text{Cs}$ chemical shifts of cesium compounds in nitromethane at 25°C. The solid lines are least-squares plots, obtained by simultaneous multiple data set fitting of all three data sets with the KINFIT program. . . . .	76
3-2.	$^{133}\text{Cs}$ chemical shifts <u>vs.</u> $[\text{L}]/[\text{Cs}^+]$ mole ratio in nitromethane at 25°C. L=18-crown-6, 15-crown-5, or 12-crown-4. The solid lines are least-squares plots. . . . .	88
3-3.	Nonlinear least-squares curve fitting of the chemical shift <u>vs.</u> $[\text{18C6}]/[\text{Cs}^+]$ mole ratio without the model of the intermediate $(\text{Cs}^+)_2(\text{18C6})_3$ . . . . .	89
3-4.	Nonlinear least-squares curve fitting of the chemical shift <u>vs.</u> $[\text{18C6}]/[\text{Cs}^+]$ mole ratio with the model of the intermediate $(\text{Cs}^+)_2(\text{18C6})_3$ . . . . .	90
3-5.	$^{133}\text{Cs}$ chemical shifts <u>vs.</u> $[\text{L}]/[\text{Cs}^+]$ mole ratio in nitromethane at 25°C. L = HMHCY, 15-crown-5, or 12-crown-4. The solid lines are least-squares plots. . . . .	99
4-1.	The series of transformations required to determine the chemical shielding or quadrupolar tensor in the PAS frame from the experimental data obtained in the laboratory frame. . . . .	109
4-2.	Crystal structure of $\text{Cs}^+(\text{18C6})_2\text{e}^-$ . A) Single molecule diagram; B) ORTEP stereo packing diagram. The anionic hole centers are indicated by the symbol $\odot$ . . . . .	110

4-3.	Single-crystal $^{133}\text{Cs}$ NMR spectra of the high-temperature phase of $\text{Cs}^+(\text{18C6})_2\text{e}^-$ at two different orientations at $\nu_L = 52.468\text{MHz}$ and at $-50^\circ\text{C}$ . . . . .	115
4-4.	Angular dependence of half the splitting of the two first satellite transitions of $\text{Cs}^+$ in site 1 from the high-temperature phase of single crystal $\text{Cs}^+(\text{18C6})_2\text{e}^-$ . . . . .	116
4-5.	Angular dependence of half the splitting of the two first satellite transitions of $\text{Cs}^+$ in site 2 from the high-temperature phase of single crystal $\text{Cs}^+(\text{18C6})_2\text{e}^-$ . . . . .	117
4-6.	Angular dependence of the chemical shift of the central transition of $\text{Cs}^+$ in site 1 from the high-temperature phase of single crystal $\text{Cs}^+(\text{18C6})_2\text{e}^-$ . . . . .	118
4-7.	Angular dependence of the chemical shift of the central transition of $\text{Cs}^+$ in site 2 from the high-temperature phase of single crystal $\text{Cs}^+(\text{18C6})_2\text{e}^-$ . . . . .	119

186

new

Pro

the

com

bicy

met

repr

elect

comp

of n

years

synth

have

of sin

EPR,

emissi

used

ethers

comple

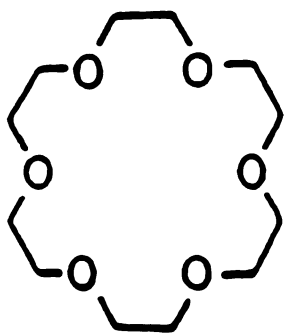
because

compar

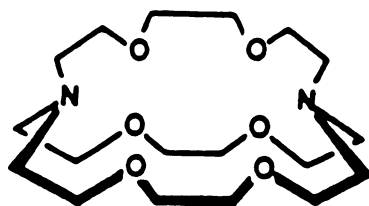
## CHAPTER 1. INTRODUCTION

The discovery of alkali metal-ammonia solutions by Weyl in 1863 has resulted in much research on this type of solution[1]. Two new types of compounds, alkalides and electrides, were discovered in Professor Dye's laboratory, while studying metal-amine solutions in the presence of complexants[2-5]. Alkalides and electrides are ionic compounds in which a metal cation is complexed by a cyclic or bicyclic polyether or polyamine. The anions in an alkalide are alkali metal anions, while those in an electride are electrons. A few representative complexants used in the synthesis of alkalides and electrides are shown in Figure 1-1.

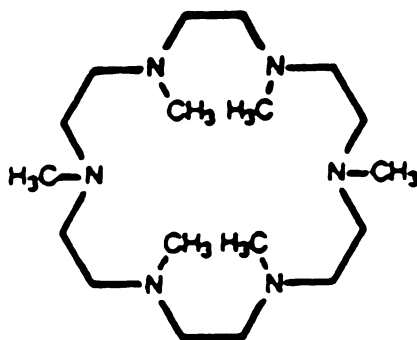
In order to advance the understanding of these unique ionic compounds, synthesis, structure determination and characterization of new alkalides and electrides are of great importance. Over the years, more than thirty alkalides and electrides have been synthesized and most of the crystal structures of these compounds have been solved since a new technique for the growth and handling of single crystals was established by S. Dawes and O. Fussa[6-8]. NMR, EPR, x-ray crystallography, powder conductivity, photoelectron emission, magnetic susceptibility and other techniques were also used to study the properties of these compounds[9-30]. But crown ethers larger than 18-crown-6 have never been used successfully as complexants for the synthesis of crystalline alkalides or electrides because of their flexible nature and their large cavity sizes compared to the radii of the alkali metal cations. The alkalides made



**18-Crown-6 (18C6)**



**Cryptand 222 (C222)**



**Hexamethyl Hexacyclen (HMHCY)**

**Figure 1-1. Representative complexants for alkali metal cations.**

wi

di

the

cro

us

cry

det

alk

con

con

exp

tem

expe

is d

indi

elec

anot

by n

toget

bette

synth

Two

synth

work.

also

model

with large crown ethers are often so 'soft' that it always presents the difficulties of growing single crystals and the problems of disorder in the crystal structures. But the hope of putting two cations into one crown ether and the interest in knowing their crystal structures led us to synthesize these compounds and to further determine their crystal structures. Among other topics, this thesis presents the details of the syntheses and crystal structure determinations of alkalides with large crown ethers as complexants.

While large crown ethers were used intentionally as complexants to synthesize alkalides, the first mixed sandwich compound,  $\text{Cs}^+(\text{18C6})(\text{15C5})\text{e}^-$ , was made accidentally during an experiment in which  $\text{Cs}^+(\text{18C6})_2\text{e}^-$  and  $\text{Cs}^+(\text{15C5})_2\text{e}^-$  were mixed as a temperature reference in  $^{133}\text{Cs}$  NMR measurements[7,31]. In this experiment, a new  $^{133}\text{Cs}$  NMR peak was observed at a position which is different from that of either  $\text{Cs}^+(\text{18C6})_2\text{e}^-$  or  $\text{Cs}^+(\text{15C5})_2\text{e}^-$ . This indicated the formation of a new compound, the mixed sandwich electrone,  $\text{Cs}^+(\text{18C6})(\text{15C5})\text{e}^-$ . After the discovery of this compound, another mixed sandwich compound,  $\text{K}^+(\text{18C6})(\text{12C4})\text{Na}^-$ , was made by mistake when samples of  $\text{K}^+(\text{18C6})\text{Na}^-$  and  $\text{K}^+(\text{12C4})_2\text{Na}^-$  were put together in an attempt to grow single crystals of  $\text{K}^+(\text{18C6})\text{Na}^-$ [32]. To better understand the nature of these mixed sandwich compounds syntheses of additional mixed sandwich complexes were carried out. Two of them,  $\text{Rb}^+(\text{18C6})(\text{12C4})\text{Na}^-$  and  $\text{Rb}^+(\text{18C6})(\text{12C4})\text{Rb}^-$ , were synthesized and their crystal structures were determined in this work. The discovery of the mixed sandwich alkalides and electrines also led to the successful synthesis and structure determination of a model salt, the mixed sandwich complex of  $\text{Rb}^+(\text{18C6})(\text{12C4})\text{I}^-$ ,

ind

cha

are

thei

ther

by

on

or

$K^+$

have

mon

the

diffi

very

rela

line

solu

$Cs^+$

addi

and

are

conv

diffe

half

field

indicating that mixed sandwich model salts indeed exist. The characterization of the mixed sandwich compounds showed that they are not only thermally stable but also have interesting properties.

It was the discovery of the mixed sandwich complexes and their thermal stability that prompted us to study the kinetics and thermodynamics of the complexation of these compounds in solution by using NMR techniques. The solution NMR studies mainly focused on the mixed sandwich complexes of the  $\text{Cs}^+$  cation with  $18\text{C6-}15\text{C5}$  or  $18\text{C6-}12\text{C4}$  although complexed  $\text{Rb}^+(18\text{C6})(12\text{C4})$  and  $\text{K}^+(18\text{C6})(12\text{C4})$  exist and are thermally stable. Both Rb and K nuclei have relatively low NMR sensitivities and large electrical quadrupole moments which give very broad NMR lines even in solutions due to the second order quadrupolar coupling. These characteristics present difficulties in the NMR studies of K or Rb nuclei. In contrast,  $\text{Cs}^+$  is a very good candidate for solution NMR studies. Its NMR sensitivity is relatively high. It has a very small electrical quadrupole moment and line broadening by quadrupolar interaction is not a factor. The solution NMR studies showed that complexed  $\text{Cs}^+(18\text{C6})(15\text{C5})$  and  $\text{Cs}^+(18\text{C6})(12\text{C4})$  indeed exist in solution as well as in solids. In addition, complexed  $\text{Cs}^+(18\text{C6})_2$ ,  $\text{Cs}^+(\text{HMHCY})_2$ ,  $\text{Cs}^+(\text{HMHCY})(15\text{C5})$ , and  $\text{Cs}^+(\text{HMHCY})(12\text{C4})$  were also studied by solution NMR.

NMR studies of half-integer spin quadrupolar nuclei in solids are becoming increasingly important since this technique can give convenient information about the structure and dynamics in many different chemical systems[33-37]. In general, the NMR spectra of half-integer spin quadrupolar nuclei depend on the local magnetic fields induced by nuclear quadrupolar coupling, chemical shift

anis

past

rela

cher

spin

inter

on

impr

that

spin

of

solid

2-D

NM

the

iden

spin

Cs-

tech

mod

NM

NM

qua

ana

is

anisotropy, and spin-spin coupling to the surrounding nuclei. In the past, NMR studies of quadrupolar nuclei were carried out in relatively low applied magnetic fields so that the field-dependent chemical shift anisotropy is small and both direct and indirect spin-spin couplings are usually negligible compared to the quadrupolar interaction. Consequently, most early studies of these nuclei focused on the investigation of the nuclear quadrupolar interaction. The improvements of NMR instrumentation in recent years have shown that measuring the influence of chemical shift anisotropy and spin-spin coupling is possible. These improvements include the application of superconducting magnets and the development of high resolution solid state techniques for quadrupolar nuclei. These techniques are 2-D NMR, dynamic angle spinning, double rotation, and zero field NMR[38-43].

Solid state NMR is one of most important techniques used for the studies of crystalline alkalides and electrides.  $\text{Na}^-$  was first identified in solution by using  $^{23}\text{Na}$  NMR[44-45]. Magic angle sample spinning NMR was also used to identify  $\text{Li}^+$ ,  $\text{Na}^+$ ,  $\text{Cs}^+$ ,  $\text{Na}^-$ ,  $\text{K}^-$ ,  $\text{Rb}^-$ , and  $\text{Cs}^-$  in powdered alkalides and electrides. In addition, other NMR techniques were used to study solid alkalides, electrides, and their model salts[9,11]. These techniques include solid state spin-echo, NMR relaxation measurements, and line-shape analysis of powder NMR spectra. Information about chemical shift anisotropy and quadrupole coupling constants can be obtained from line-shape analysis of static and magic angle spinning NMR spectra.

$^{133}\text{Cs}$  is an ideal nucleus for solid state NMR studies because it is 100% naturally abundant and has a relatively small quadrupole

moment. A number of  $\text{Cs}^+$  alkalides and their model salts have been studied by using static powder and magic angle sample spinning NMR. The line-shape analysis of the NMR spectra of these compounds gave some information about the quadrupolar interactions and chemical shift anisotropy of the  $\text{Cs}^+$  cations in these compounds. In spite of the success of  $\text{Cs}^+$  powder NMR studies, there are limitations that can only be eliminated by single-crystal NMR studies. Single-crystal NMR studies can give accurate quadrupolar coupling constant values, asymmetry parameters, and the orientations of the principal axes. The separation of the effects of chemical shift anisotropy and quadrupolar interaction also requires single-crystal NMR studies. The first and only single-crystal NMR study carried out in our laboratory is the single-crystal NMR investigation of  $\text{Na}^+(\text{C}_{222})\text{Na}^-$  by J. Kim[46]. This successful single-crystal NMR study showed that it is possible to carry out this type of study for alkalides and electrides, although they are temperature- and air-sensitive.

$\text{Cs}^+(\text{18C6})_2\text{e}^-$  was the first electride synthesized and is the most stable one of the five electrides whose structures have been determined. After its synthesis,  $\text{Cs}^+(\text{18C6})_2\text{e}^-$  was intensively studied by using numerous techniques including powder NMR, EPR, conductivity, magnetic susceptibility and others because of its unique physical properties. All of these led us to carried out the first single-crystal  $^{133}\text{Cs}$  NMR study of  $\text{Cs}^+(\text{18C6})_2\text{e}^-$ .

I.

imp

one

of

or,

con

hav

as

in t

and

cati

struc

crys

comp

impe

com

deco

low

deco

comp

soluti

## CHAPTER 2. SYNTHESIS, STRUCTURE DETERMINATION AND CHARACTERIZATION OF ALKALIDES

### I. Introduction

The synthesis of new alkalides and electrides is one of the most important goals in the studies of these compounds. For this purpose, one has to have suitable complexants. It appears that the synthesis of electrides requires encapsulation of the cation in a cage structure or, for crown ethers, by sandwich formation in which a 2:1 ratio of complexants to alkali metal cations is used. So far, electrides only have a 1:1 ratio of complexants to cations when cryptands are used as ligands. The size of the complexants also plays an important role in the formation of electrides. By contrast, alkalides can have 2:1, 1:1, and other ratios. They can also have solvent molecules bound to the cations or have free complexant molecules in the crystal structure[32, 47-48]. These different molecular structures and the crystal packing of alkalides depend greatly on the sizes of the complexants and the cations. Control of the temperature is also very important for the synthesis of alkalides and electrides since these compounds are temperature-sensitive and some compounds decompose, decomplex or undergo phase changes at temperatures as low as  $-50^{\circ}\text{C}$ . For example,  $(\text{Cs}^+)_2(21\text{C}7)_2(\text{Na}^-)_2$  in solution starts to decomplex at a temperature of about  $-49^{\circ}\text{C}$ . With the same complexant, 21-crown-7,  $(\text{K}^+)_2(21\text{C}7)_3(\text{MeNH}_2)(\text{Na}^-)_2$  is still stable in solution at a temperature as high as  $-32^{\circ}\text{C}$ .

app

atta

use

cell

Becc

glas

alka

wast

Char

B, a

could

then

comp

meth

evapo

are s

over

in th

witho

appar

with

decom

in one

could

finger.

Alkalides and electrides can be prepared in a K-cell or a glass apparatus called a three-chamber cell which has a third chamber attached to the K-cell as shown in Figure 2-1. Synthesis methods that use a K-cell have been described elsewhere[4-5]. The three-chamber cell is used especially for the synthesis of Li or Ba compounds. Because Li and Ba have relatively high melting points and react with glass, neither can be distilled by the usual methods used to distill alkali metals. Li or Ba was dropped into chamber C directly and washed with ammonia to chamber B through the frit between Chamber B and C. Once the metal ammonia solution was in chamber B, ammonia was removed by vacuum distillation and clean metal could be obtained in chamber B. Chamber C with its impurities could then be sealed off. After this procedure, the synthesis of Li or Ba compounds is similar to the others.

There are many ways of growing single crystals, but the two methods used most often in our laboratory are slow solvent evaporation and temperature scanning. Although these two methods are still being used, the strategy of crystal growth had been changed over the years. Nowadays, crystal growth can be carried out directly in the same K-cell in which the sample had just been synthesized without removing solvent and reloading the sample into another apparatus. Crystals can also be grown and harvested several times with the same sample and apparatus as long as the sample has not decomposed. In this case, a portion of the crystals could be collected in one or even half of one of the sample fingers so that some sample could be left to grow crystals at another time; the remaining sample fingers could then be used to collect crystals that were grown later.

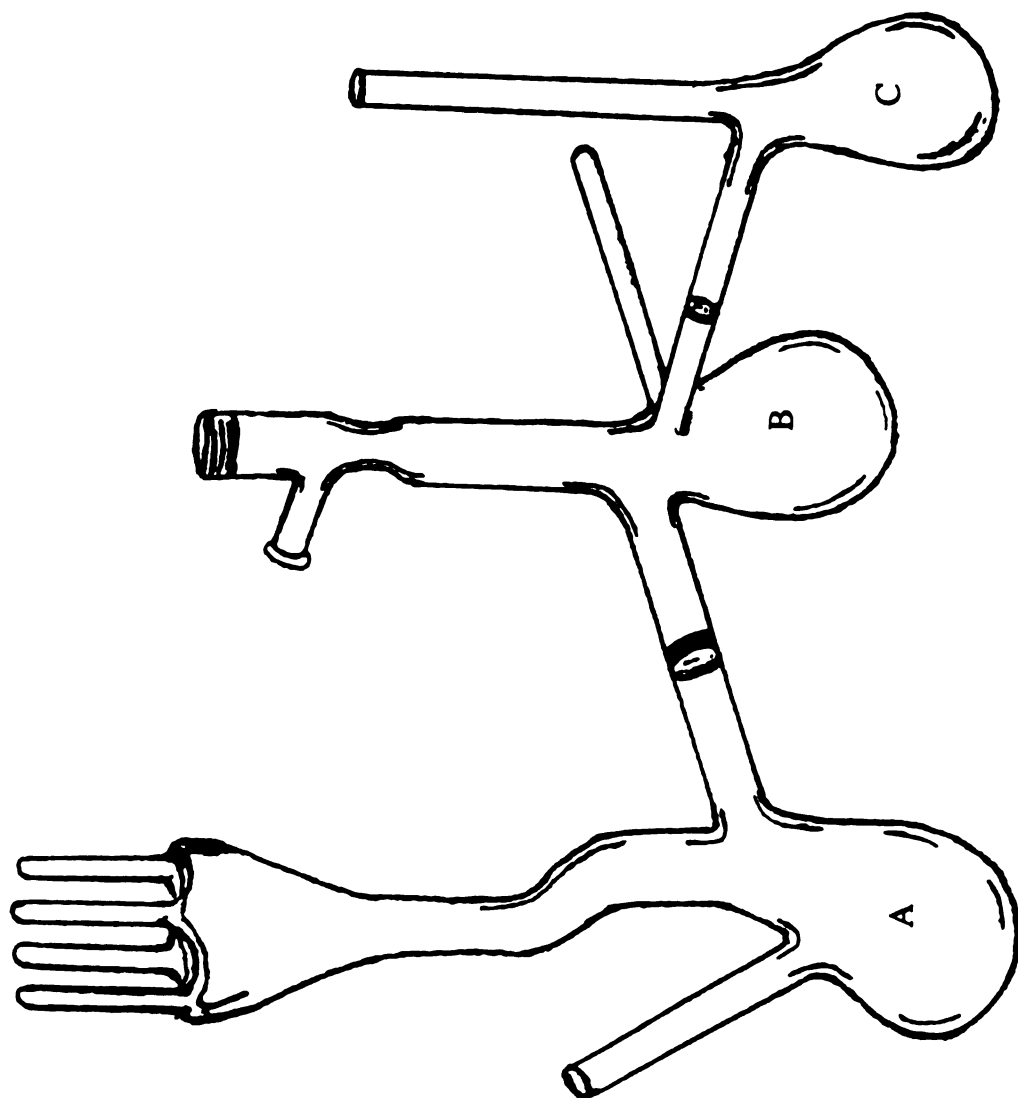


**Figure 2-1. Vacuum apparatus for the synthesis of alkali metal and  
electrides [3-chamber K-Cell].**

This

same

and

ray

prov

sand

was

been

othe

dete

actua

in th

II.

carrie

solve

single

alkali

7, di

obtain

viscon

vacuu

liquid

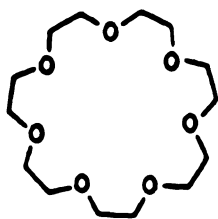
found

This can be repeated several times until no sample is left or the sample fingers are all used.

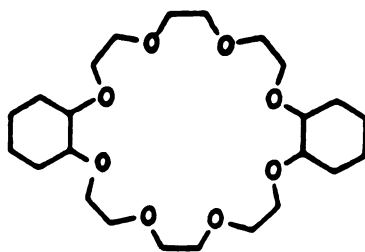
To determine the identity and stoichiometry of a compound and to help in understanding its physical properties, single crystal X-ray diffraction is the most direct and reliable method. This has been proved in our laboratory before. For example, the only mixed sandwich electride, first synthesized by S. B. Dawes and J. L. Eglin, was thought to be  $\text{Cs}^+(\text{18C6})(\text{15C5})\text{e}^-$  even after this electride had been studied with NMR, magnetic susceptibility, conductivity and other techniques by J. L. Eglin[48]. But the crystal structure determined by Rui Huang shows that its molecular formula is actually  $[\text{Cs}^+(\text{18C6})(\text{15C5})\text{e}^-]_6(\text{18C6})$  in which a free 18-crown-6 sits in the center of six  $\text{Cs}^+(\text{18C6})(\text{15C5})\text{e}^-$  members[50].

## II. Experimental

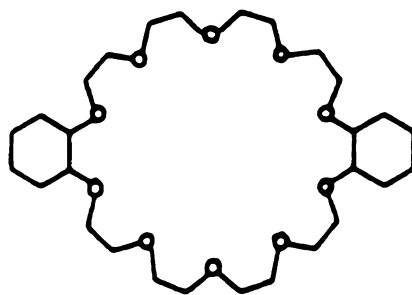
Syntheses and crystal growth of alkalides in this work were carried out with two different crystal growing methods and different solvent combinations in order to find out the best way to grow good single crystals. The large crown ethers used for the synthesis of alkalides are shown in Figure 2-2. All large crown ethers, 21-crown-7, dicyclohexano-24-crown-8, and dicyclohexano-30-crown-10, were obtained from Parish Chemical Co. These large crown ethers are very viscous liquids. Before being used, the complexants were purified by vacuum distillation at  $190^\circ\text{C}$  under  $2 \times 10^{-5}$  torr to yield a clear liquid. The methods of synthesis of alkalides and electrides can be found elsewhere[4-5]. The temperature scanning method for crystal



**21-Crown-7 (21C7)**



**Dicyclohexano-24-Crown-8 (Dicyclohexano-24C8)**



**Dicyclohexano-30-Crown-10 (Dicyclohexano-30C10)**

**Figure 2-2. Large crown ethers used for the synthesis of alkalides.**

growth with a programmable NESLAB LT-9 bath has been described in detail by Rui Huang[51]. When the slow solvent evaporation method was used, the mixed solvents of dimethyl ether or methyl amine with either diethyl ether or trimethyl amine were slowly evaporated into a liquid nitrogen trap through a series of frits under dynamic vacuum( $10^{-5}$  torr) for 3-4 days after the samples had been synthesized. Each frit has a bypass so that the speed of the solvent evaporation could be controlled.

A complete description of the techniques for the examination and mounting of single crystals for the X-ray diffraction is given by S. B. Dawes and O. Fussa[6-8].

X-ray data collection was carried out in a Nicolet P3F diffractometer with a LT-1 low temperature device. Cold nitrogen gas was used to keep the crystals under an inert atmosphere at low temperature throughout the entire data collection. The temperature of the crystals was kept at  $-70^{\circ}\text{C}$  or  $-80^{\circ}\text{C}$ .

$^7\text{Li}$ ,  $^{23}\text{Na}$ ,  $^{87}\text{Rb}$ , and  $^{133}\text{Cs}$  NMR spectra of the samples were obtained on a Varian VXR-400 superconducting NMR spectrometer equipped with a variable temperature controller. Various NMR techniques were used including static powder, solid state spin echo, and magic angle sample spinning. Static and solid state spin echo NMR measurements were carried out with a 45 to 165 MHz broadband probe, while the magic angle sample spinning measurements were made with a Varian 7-mm VT CP/MAS probe. The sample holder was a Zirconia rotor designed to allow sample loading and NMR measurements at low temperatures. After the samples were loaded into the NMR rotor under a nitrogen gas atmosphere and at or

v  
v  
v  
i  
  
r  
r  
f  
l  
t  
t  
a  
a  
  
L  
i  
t  
  
I  
  
I  
  
te  
at  
-7  
di

near liquid nitrogen temperature, the rotor containing the sample was transferred to a precooled NMR probe. Cold nitrogen gas was used to control the temperature and to keep the samples under an inert gas atmosphere during the NMR measurement.

A Model 260 Guided Wave Spectrophotometer was used to measure the optical absorption spectra. After the samples were reloaded into an optical apparatus at low temperature in a nitrogen-filled glove bag, the optical cell was pumped on a vacuum line, while being kept cold at  $-78^{\circ}\text{C}$ . Solutions of the compounds were made by the addition of methylamine or dimethyl ether. The thin films were then prepared by pouring the solution over the quartz cell window and rapidly distilling the solvent to another side-arm of the apparatus.

Differential Scanning Calorimetry(DSC) was performed on a DuPont 910 Differential Scanning Calorimeter. Samples were sealed in aluminum pans under nitrogen gas atmosphere at liquid nitrogen temperature.

### III. Results and Discussion

#### III.A. $(\text{Cs}^+)_2(21\text{C}7)_2(\text{Na}^-)_2$

Single crystals of  $(\text{Cs}^+)_2(21\text{C}7)_2(\text{Na}^-)_2$  were grown by the temperature-scanning technique. Since this compound decomplexed at about  $-49^{\circ}\text{C}$ , the temperature scan range was set from  $-50^{\circ}\text{C}$  to  $-70^{\circ}\text{C}$ . Methylamine or dimethyl ether with either trimethylamine or diethyl ether were tried as first and second solvents to form

stru  
fin.  
Rw  
isc  
we  
by  
w  
3-  
fo  
w  
c  
-  
c  
c  
c  
f  
l  
i

different solvent combinations for the synthesis and crystal growth. But only the combination of methylamine and diethyl ether was suitable for crystal growth. The crystals obtained were very small. Attempts to grow bigger crystals were not successful, probably because of the small temperature scan range. The crystals were purple in color.

The single crystal used for the X-ray study had the approximate dimensions of  $0.1 \times 0.2 \times 0.4 \text{ mm}^3$ . The unit cell parameters and orientation matrix were determined by least squares from the setting angles of 16 reflections in the range of  $15^\circ < 2\theta < 20^\circ$ . The space group of the crystal is triclinic  $P1$  with  $Z=1$  and the cell parameters are  $a=10.469(4)$ ,  $b=10.032(6)$ ,  $c=12.708(6)$ ,  $\alpha=90.919(42)^\circ$ ,  $\beta=73.385(30)^\circ$ , and  $\gamma=107.453(38)^\circ$ . These yield a calculated cell volume of  $1216.5(2.1)\text{\AA}^3$ . The crystal was kept at  $-70^\circ\text{C}$  throughout the entire data collection. Intensity data were collected by using the  $\theta$ - $2\theta$  scan method at  $3^\circ/\text{min.}$ (in  $2\theta$ ) with minimum  $2\theta=3.5^\circ$  and maximum  $2\theta=45^\circ$ . A linear decay correction was based on the intensities of three standard reflections measured for every 150 reflections. The number of reflections measured was 3485 and the number of reflections used in refinement was 2296 with a data cut-off of  $I > 3 \text{ sigma}(\sigma)$ . The crystal structure was solved by using direct methods with the Texsan Program. Hydrogen atoms were constrained to ride on their bonded C-atoms with fixed isotropic thermal parameters. The R factors were  $R=0.063$  and  $R_w=0.051$  with R defined as  $(\sum ||F_o| - |F_c||) / \sum |F_o|$ . Peak heights in the final difference map ranged from  $-0.91$  to  $0.67 \text{ e/\AA}^3$ . The molecular structure and numbering of the atoms are shown in Figure 2-3 and

the  
para  
A-2.

Tabl

Spac  
Cell

Volu  
Z  
R fac  
d

large  
show  
structu  
crown  
molar  
seven  
the se  
cations  
 $\text{Cs}^+(2)$   
Figure  
cations

the stereo packing diagram is shown in Figure 2-4. The positional parameters, bond distances, and bond angles are given in Tables A-1, A-2, and A-3 in Appendix A.

Table 2-1. Summary of Crystallographic Data for  $(\text{Cs}^+)_2(21\text{C}7)_2(\text{Na}^-)_2$

Space Group	Triclinic $P_1$
Cell Parameters	$a=10.469(4)\text{\AA}$ , $b=10.032(6)\text{\AA}$ , $c=12.708(6)\text{\AA}$ , $\alpha=90.919(42)^\circ$ , $\beta=73.385(30)^\circ$ , $\gamma=107.453(38)^\circ$
Volume	$1216.5(2.1)\text{\AA}^3$
Z	1
R factors	$R=0.063$ , $R_w=0.051$
d	$1.267\text{g/cm}^3$

$(\text{Cs}^+)_2(21\text{C}7)_2(\text{Na}^-)_2$  was the first alkalide synthesized with a large crown ether as complexant. The X-ray crystal structure data show that its crystal structure is completely different from the structures known for other alkalides. There are two  $\text{Cs}^+$  cations, two crown ethers, and two  $\text{Na}^-$  anions in one molecule although their molar ratio is 1:1:1. Each  $\text{Cs}^+$  cation in the molecule is bonded to all seven oxygen atoms in one 21-crown-7 and surprisingly to one of the seven oxygen atoms from another 21-crown-7. This gave the  $\text{Cs}^+$  cations a coordination number of eight and connected the two  $\text{Cs}^+(21\text{C}7)\text{Na}^-$  units together to form  $(\text{Cs}^+)_2(21\text{C}7)_2(\text{Na}^-)_2$  as shown in Figure 2-3. Even more surprisingly, the distance between the two  $\text{Cs}^+$  cations is only  $5.283(4)\text{\AA}$  and the  $\text{Na}^-$  anions and  $\text{Cs}^+$  cations form

Figure  
in  $\text{Cs}^+$

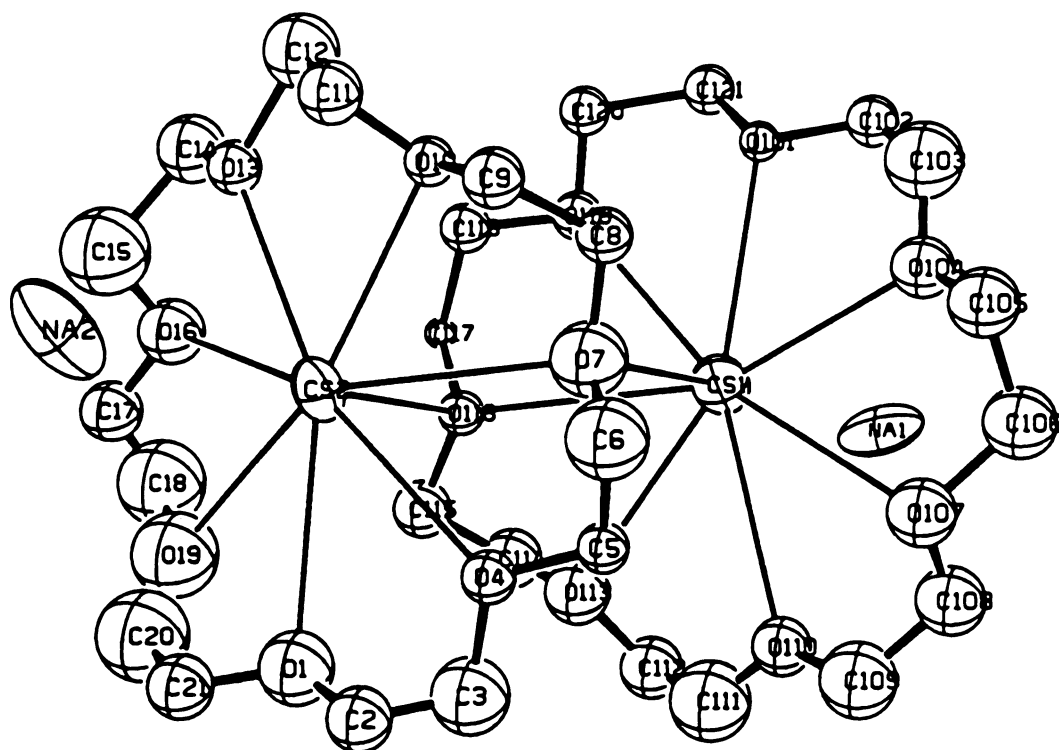


Figure 2-3. The molecular structure and the numbering of atoms in  $(\text{Cs}^+)_2(21\text{C}7)_2(\text{Na}^-)_2$ .

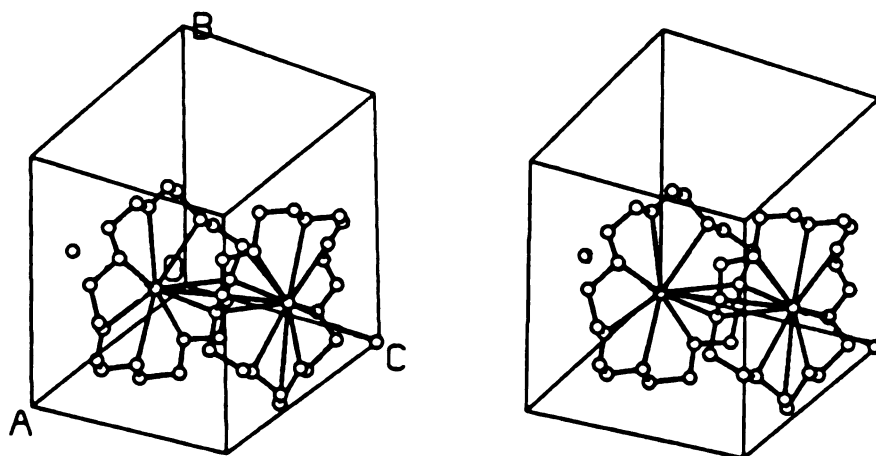


Figure 2-4. Stereo packing diagram of  $(\text{Cs}^+)_2(21\text{C}7)_2(\text{Na}^-)_2$ .

Table 2-2. selected bond distances and bond angles  
for  $(\text{Cs}^+)_2(21\text{C7})_2(\text{Na}^-)_2$

Bond	Length(Å)
Cs1-O7	3.25(3)
Cs1-O116	3.47(3)
Cs2-O7	3.45(3)
Cs2-O116	3.13(3)
Bond angle	Angle(degree)
O7-Cs1-O116	73.9(7)
O7-Cs2-O116	75.7(6)
Cs1-O7-Cs2	104.1(8)
Cs1-O116-Cs2	106.2(7)

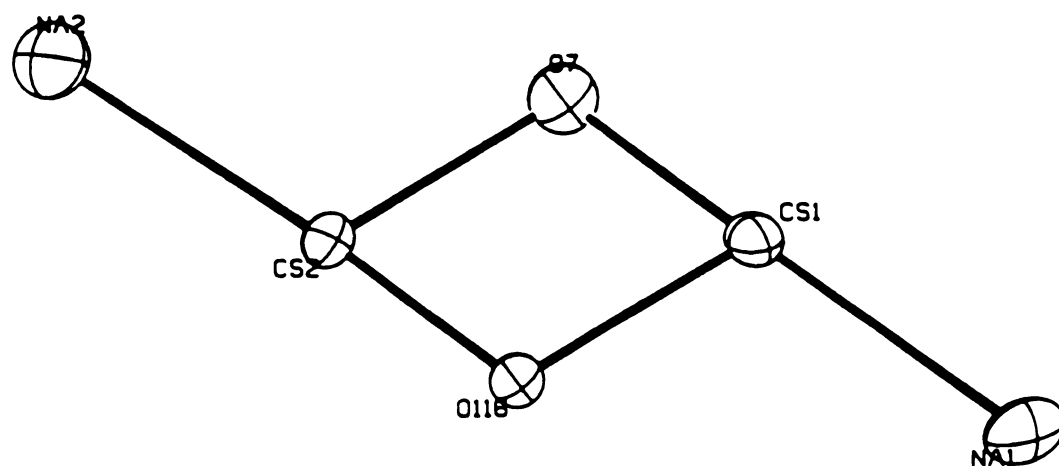


Figure 2-5. ORTEP plot of selected atoms in  $(\text{Cs}^+)_2(21\text{C}7)_2(\text{Na}^-)_2$ .

two cation-anion ion pairs on both sides of the molecule. The distances from the  $\text{Na}^-$  anions to the  $\text{Cs}^+$  cations are almost the same, 4.44(2)Å and 4.52(3)Å respectively. This is the only alkalide that has two cation-anion ion pairs in one molecule with two closely separated cations. Aside from these short Cs-Cs and Cs-Na distances in the molecule, the shortest Cs-Cs, Cs-Na, and Na-Na distances in the crystal structure are 8.904(4), 7.67(2), and 7.18(1)Å respectively. The bond distances of Cs1-O7, Cs1-O116, Cs2-O7, and Cs2-O116 are 3.25(3), 3.47(3), 3.45(3), and 3.13(3)Å respectively and the bond angles of O7-Cs1-O116, O7-Cs2-O116, Cs1-O7-Cs2, and Cs1-O116-Cs2 are 73.9(7)°, 75.7(6)°, 104.2(8)°, and 106.2(7)° respectively. These data are summarized in Table 2-2 and show that the four atoms formed a nearly symmetric parallelogram as shown in Figure 2-5. The two cation-anion ion pairs are on both sides of the  $\text{Cs}^+$  cations to give rather interesting twin ion pairs in the molecule.

This crystal belongs to the space group triclinic  $P_1$  and there is only one molecule in the unit cell. This is the first alkalide without any symmetry elements although most of the more than thirty alkalides and electrides belong to low symmetry space groups. The Cs1-O distances range from 3.18(2) to 3.55(2)Å with an average distance of 3.34Å and the Cs2-O distances range from 3.10(2) to 3.48(3)Å with an average distance of 3.30Å. The average distances of 3.34Å for Cs1-O and 3.30Å for Cs2-O are very close to those in  $\text{Cs}^+(\text{18C6})_2\text{Na}^-(3.36\text{Å})$ [7,52] and  $\text{Cs}^+(\text{18C6})_2\text{Cs}^-(3.31\text{Å})$ [51], and  $\text{Cs}^+(\text{18C6})_2\text{e}^-(3.35\text{Å})$ [6]. The two  $\text{Cs}^+$  cations in the unit cell are expected to be inequivalent because of their nonsymmetric positions in the crystal structure, regardless of the difference between their

average Cs-O distances. In fact, static powder and magic angle sample spinning NMR spectra in Figure 2-6 showed that there are two distinct  $^{133}\text{Cs}$  peaks, at chemical shift values of +60ppm and -28ppm, separated by 88ppm. The two  $^{133}\text{Cs}$  peaks are temperature independent. The large separation between the two peaks not only indicated the two  $\text{Cs}^+$  cations are asymmetric in the molecule, but also confirmed that they are chemically inequivalent because of differences in the Cs-O distances.

Perhaps the most interesting feature of this molecular structure is the twin cation-anion ion pairs. Taking the effective radius of  $\text{Cs}^+$  to be 1.69Å[53] and that of  $\text{Na}^-$  to be between 2.50 and 2.70Å determined from the anionic cavity size in other sodides[7, 8, 51, 54], the separation between the Van der Waals surfaces of the cation and anion is between 0.00 and 0.20Å. It is remarkable that the  $^{23}\text{Na}$  NMR and the optical absorption spectra of  $\text{Na}^-$  show no evidence of appreciable charge transfer to the cations in spite of the close contact of the anions and the cations; that is, the optical and NMR properties of  $\text{Na}^-$  are the same as those for other sodides in which  $\text{Na}^-$  is well isolated from the cations. The optical absorption spectrum of  $\text{Na}^-$  in  $(\text{Cs}^+)_2(21\text{C7})_2(\text{Na}^-)_2$  is shown in Figure 2-7. The single absorption peak at approximately 650nm in the spectrum of the thin film produced by solvent evaporation is attributed to the electronic transition of  $\text{Na}^-$  from the ground state,  $3s^2$ , to the excited state,  $3s3p$ . The two  $\text{Na}^-$  anions in the molecule show no differences in their optical properties and the absorption spectrum is very similar to those of the typical  $\text{Na}^-$  anions. The transition was temperature independent from -120°C to -20°C.

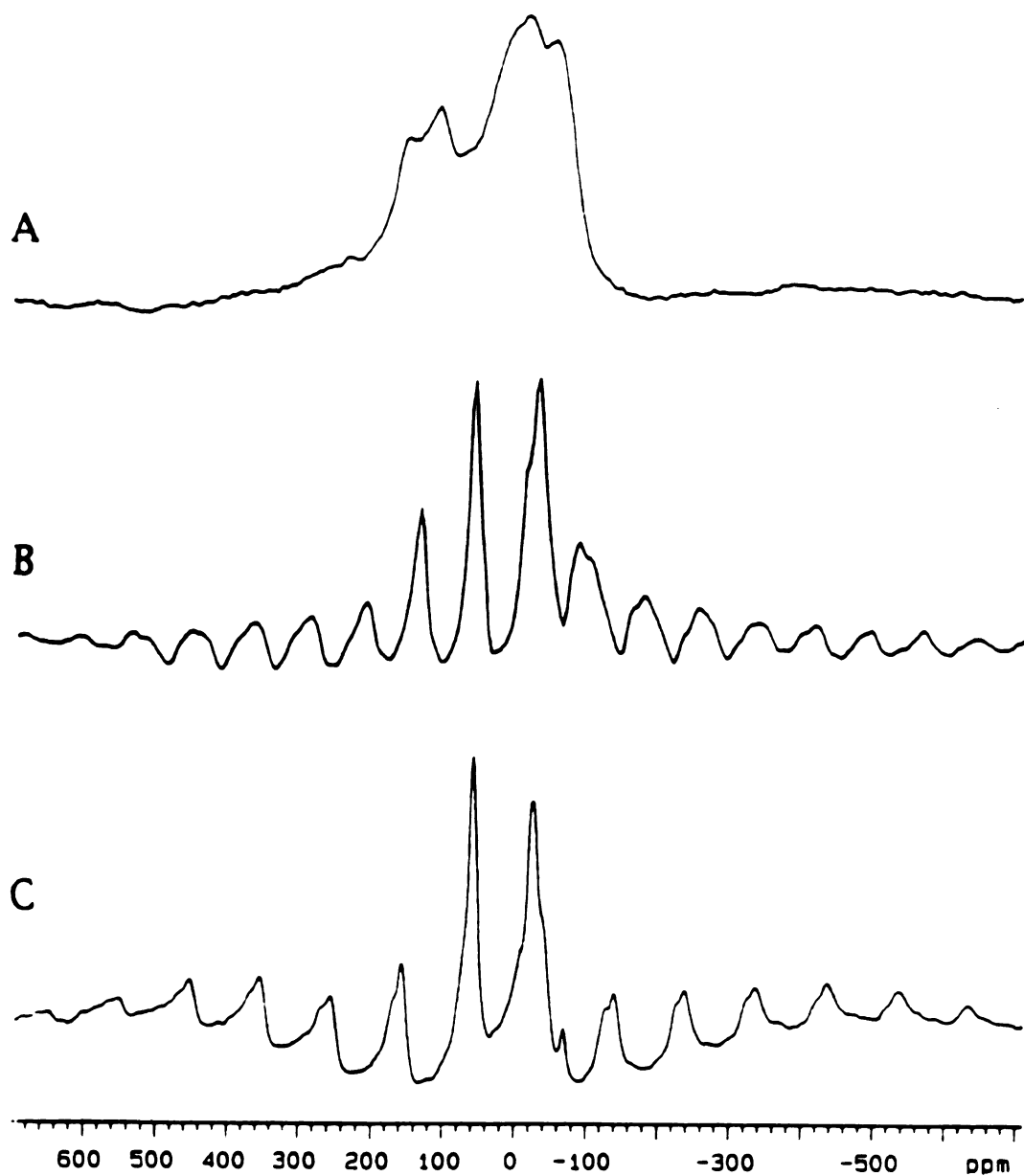


Figure 2-6.  $^{133}\text{Cs}$  static and MAS NMR spectra of  $(\text{Cs}^+)_2(21\text{C}7)_2(\text{Na}^-)_2$  at  $-60^\circ\text{C}$ ; A) Static; B) MAS,  $f=3.6\text{KHz}$ ; and C) MAS,  $f=5.0\text{KHz}$ .

Figure 2-8 shows the  $^{23}\text{Na}$  static powder NMR spectrum of  $(\text{Cs}^+)_{2}(\text{21C7})_{2}(\text{Na}^-)_{2}$ . The spectrum has a single  $^{23}\text{Na}$  NMR peak at a chemical shift value of  $-56.3\text{ppm}$  and shows no evidence of difference between the two  $\text{Na}^-$  cations. The chemical shift of  $-56.3\text{ppm}$  is well within the range of typical  $\text{Na}^-$  NMR spectra about  $-60\text{ppm}$  in other sodides considering the rather broad half height line width of  $40\text{ppm}$ . Again, the chemical shift is temperature independent. Both the optical and NMR properties of  $\text{Na}^-$  in  $(\text{Cs}^+)_{2}(\text{21C7})_{2}(\text{Na}^-)_{2}$  indeed show no evidence of charge transfer from the anion to the cation, similar to the results obtained with  $\text{M}^+(\text{HMHCY})\text{Na}^-$ , which also contains ion pairs for  $\text{M}=\text{K}$ ,  $\text{Rb}$ , and  $\text{Cs}$ [55].

The stability of this compound is of interest because of the large size of the complexant. According to Pedersen and Izatt[56-58], the cation radius and cavity size of the complexant are the most important factors which determine the stability of the complex. The difficulties encountered while trying to grow good quality crystals and to refine the crystal structure indicated that there is some kind of disorder in the crystal structure that was probably caused by thermal motion or packing disorder of the crown ethers during the crystallization. These effects are probably caused by the flexible nature of the crown ether and its large cavity size compared to the  $\text{Cs}^+$  cation radius. All crown ether atoms had to be refined isotropically because of this kind of disorder. This does not necessarily mean that this complex is unstable, but rather that a variety of crown ether conformations can be accommodated. DSC studies indicated that, at a ramping rate of  $5^{\circ}\text{C}/\text{min.}$ , this compound decomposes at about  $120^{\circ}\text{C}$  with a  $\Delta H$  value of  $-168\text{kJ}/\text{mole}$ .

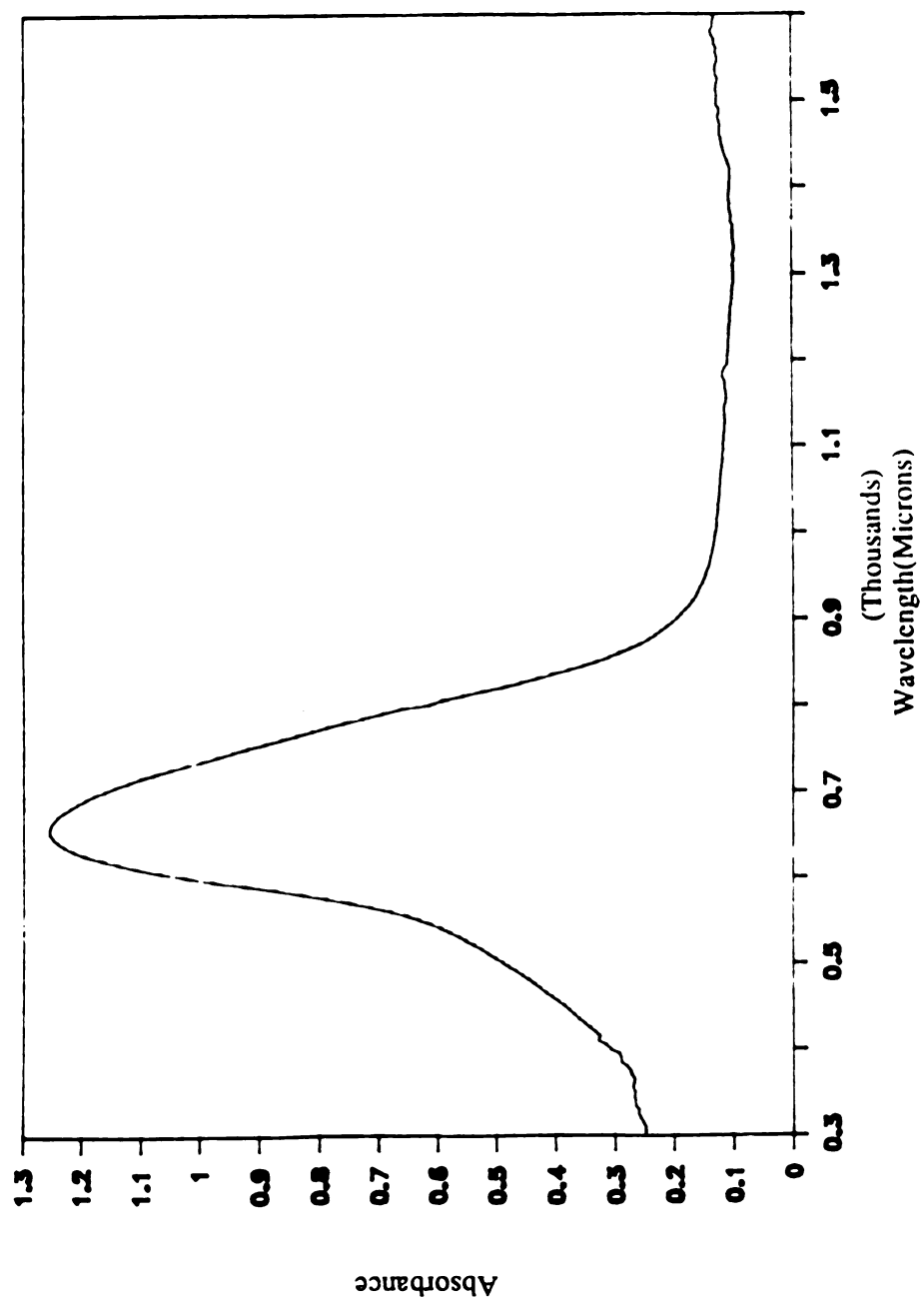


Figure 2-7. Optical absorption spectrum of a thin film of  $(\text{Cs}^+)_2(21\text{C7})_2(\text{Na}^-)_2$  at  $-60^\circ\text{C}$ , prepared by rapid evaporation of the methyllamine solvent.

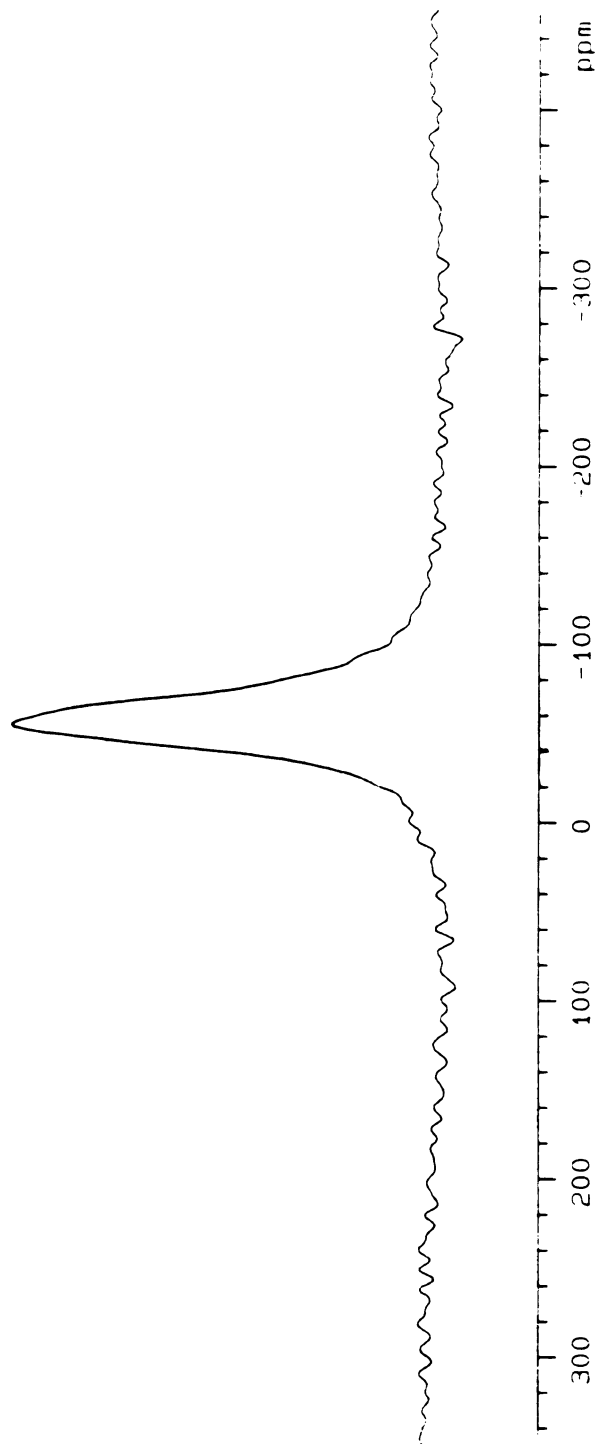


Figure 2-8.  $^{23}\text{Na}$  static NMR spectrum of  $(\text{Cs}^+)_2(2\text{IC}7)_2(\text{Na}^-)_2$  at  $-60^\circ\text{C}$ .

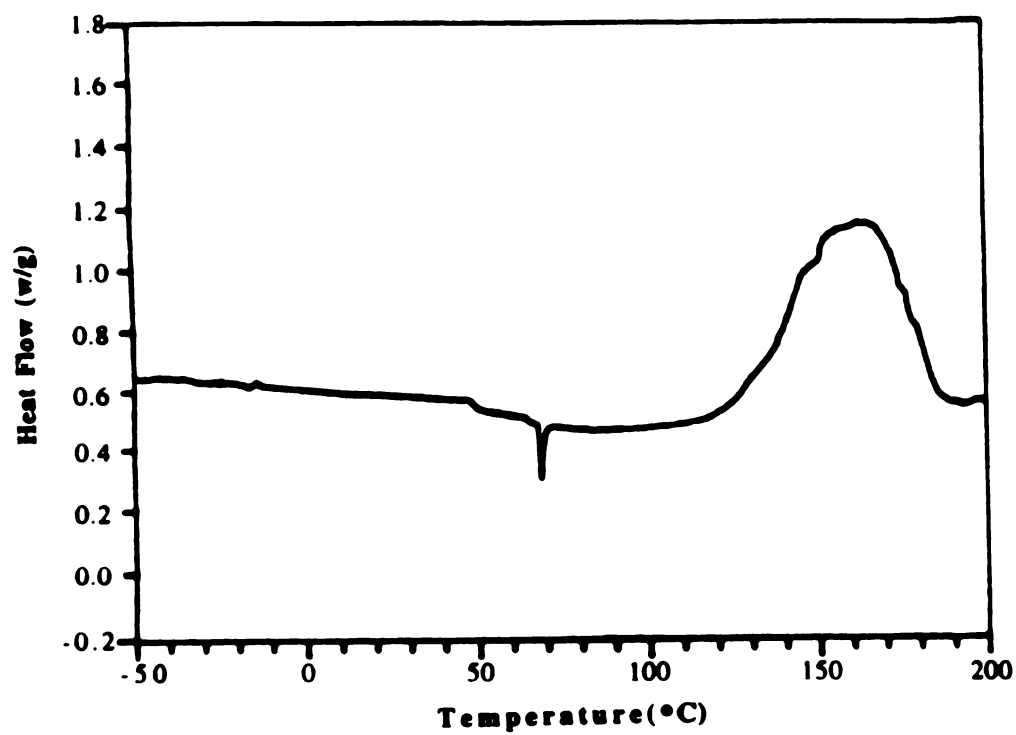


Figure 2-9. Differential Scanning Calorimetry trace of  $(\text{Cs}^+)_2(21\text{C}7)_2(\text{Na}^-)_2$  at a ramping rate of  $5^\circ\text{C}/\text{min}$ .

$(\text{Cs}^+)_2(21\text{C}7)_2(\text{Na}^-)_2$  also undergoes an irreversible endothermic transition with a  $\Delta H$  value of about 5kJ/mole at about 68°C before decomposition. The cause of the transition is not known, although it could be due to decomplexation. The DSC trace of  $(\text{Cs}^+)_2(21\text{C}7)_2(\text{Na}^-)_2$  is shown in Figure 2-9. The absence of low temperature peaks due to decomplexation and the high decomposition temperature show that  $(\text{Cs}^+)_2(21\text{C}7)_2(\text{Na}^-)_2$  is rather stable in the solid state, although it decomplexes even at -49°C in solution.

The stability of this compound may be attributed to the extensive coordination of the  $\text{Cs}^+$  cations to the complexants and to the presence of cation-anion contact ion pairs. These unusual features show that the  $\text{Cs}^+$  cations are well coordinated, leaving no open space around the  $\text{Cs}^+$  cations, which in turn stabilizes the complex. In solution, the Cs-O bond formed between a  $\text{Cs}^+$  cation and the oxygen atom from the second 21-crown-7 might be easily dissociated to form two  $\text{Cs}^+(21\text{C}7)\text{Na}^-$  molecules. Another possibility is that the cation-anion ion pairs might not be as stable as in the solid state.

EPR studies of this compound, being carried out by K. Reidy-Cedergren and Dr. J. McCracken of Michigan State University, are being used to determine the interactions of defect electrons trapped at the  $\text{Na}^-$  positions with nearby  $\text{Cs}^+$  cations and other nuclei[59].

### III.B. $(\text{K}^+)_2(21\text{C}7)_3(\text{MeNH}_2)(\text{Na}^-)_2$

In contrast to  $\text{Cs}^+(21\text{C}7)\text{Na}^-$ , this compound is much more stable in solution. Single crystals of  $(\text{K}^+)_2(21\text{C}7)_3(\text{MeNH}_2)(\text{Na}^-)_2$

were grown by using the temperature-scanning technique. The temperature scan range was set from  $-45^{\circ}\text{C}$  to  $-70^{\circ}\text{C}$  at a scan rate of  $1^{\circ}\text{C}/\text{hour}$ . Methylamine and diethyl ether were used as first and second solvents. The crystals were shiny brown in color.

The single crystal used for the X-ray study had the approximate dimensions of  $0.25 \times 0.4 \times 0.7 \text{ mm}^3$ . The unit cell parameters and orientation matrix were determined by least squares from the setting angles of 46 reflections in the range of  $4^{\circ} < 2\theta < 20^{\circ}$ . The space group of the crystal is monoclinic  $P2_1/n$  with  $Z=4$  and the cell parameters are  $a=9.140(3)$ ,  $b=36.574(8)$ ,  $c=19.475(5)$ , and  $\beta=94.630(23)^{\circ}$ . These yield a calculated cell volume of  $6489.0(5.4) \text{ \AA}^3$ . The crystal was kept at  $-80^{\circ}\text{C}$  throughout the entire data collection. Intensity data were collected by using the  $\theta$ - $2\theta$  scan method at  $4^{\circ}/\text{min. (in } 2\theta)$  with minimum  $2\theta=3.5^{\circ}$  and maximum  $2\theta=45^{\circ}$ . A linear decay correction was based on the intensities of three standard reflections measured for every 100 reflections. The number of reflections measured was 9634 and the number of reflections used in refinement was 3443 with a data cut-off of  $I > 3 \text{ sigma}(\sigma)$ . The crystal structure was solved by using direct methods with the Texsan Program. Hydrogen atoms were constrained to ride on their bonded C-atoms with fixed isotropic thermal parameters. The R factors were  $R=0.102$  and  $R_w=0.052$  with R defined as  $(\sum ||F_o| - |F_c||) / \sum |F_o|$ . Peak heights in the final difference map ranged from  $-0.46$  to  $0.86 \text{ e/\AA}^3$ . The molecular structure and numbering of the atoms are shown in Figure 2-10 and the stereo packing diagram is shown in Figure 2-11. The positional parameters, bond distances, and bond angles are given in Tables A-4, A-5, and A-6 in Appendix A.

Table 2-3. Summary of Crystallographic Data for  
 $(K^+)_2(21C7)_3(MeNH_2)(Na^-)_2$

Space Group	Monoclinic $P2_1/n$
Cell Parameters	$a=9.140(3)\text{\AA}$ , $b=36.574(8)\text{\AA}$ , $c=19.475(5)\text{\AA}$ , $\beta=94.630(23)^\circ$
Volume	$6489.0(5.4)\text{\AA}^3$
Z	4
R factors	$R=0.102$ , $R_w=0.052$
d	$1.131\text{g/cm}^3$

This is another unusual crystal structure. In this compound, there is a third 21-crown-7 that serves as a bridge that connects the two  $K^+$  ions in the molecule, while a solvent molecule,  $MeNH_2$ , forms a bond to one of the two  $K^+$  cations. The two  $K^+$  cations in the molecule have completely different coordination features. One is coordinated by all seven oxygen atoms from a 21-crown-7 and an eighth oxygen atom from the third 21-crown-7, giving it a coordination number of eight. By contrast, the other  $K^+$  ion is coordinated by only five of the seven oxygen atoms from a second 21-crown-7 and one from the third 21-crown-7. It is also bonded to a solvent molecule,  $MeNH_2$ . This gives the second  $K^+$  ion a total coordination number of seven. These two  $K^+$  cations, therefore, are clearly chemically inequivalent. The K1-K2 distance within the molecule is  $9.985(7)\text{\AA}$ , while the shortest K-K, K-Na, and Na-Na

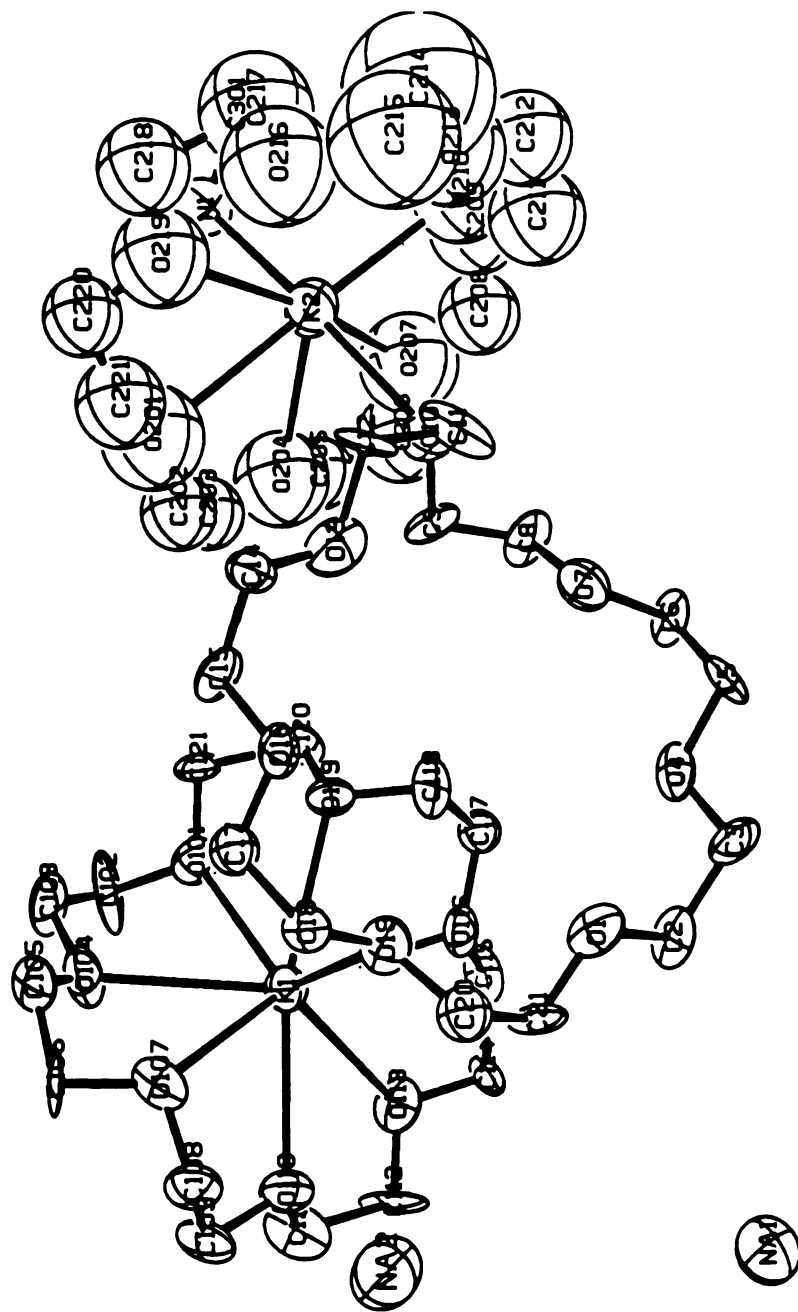


Figure 2-10. The molecular structure and the numbering of atoms in  $(K^+)_2(21C7)_3(MeNH_2)_2(Na^+)_2$ .

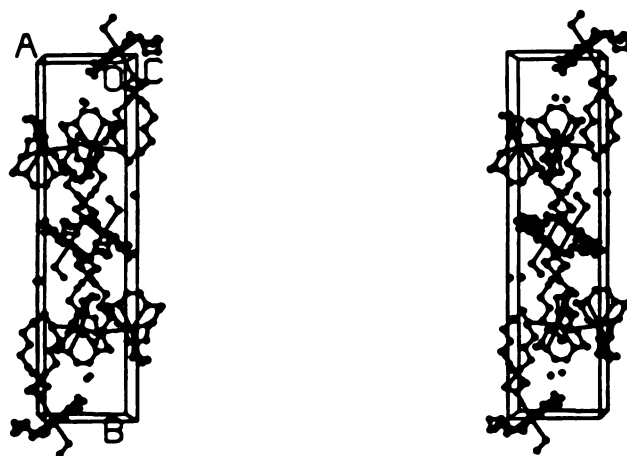


Figure 2-11. Stereo packing diagram of  $(K^+)_2(21C7)_3(MeNH_2)(Na^+)_2$ .

t  
t  
c  
t  
K  
c  
a  
in  
cr  
-7  
co  
re  
we  
tha  
the  
dis

distances in the crystal structure are 8.819(7), 6.41(1), and 8.21(1)Å respectively. The K1-O bond distances range from 2.84(1) to 3.12(1)Å with an average bond distance of 2.93Å. The K2-O bond distances range from 2.92(2) to 3.05(4)Å with an average bond distance of 2.98Å. These average K<sup>+</sup>-O distances are very close to those in K<sup>+</sup>(18C6)(12C4)Na<sup>-</sup>(2.98Å), K<sup>+</sup>(18C6)(12C4)K<sup>-</sup>(2.99Å), and K<sup>+</sup>(18C6)(12C4)K<sup>-</sup>(18C6)(3.02Å)[32], but are slightly longer than those in K<sup>+</sup>(C222)Na<sup>-</sup>(2.82Å) and K<sup>+</sup>(C222)e<sup>-</sup>(2.83Å)[51]. The K-N bond distance is 2.94(2)Å. The distances between K<sub>2</sub> and O213 and O216 are 3.45(4)Å and 3.64(3)Å respectively, indicating that these two oxygen atoms are too far away from the K<sup>+</sup> cation to form bonds between them. This type of crystal structure is very unusual because the second K<sup>+</sup> cation does not have the same surroundings and coordination number as does the first K<sup>+</sup> cation on the other side of the molecule, even though there could be similar conditions for the K<sup>+</sup> ion to do so. In the first structure determination, the results for a crystal that was grown by the temperature-scanning technique with a scan range from -32°C to -70°C showed that all atoms except those in the second 21-crown-7 could be well refined. The second set of crystals was grown with a temperature scan range from -45°C to -70°C, and the temperature for the entire X-ray diffraction data collection was also lowered to -80°C, in the hope that this would reduce the disorder due to thermal motion. However, the results were exactly the same as those obtained the first time. This indicated that the temperatures for crystal growth and data collection were not the cause of the disorder problem. It might be attributed to disordered packing of the second 21-crown-7 because the

c

f

R

t

2

i

c

(

(

e

b

la

la

in

st

2

bo

ca

in

un

cr

Th

we

M

coordination number between the  $K^+$  ion and 21-crown-7 is only five, leaving part of the crown ether free and more flexible.

The optical absorption spectrum of this compound is shown in Figure 2-12. The single absorption peak at approximately 690nm is typical for  $Na^-$  anions. The NMR spectrum in Figure 2-13 has a single  $^{23}Na$  NMR peak at -60.80ppm. Both optical and NMR spectra indicated that this compound is a typical sodide and there is no observable difference between the two  $Na^-$  anions in  $(K^+)_2(21C7)_3(MeNH_2)(Na^-)_2$ . The  $^{39}K$  solid state NMR peaks of  $(K^+)_2(21C7)_3(MeNH_2)(Na^-)_2$  could not be observed because of the expected large second order quadrupolar coupling. This would broaden the NMR lines greatly and bury them into the base line. This large second order quadrupolar coupling can be attributed to the large quadrupole moment of potassium and the very asymmetric interaction between the  $K^+$  cations and their surroundings.

The DSC trace of  $(K^+)_2(21C7)_3(MeNH_2)(Na^-)_2$  in Figure 2-14 shows that this compound decomposed at about 65°C with  $\Delta H = -233\text{kJ/mole}$  at a ramping rate of 5°C/min. There was no sign of K-N bond dissociation between the solvent molecule,  $MeNH_2$  and the  $K^+$  cation even when temperature reached the decomposition point. This indicated that the K-N bond is rather strong.

The disorder problem was believed to be caused by the unusual stereo-coordination nature of the second  $K^+$  cation and 21-crown-7 and the presence of a coordinated solvent molecule. Therefore, attempts to synthesize and to crystallize K-(21C7) sodide were carried out with dimethyl ether as a first solvent instead of  $MeNH_2$ , in the hope that the second  $K^+$  and 21-crown-7 would be

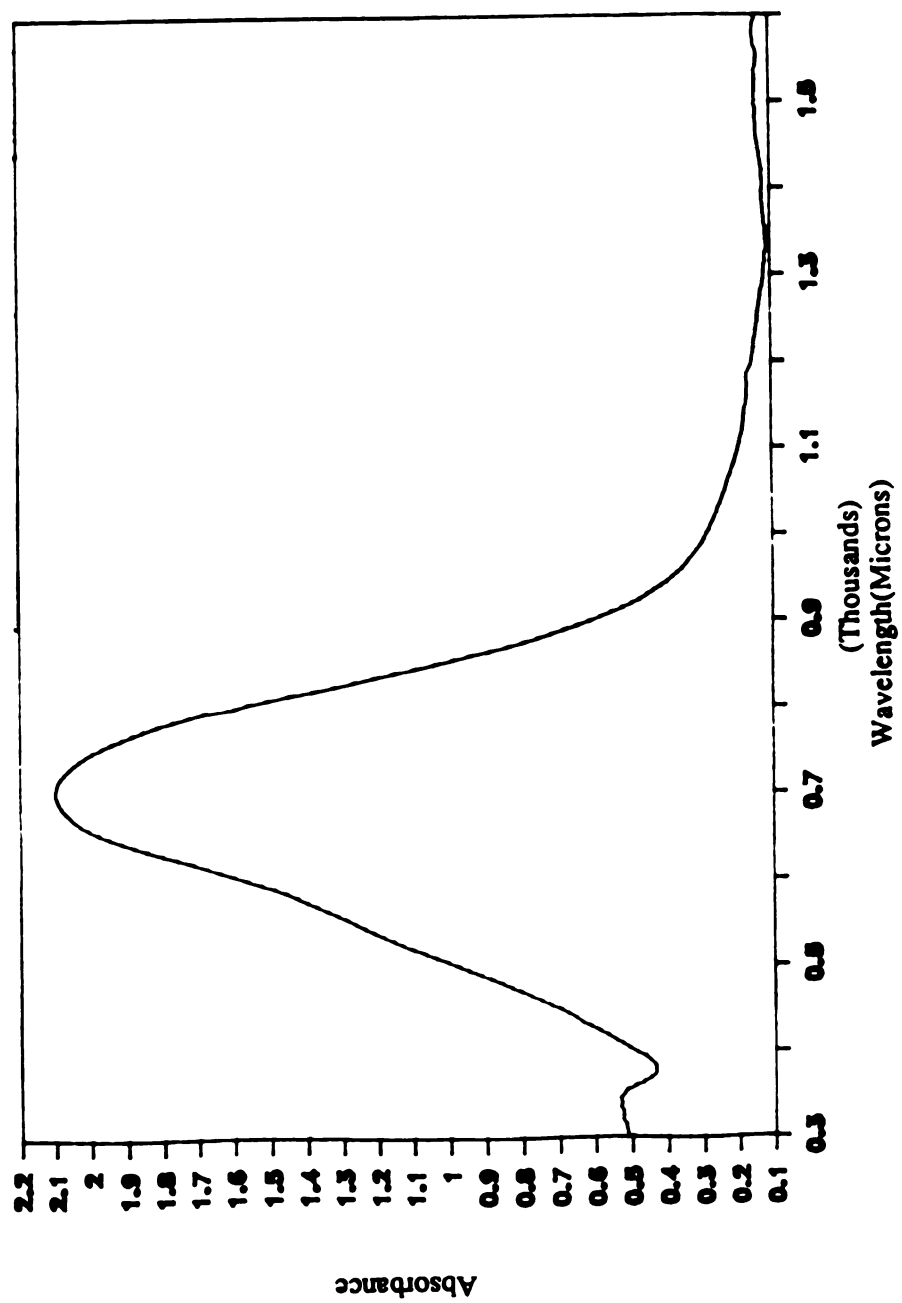


Figure 2-12. Optical absorption spectrum of a thin film of  $(K^+)_2(21C7)_3(MeNH_2)_3(Na^+)_2$  at  $-60^\circ C$ , prepared by rapid evaporation of the methylamine solvent.

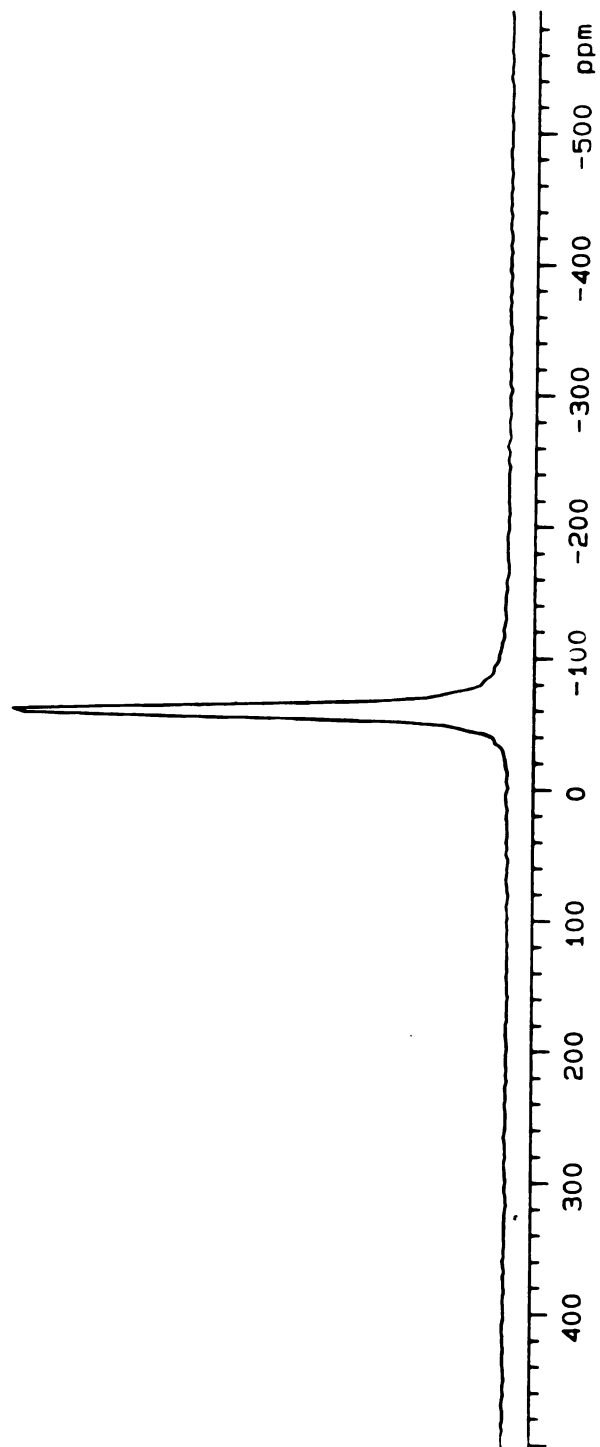


Figure 2-13.  $^{23}\text{Na}$  static NMR spectrum of  $(\text{K}^+)_2(21\text{C7})_3(\text{MeNH}_2)_2(\text{Na}^-)_2$  at  $-60^\circ\text{C}$ .

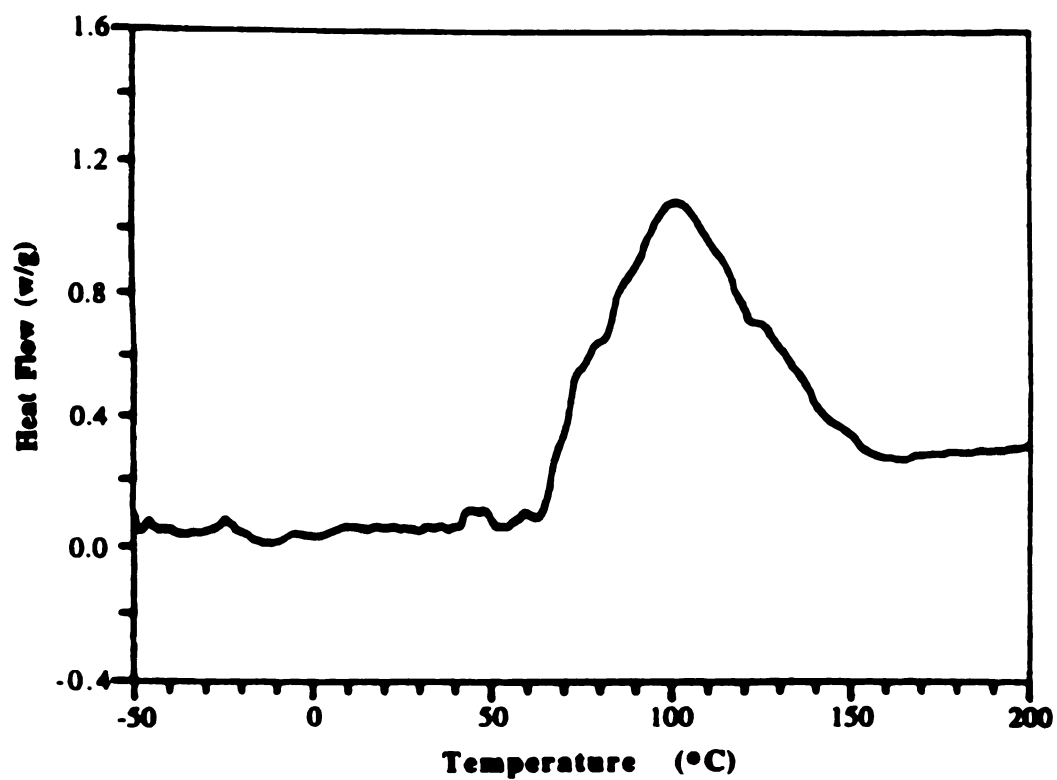


Figure 2-14. Differential Scanning Calorimetry trace of  $(\text{K}^+)_2(21\text{C7})_3(\text{MeNH}_2)(\text{Na}^-)_2$  at a ramping rate of  $5^\circ\text{C}/\text{min}$ .

forced to coordinate to each other in a similar fashion to that of the first  $K^+$  and 21-crown-7, because the K-N bond would no longer be available for coordination. Unfortunately, only powder samples were obtained when dimethyl ether was used as the first solvent.

### III.C. $K^+(\text{dicyclohexano-24C8})Na^-$

$K^+(\text{dicyclohexano-24C8})Na^-$  is the only alkalide complexed by a crown ether as large as 24-crown-8 that could be crystallized. Crystals were obtained by using the temperature-scanning technique. The temperature scan range was set from  $-40^\circ\text{C}$  to  $-70^\circ\text{C}$  at a scan rate of  $1^\circ\text{C}/\text{hour}$ . Methylamine and diethyl ether were the solvents for synthesis and crystal growth. The crystals were golden in color.

The single crystal used for the X-ray study had the approximate dimensions of  $0.2 \times 0.4 \times 0.8 \text{ mm}^3$ . The unit cell parameters and orientation matrix were determined by least squares from the setting angles of 32 reflections in the range of  $4^\circ < 2\theta < 20^\circ$ . The space group of the crystal is orthorhombic  $P2_12_12$  with  $Z=4$  and the cell parameters are  $a=10.439(5)$ ,  $b=10.954(7)$ , and  $c=27.773(13)$ . These yield a calculated cell volume of  $3175.8(5.0)\text{\AA}^3$ . The crystal was kept at  $-70^\circ\text{C}$  throughout the entire data collection. Intensity data were collected by using the  $\theta$ - $2\theta$  scan method at  $2^\circ/\text{min}$ . (in  $2\theta$ ) with minimum  $2\theta=3.5^\circ$  and maximum  $2\theta=45^\circ$ . A linear decay correction was based on the intensities of three standard reflections measured for every 100 reflections. The number of reflections measured was 1285 and the number of reflections used in

Table 2-4. Summary of Crystallographic Data for  
 $\text{K}^+(\text{dicyclohexano-24C8})\text{Na}^-$

---

Space Group	Orthorhombic $P2_12_12$
Cell Parameters	$a=10.439(5)\text{\AA}$ , $b=10.954(7)\text{\AA}$ , $c=27.773(13)\text{\AA}$ ,
Volume	$3175.8(5.0)\text{\AA}^3$
Z	4
R factors	$R=0.147$ , $R_w=0.067$
d	$1.093\text{g/cm}^3$

---

refinement was 272 with a data cut-off of  $I > 3 \sigma(\sigma)$ . The crystal structure was solved by using direct methods with the Texsan Program. Hydrogen atoms were constrained to ride on their bonded C-atoms with fixed isotropic thermal parameters. The R factors were  $R=0.147$  and  $R_w=0.067$  with R defined as  $(\sum ||F_o| - |F_c||) / \sum |F_o|$ . Peak heights in the final difference map ranged from -0.73 to 0.79 e/Å<sup>3</sup>. The molecular structure and numbering of the atoms are shown in Figure 2-15 and the stereo packing diagram is shown in Figure 2-16. The positional parameters, bond distances, and bond angles are given in Tables A-7, A-8, and A-9 in Appendix A.

It was thought that a dicyclohexano-24-crown-8 molecule might be able to complex two K<sup>+</sup> cations because this crown ether has a large size compared to that of K<sup>+</sup>. But the single crystal X-ray diffraction study showed that this compound has a 1:1 ratio of K<sup>+</sup> to dicyclohexano-24-crown-8. Because of the mismatch of sizes between dicyclohexano-24-crown-8 and K<sup>+</sup> cation, the crown ether twists around the K<sup>+</sup> in order to have all eight oxygen atoms form bonds to the cation. Despite the twist of dicyclohexano-24-crown-8 around the potassium cation and the flexibility of its two six-carbon member rings, which could let any possible symmetry within the molecule disappear, only one half of the crown ether is crystallographically unique and both the cations and the anions are in special positions. It is also interesting to note that there are two types of crystallographically non-equivalent molecules in the unit cell while only one half of each of the two inequivalent molecules is crystallographically unique. The K1-O distances range from 2.71(3) to 2.83(2) Å with an average distance of 2.79 Å and K2-O distances range

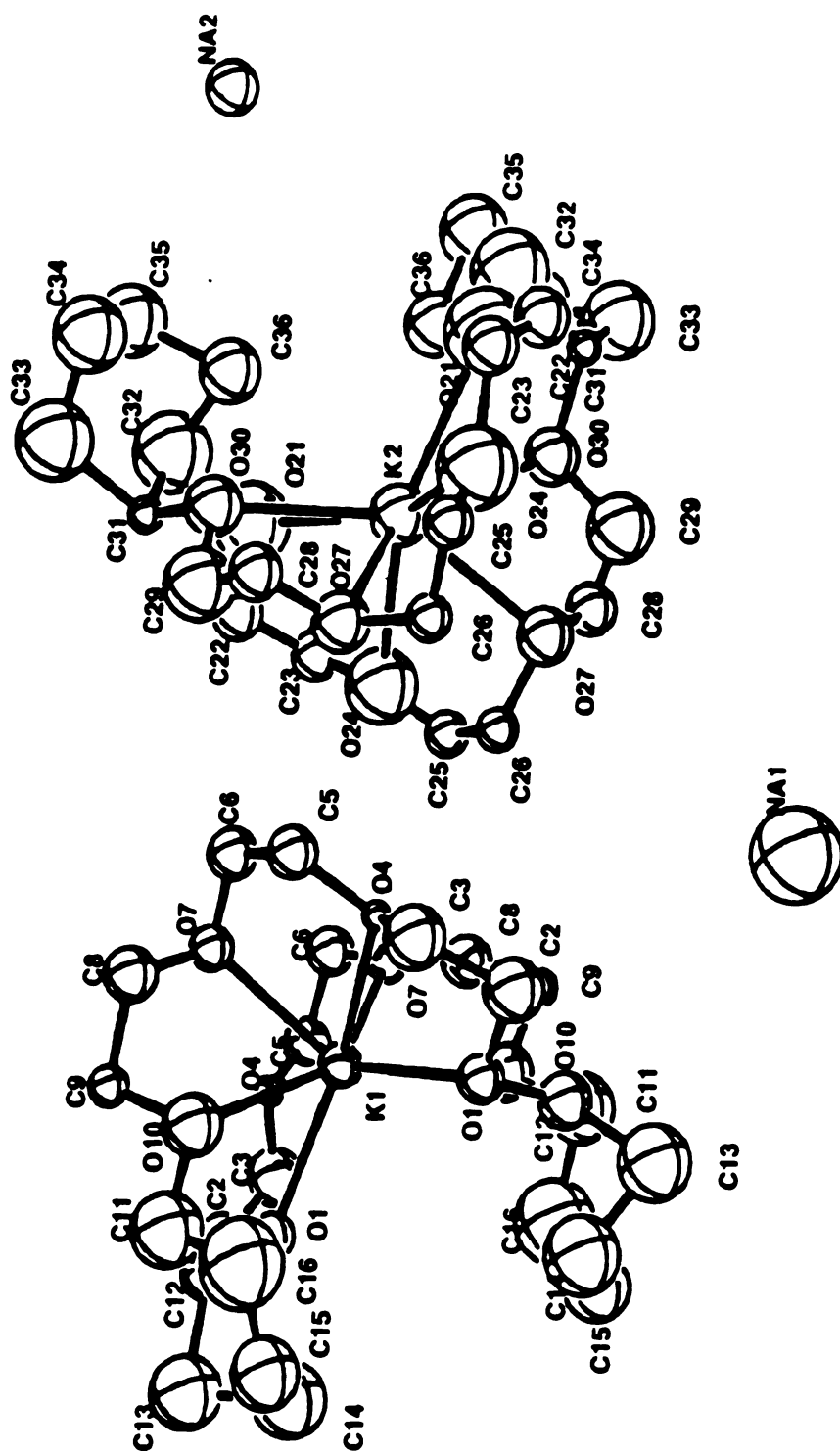


Figure 2-15. The molecular structure and the numbering of atoms in  $\text{K}^+(\text{dicyclohexano-24C8})\text{Na}^+$ .

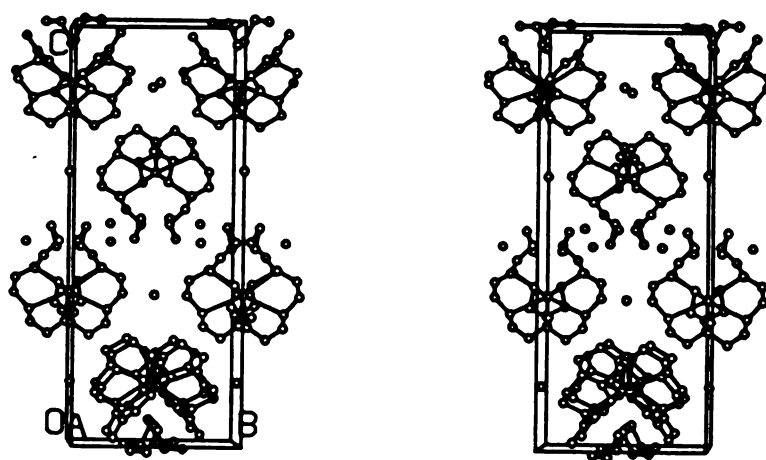


Figure 2-16. Stereo packing diagram of  $\text{K}^+(\text{dicyclohexano-24C8})\text{Na}^-$ .

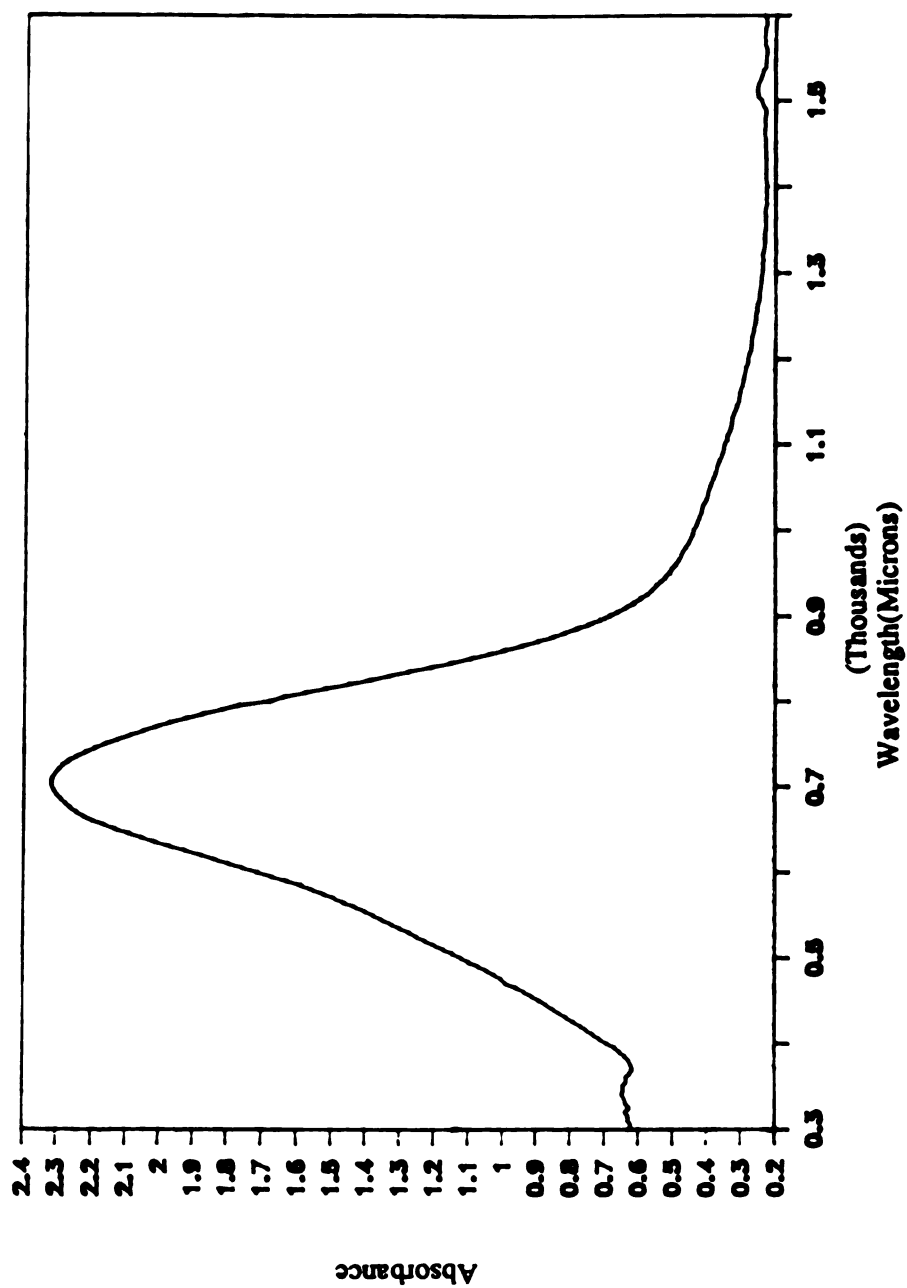


Figure 2-17. Optical absorption spectrum of a thin film of  $\text{K}^+(\text{dicyclohexano-24C8})\text{Na}^-$  at  $-60^\circ\text{C}$ , prepared by rapid evaporation of the methyllamine solvent.

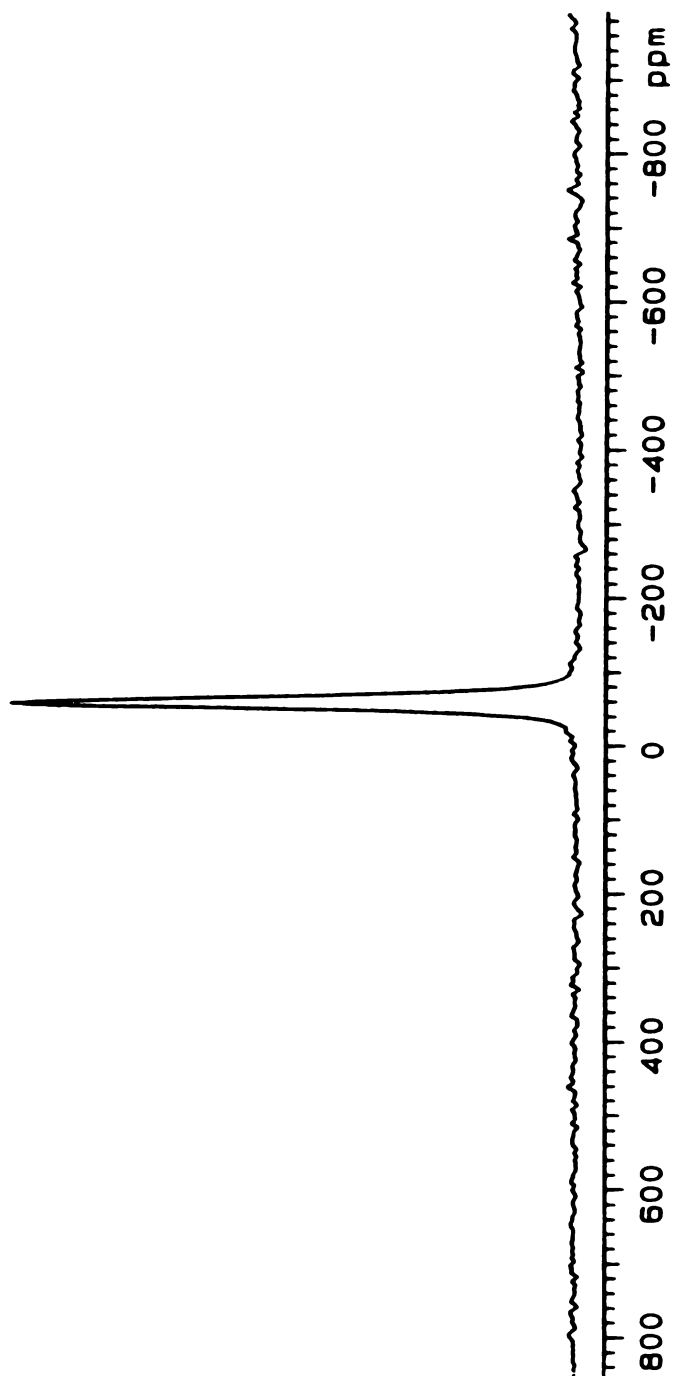


Figure 2-18.  $^{23}\text{Na}$  static NMR spectrum of  $\text{K}^+(\text{dicyclohexano-24C8})\text{Na}^+$  at  $-60^\circ\text{C}$ .

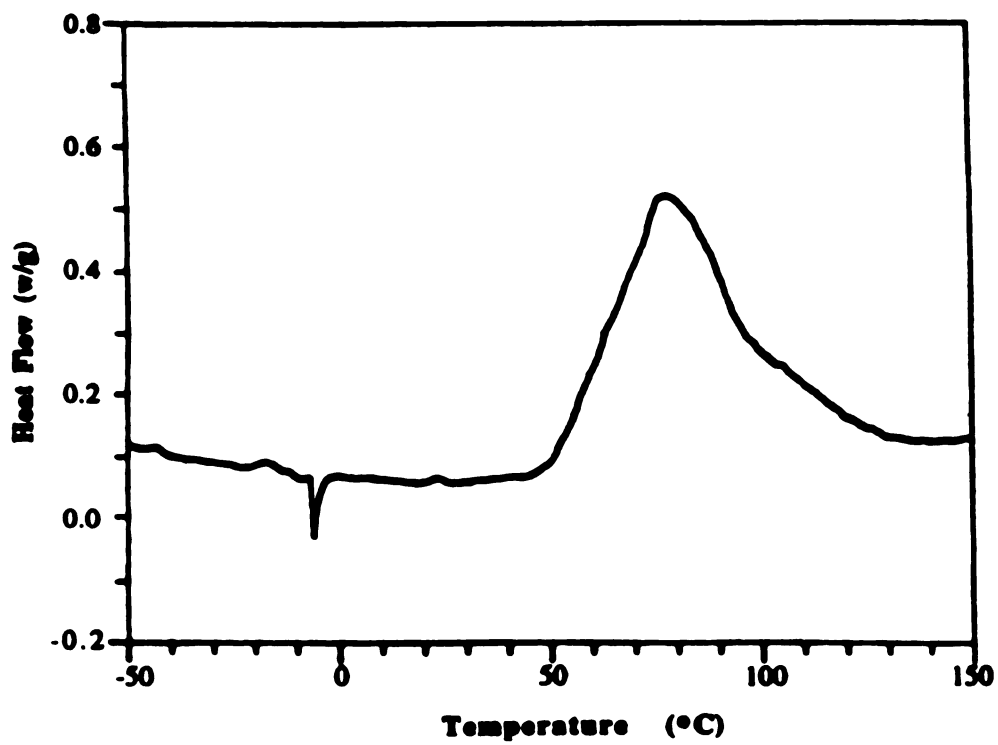


Figure 2-19. Differential Scanning Calorimetry trace of  $\text{K}^+(\text{dicyclohexano-24C8})\text{Na}^-$  at a ramping rate of  $5^\circ\text{C}/\text{min}$ .

from 2.81(3) to 2.92(3)Å with an average distance of 2.86Å. These average  $K^+$ -O distances are close to those in  $K^+(C222)I^-(2.79\text{\AA})$ [60],  $K^+(C222)Na^-(2.82\text{\AA})$ , and  $K^+(C222)e^-(2.83\text{\AA})$ [51], but are shorter than those in  $K^+(18C6)(12C4)Na^-(2.98\text{\AA})$ , and  $K^+(18C6)(12C4)K^-(2.99\text{\AA})$ [32].

The optical absorption and  $^{23}Na$  solid state NMR spectra of  $K^+(\text{dicyclohexano-}24C8)Na^-$  are given in Figure 2-17 and Figure 2-18. The absorption peak is at about 700nm and the  $^{23}Na$  NMR peak is at -61.22ppm. These results indicated that  $K^+(\text{dicyclohexano-}24C8)Na^-$  is a typical sodide. The  $^{39}K$  solid state NMR spectrum could not be obtained because of the large second order quadrupolar coupling as was the case for  $(K^+)_2(21C7)_3(MeNH_2)(Na^-)_2$ . The DSC studies of this compound showed decomposition at about 55°C with  $\Delta H = -72\text{kJ/mole}$  at a ramping rate of 5°C/min. An irreversible endothermic transition at about -5°C was also observed. The cause of this transition is unclear, but it could be due to decomplexation or melting. The DSC trace of this compound is shown in Figure 2-19.

### III.D. $Rb^+(21C7)Na^-$ and Five Other Sodides

It took several attempts to get single crystals of  $Rb^+(21C7)Na^-$  for single crystal X-ray structure determination. Methylamine and diethyl ether were used as the solvents. Crystals were grown by the temperature-scanning technique with a scan range set from -45°C to -70°C. The crystals are golden in color.

The single crystal used for X-ray study had the approximate dimensions of  $0.15 \times 0.30 \times 0.40\text{ mm}^3$ . The unit cell parameters and

orientation matrix were determined by least squares from the setting angles of 44 reflections in the range of  $4^{\circ} < 2\theta < 20^{\circ}$ . The space group of the crystal is monoclinic C2/c and the cell parameters are  $a=16.832(4)$ ,  $b=15.205(4)$ ,  $c=25.362(5)$ , and  $\beta=91.262(16)^{\circ}$  with cell volume of  $6489.2(2.6)\text{\AA}^3$ . The crystal was kept at  $-80^{\circ}\text{C}$  throughout the entire data collection. Intensity data were collected by using the  $\theta$ - $2\theta$  scan method at  $4^{\circ}/\text{min.}$ (in  $2\theta$ ) with minimum  $2\theta=3.5^{\circ}$  and maximum  $2\theta=45^{\circ}$ . A linear decay correction was based on the intensities of three standard reflections measured for every 150 reflections. The number of reflections measured was 9434 and the number of reflections used in refinement was 2404 with a data cut-off of  $I > 3 \text{ sigma}(\sigma)$ . Direct methods with the Texsan Program was used in the attempt to solve the crystal structure. Unfortunately, the complete crystal structure could not be solved in this case, probably because of the disorder problem.

No crystalline sodide could be made with  $\text{Cs}^+(\text{dicyclohexano-30C10})$ . This compound appeared to be an amorphous material in the solid state at temperatures below  $-30^{\circ}\text{C}$ . At higher temperature, it became a sticky blue-brown liquid and could even flow inside the K-cell. When it was cooled to below  $-30^{\circ}\text{C}$ , a brown solid was formed again. After this attempt, four more sodides were made with  $\text{Rb}^+$  and  $\text{Cs}^+(\text{dicyclohexano-24C4})$  and  $\text{K}^+$  and  $\text{Rb}^+(\text{dicyclohexano-30C10})$  in order to obtain a more systematic idea about these large crown ether complexes. Methylamine and diethyl ether were used as solvents for synthesis. As with the sodide of  $\text{Cs}^+(\text{dicyclohexano-30C10})$ ,  $\text{K}^+$  and  $\text{Rb}^+(\text{dicyclohexano-30C10})$  sodides are amorphous-like solid compounds at low temperature and sticky liquids at higher

temperature. The two other sodides made with  $\text{Rb}^+(\text{dicyclohexano-24C8})$  and  $\text{Cs}^+(\text{dicyclohexano-24C8})$  seem to be very 'soft' solids and could become very sticky liquid-like compounds at higher temperature, but DSC studies show that both of them undergo irreversible transitions at  $-7^\circ\text{C}$  and  $-9^\circ\text{C}$  respectively, and no melting processes were observed up to the decomposition temperature. The DSC results of all six sodides are summarized in Table 2-5.

Attempts to crystallize these compounds failed, probably because they are too 'soft' and disordered because of the flexible nature of the large crown ethers. It seems that the larger the crown ether, the more flexible it is. Consequently, the alkalide made with it will be 'softer'.

Since no crystal structures were obtained for these six sodides, methylamine tests were performed to determine if solvent molecules were present in the complexes. The testing method has been described in detail elsewhere[49]. The testing results indicated that methylamine was not present in any one of the six complexes.  $^{23}\text{Na}$  solid state NMR experiments showed that all six compounds are sodides with  $^{23}\text{Na}$  NMR peaks at about  $-60\text{ppm}$ .  $^{133}\text{Cs}$  solid state NMR spectra of the sodides of  $\text{Cs}^+(\text{dicyclohexano-24C8})$  and  $\text{Cs}^+(\text{dicyclohexano-30C10})$  are shown in Figure 2-20. and their  $^{133}\text{Cs}$  chemical shift values are summarized in Table 2-6. The wide range of chemical shift values of these  $\text{Cs}^+$ -large crown ether complexes is indicative of differences in their  $\text{Cs-O}$  coordination numbers and distances.

Table 2-5. Summary of thermal processes that occur in the DSC traces with a heating rate of 5°C/min. in °C.

Compound	M.P. or Phase Change	Decomposition Temperature
$(K^+)_2(21C7)_3(MeNH_2)(Na^-)_2$	--	65
$Rb^+(21C7)Na^-$	--	87
$(Cs^+)_2(21C7)_2(Na^-)_2$	68	120
$K^+(Di-24C8)Na^-$	-5	55
$Rb^+(Di-24C8)Na^-$	-7	54
$Cs^+(Di-24C8)Na^-$	-9	60
$K^+(Di-30C10)Na^-$	-25	65
$Rb^+(Di-30C10)Na^-$	-28	70
$Cs^+(Di-30C10)Na^-$	-30	67

Table 2-6.  $^{133}Cs$  NMR chemical shifts of the complexed cations in three sodides.

compound	Chemical shift(ppm)
$(Cs^+)_2(21C7)_2(Na^-)_2$	+60, -28
$Cs^+(Di-24C8)Na^-$	-83
$Cs^+(Di-30C10)Na^-$	-174

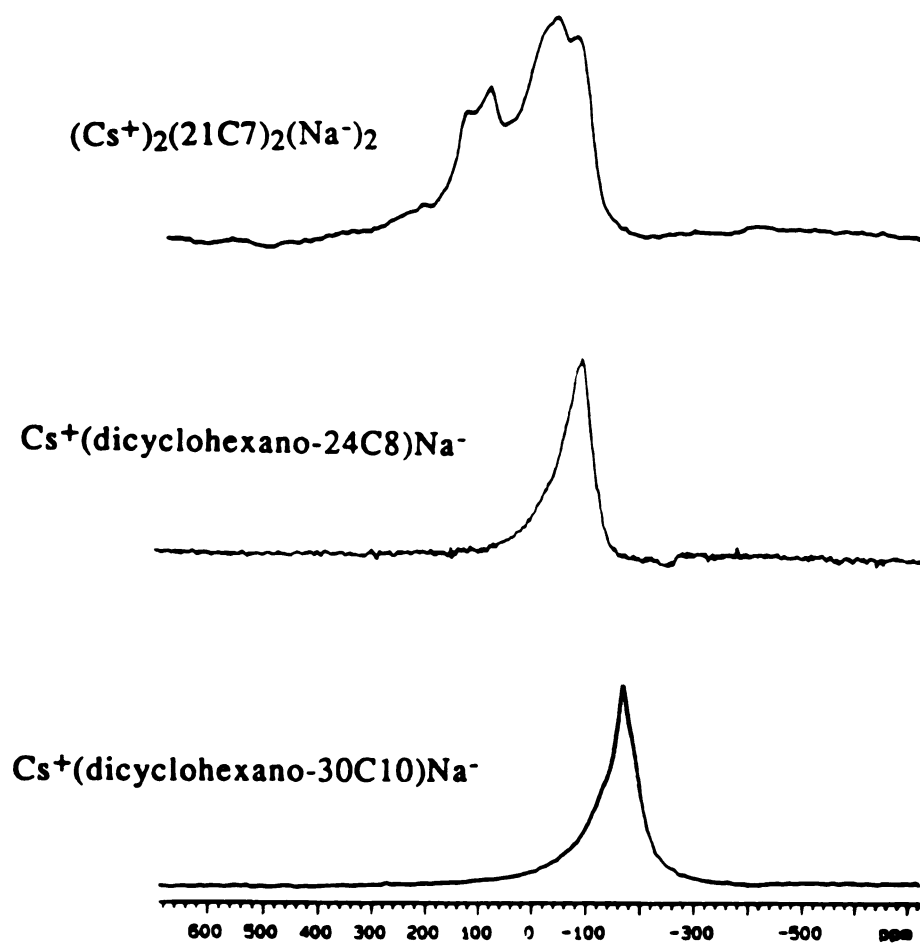


Figure 2-20.  $^{133}\text{Cs}$  static NMR spectra of three alkalides.

### III.E. $\text{Rb}^+(18\text{C}6)(12\text{C}4)\text{Na}^-$ and $\text{Rb}^+(18\text{C}6)(12\text{C}4)\text{Rb}^-$

The synthesis of these two mixed sandwich complexes followed the same procedures used for the synthesis of normal sandwich compounds[4-5], but 18-crown-6 and 12-crown-4 were used in a 1:1 molar ratio. The K-cell used for the synthesis had to be cooled during evacuation to prevent loss of the more volatile 12-crown-4.

$\text{Rb}^+(18\text{C}6)(12\text{C}4)\text{Na}^-$  can be synthesized with the solvent combination of dimethyl ether or methylamine together with either diethyl ether or trimethylamine. Beautiful prism-shaped crystals were obtained with dimethyl ether and diethyl ether as solvents. The temperature scan range was set from  $-35^\circ\text{C}$  to  $-70^\circ\text{C}$  to grow crystals by using temperature-scanning method at a scan rate of  $1^\circ\text{C}/\text{hour}$ . The crystals are bright green in color. A very difficult problem of disorder was encountered during the refinement when crystals grown with dimethyl ether as first solvent were used for the single crystal X-ray diffraction studies. In order to obtain better quality crystals, methylamine was used instead of dimethyl ether. Large size crystals with approximate dimensions of  $5 \times 5 \times 5 \text{ mm}^3$  or larger could be obtained with methylamine and diethyl ether as solvents and by using the temperature-scanning method with a scan range from  $-35^\circ\text{C}$  to  $-70^\circ\text{C}$ . The temperature scan range was set from  $-45^\circ\text{C}$  to  $-63^\circ\text{C}$  to grow smaller size crystals for the single crystal X-ray diffraction studies. The crystals appeared to be rod-shaped and green in color when methylamine was used as first solvent. The single crystal X-ray diffraction studies proved methylamine to be

indeed a better solvent for growing better quality crystals of  $\text{Rb}^+(\text{18C6})(\text{12C4})\text{Na}^-$ .

The single crystal used for X-ray diffraction study of  $\text{Rb}^+(\text{18C6})(\text{12C4})\text{Na}^-$  had the dimensions of  $0.4 \times 0.4 \times 0.5 \text{ mm}^3$ . The unit cell parameters and orientation matrix were determined by least squares from the setting angles of 34 reflections in the range of  $3.5^\circ < 2\theta < 22^\circ$ . The space group of the crystal is orthorhombic  $\text{Pnma}$  with  $Z=4$  and the cell parameters are  $a=13.989(5)$ ,  $b=13.677(14)$ , and  $c=16.683(5)$ . These yield a calculated cell volume of  $3191.9(5.4) \text{ \AA}^3$ . The crystal was kept at  $-90^\circ\text{C}$  throughout the entire data collection. Intensity data were collected by using the  $\theta$ - $2\theta$  scan method at  $4^\circ/\text{min. (in } 2\theta)$  with minimum  $2\theta=3.5^\circ$  and maximum  $2\theta=45^\circ$ . A linear decay correction was based on the intensities of three standard reflections measured for every 200 reflections. The number of reflections measured was 9170 and the number of reflections used in refinement was 2060 with a data cut-off of  $I > 3 \text{ sigma}(\sigma)$ . The crystal structure was solved by using direct methods with the Texsan Program. Hydrogen atoms were constrained to ride on their bonded C-atoms with fixed isotropic thermal parameters. The R factors were  $R=0.072$  and  $R_w=0.050$  with R defined as  $(\sum ||F_o| - |F_c||) / \sum |F_o|$ . Peak heights in the final difference map ranged from  $-0.67$  to  $0.66 \text{ e/\AA}^3$ . The molecular structure and numbering of the atoms are shown in Figure 2-21 and the stereo packing diagram is shown in Figure 2-22. A summary of crystallographic data for  $\text{Rb}^+(\text{18C6})(\text{12C4})\text{Na}^-$  is given in Table 2-7. The positional parameters, bond distances, and bond angles are given in Tables A-10, A-11, and A-12 in Appendix A.

The carbon atoms on 12-crown-4 were found to have large temperature factors during the refinement. It was caused primarily by the apparent mirror symmetry of the space group, Pnma. The 12-crown-4 molecule does not usually possess mirror symmetry. The oxygen atoms of the 12-crown-4 molecule were refined well with normal temperature factors, indicating that they are well described by the mirror symmetry. But the carbon atoms of the 12-crown-4 must be divided into two configurations which are mirror images of each other. Therefore, these carbon atoms were refined isotropically with disorder, resulting in much lower temperature factors. The  $\text{Rb}^+$  cation is  $1.24\text{\AA}$  out of the least-squares plane of the six oxygen atoms of 18-crown-6 and  $2.30\text{\AA}$  out of the plane of the four oxygen atoms of 12-crown-4. The  $\text{Rb}^+\text{-O}$  distances range from  $2.969(9)$  to  $3.101(8)\text{\AA}$  with an average distance of  $3.038\text{\AA}$  for the oxygen atoms of the 18-crown-6 and are  $2.988(6)$  and  $3.128(7)\text{\AA}$  with an average distance of  $3.058\text{\AA}$  for the oxygen atoms of the 12-crown-4. The shortest  $\text{Na}^+\text{-Na}^+$  and  $\text{Na}^+\text{-Rb}^+$  distances in the crystal are  $7.891(7)$  and  $7.960(7)\text{\AA}$  respectively, indicating that  $\text{Na}^+$  is well isolated from other  $\text{Na}^+$  anions and  $\text{Rb}^+$  cations. The bond distances and angles for the atoms of 18-crown-6 are well within the normal values, but those of 12-crown-4 deviate substantially from normal, probably due to the disorder. In contrast to those of the 18-crown-6 configuration, in which the oxygen and carbon atoms alternate on both sides of the least-squares plane of the six oxygen atoms, the carbon atoms of 12-crown-4 are all on one side of the plane of the four oxygen atoms, away from the  $\text{Rb}^+$ .

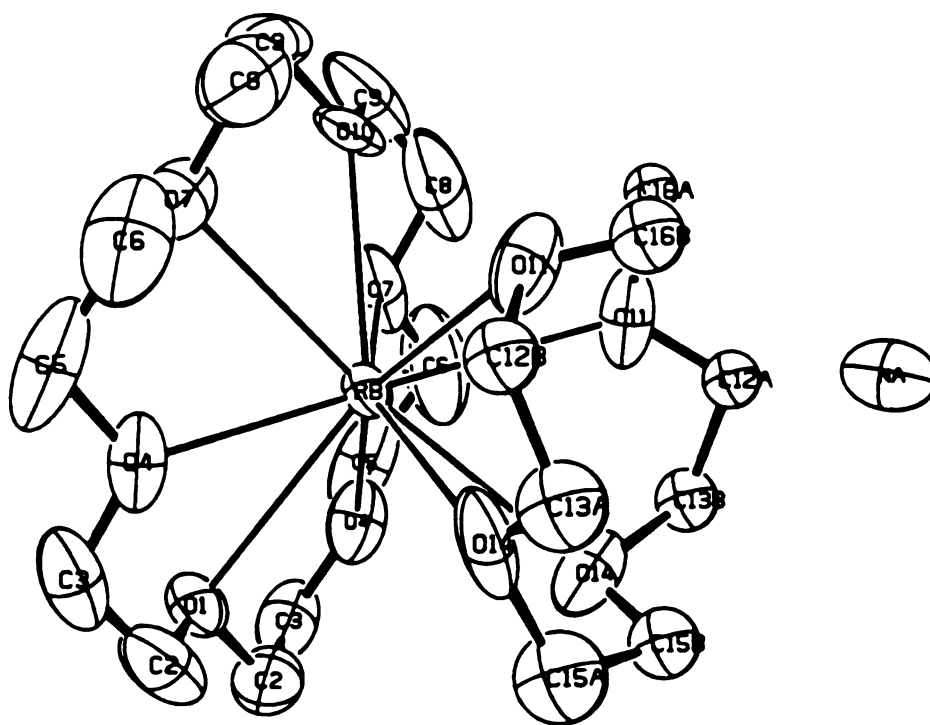


Figure 2-21. The molecular structure and the numbering of atoms in  $\text{Rb}^+(18\text{C}6)(12\text{C}4)\text{Na}^-$ .

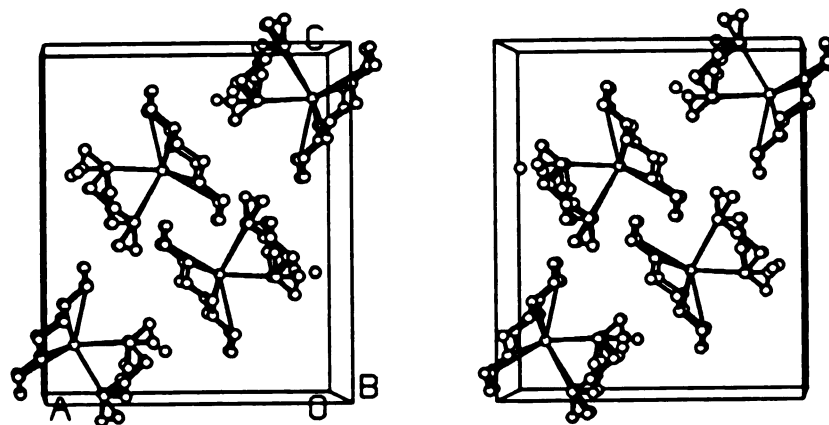


Figure 2-22. Stereo packing diagram of  $\text{Rb}^+(18\text{C}6)(12\text{C}4)\text{Na}^-$ .

Table 2-7. Summary of Crystallographic Data for  
 $\text{Rb}^+(18\text{C}6)(12\text{C}4)\text{Na}^-$ -(I) and  $\text{Rb}^+(18\text{C}6)(12\text{C}4)\text{Rb}^-$ -(II)

	I	II
Space Group	Orthorhombic Pnma	Orthorhombic Pnma
Cell Parameters		
a(Å)	13.989(5)	14.063(10)
b(Å)	13.677(14)	14.167(10)
c(Å)	16.683(5)	17.030(10)
Volume(Å <sup>3</sup> )	3191.9(5.4)	3392.9(6.6)
Z	4	4
R	0.072	0.059
R <sub>w</sub>	0.050	0.031
d	1.142g/cm <sup>3</sup>	1.197g/cm <sup>3</sup>

Dimethyl ether and diethyl ether were used for the synthesis and crystal growth of  $\text{Rb}^+(18\text{C}6)(12\text{C}4)\text{Rb}^-$ . Crystals were grown by the temperature-scanning method with a scan range from  $-35^\circ\text{C}$  to  $-70^\circ\text{C}$  at a scan rate of  $1^\circ\text{C}/\text{hour}$ . The crystals appeared to be rod-shaped and golden in color.

The single crystal used for the X-ray diffraction study of  $\text{Rb}^+(18\text{C}6)(12\text{C}4)\text{Rb}^-$  had the approximate dimensions of  $0.3 \times 0.4 \times 0.5 \text{ mm}^3$ . The unit cell parameters and orientation matrix were determined by least squares from the setting angles of 20 reflections in the range of  $3.5^\circ < 2\theta < 22^\circ$ . The space group of the crystal is orthorhombic  $\text{Pnma}$  with  $Z=4$  and the cell parameters are  $a=14.063(10)$ ,  $b=14.167(10)$ , and  $c=17.030(10)$ . These yield a calculated cell volume of  $3392.9(6.6)\text{\AA}^3$ . The crystal was kept at  $-90^\circ\text{C}$  throughout the entire data collection. Intensity data were collected by using the  $\theta$ - $2\theta$  scan method at  $4^\circ/\text{min.}$ (in  $2\theta$ ) with minimum  $2\theta=3.5^\circ$  and maximum  $2\theta=45^\circ$ . A linear decay correction was based on the intensities of three standard reflections measured for every 150 reflections. The number of reflections measured was 3471 and the number of reflections used in refinement was 1135 with a data cut-off of  $I > 3 \text{ sigma}(\sigma)$ . The crystal structure was solved by using direct methods with the Texsan Program. Hydrogen atoms were constrained to ride on their bonded C-atoms with fixed isotropic thermal parameters. The R factors were  $R=0.059$  and  $R_w=0.031$  with R defined as  $(\sum ||F_o| - |F_c||) / \sum |F_o|$ . Peak heights in the final difference map ranged from  $-0.47$  to  $0.47 \text{ e/\AA}^3$ . The molecular structure and numbering of the atoms are shown in Figure 2-23 and the stereo packing diagram is shown in Figure 2-24. The positional

parameters, bond distances, and bond angles are given in Tables A-13, A-11, and A-12 in Appendix A.

This mixed sandwich compound,  $\text{Rb}^+(\text{18C6})(\text{12C4})\text{Rb}^-$ , is isostructural with  $\text{Rb}^+(\text{18C6})(\text{12C4})\text{Na}^-$ . Again the refinement was performed with disorder of the carbon atoms of 12-crown-4 and they were refined isotropically. The location and coordination of the complexed  $\text{Rb}^+$  cation in this compound is very similar to that in  $\text{Rb}^+(\text{18C6})(\text{12C4})\text{Na}^-$ . The  $\text{Rb}^+$  cation is 1.20 Å out of the 18-crown-6 oxygen plane and 2.30 Å out of the plane of the 12-crown-4 oxygen atoms, with oxygen and carbon atoms of the 18-crown-6 ring alternately above and below the plane. All carbons of 12-crown-4 are on one side of the plane of the four oxygen atoms, staying away from the  $\text{Rb}^+$  cation. The  $\text{Rb}^+\text{-O}$  distances range from 2.98(2) to 3.08(1) Å with an average distance of 3.03 Å for the oxygen atoms of the 18-crown-6 and are 2.964(7) and 3.155(9) Å with an average distance of 3.060 Å for the oxygen atoms of the 12-crown-4. The shortest  $\text{Rb}^+\text{-Rb}^+$  and  $\text{Rb}^+\text{-Rb}^-$  distances in the crystal are 7.843(5) and 8.166(5) Å respectively, indicating that  $\text{Rb}^+$  is well isolated from other  $\text{Rb}^+$  anions and  $\text{Rb}^+$  cations. The bond distances and angles for atoms of 18-crown-6 are well within the normal values, but those of 12-crown-4 deviate substantially from normal.

These two compounds were synthesized and characterized following the synthesis of the  $\text{Cs-18C6-15C5}$  and  $\text{K-18C6-12C4}$  systems.  $\text{Rb}^+(\text{18C6})(\text{12C4})\text{Na}^-$  is thermodynamically more stable than its 'parent' compounds,  $\text{Rb}^+(\text{12C4})_2\text{Na}^-$  and  $\text{Rb}^+(\text{18C6})\text{Na}^-(\text{MeNH}_2)$ .  $\text{Rb}^+(\text{12C4})_2\text{Na}^-$  hardly exists in solid state and easily decomplexes in solution at higher temperature. In fact, several attempts to

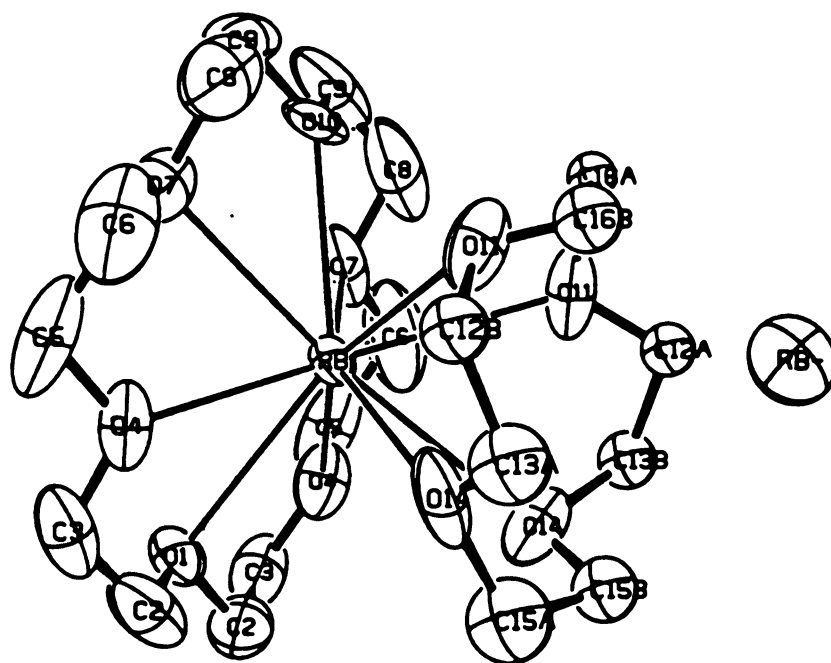


**Figure 2-23.** The molecular structure and the numbering of atoms in  $\text{Rb}^+(18\text{C}6)(12\text{C}4)\text{Rb}^-$ .

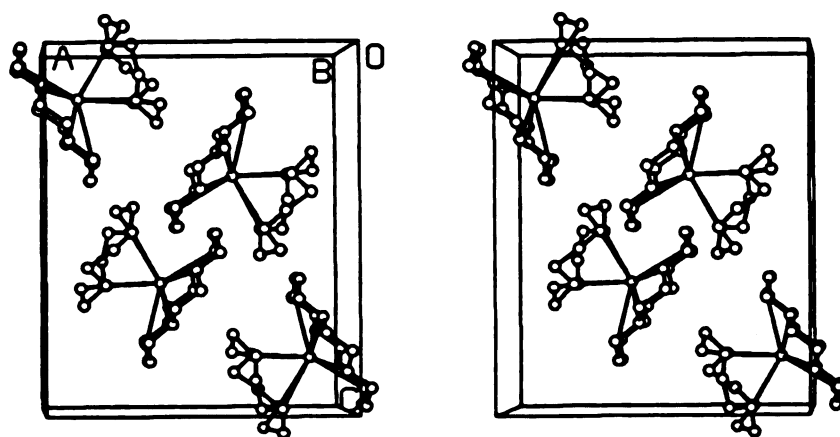


Figure 2-24. Stereo packing diagram of  $\text{Rb}^+(18\text{C}6)(12\text{C}4)\text{Rb}^-$ .

crystallize  $\text{Rb}^+(\text{12C4})_2\text{Na}^-$  failed, simply because it is very unstable when the solvent is removed. Another 'parent' compound,  $\text{Rb}^+(\text{18C6})\text{Na}^-(\text{MeNH}_2)$ , crystallizes with a solvent molecule,  $\text{MeNH}_2$ , on one side of the 18-crown-6, while the  $\text{Rb}^+$  cation sits in the cavity of the 18-crown-6.  $\text{Na}^-$  anion also forms cation-anion ion pairs with  $\text{Rb}^+$  on the same side as the solvent molecule is. Apparently, the solvent molecule and cation-anion ion pair formation are necessary in the crystal in order to stabilize the complexed  $\text{Rb}^+(\text{18C6})$  cation. Examples of the sandwich complexed ion  $\text{Rb}^+(\text{18C6})_2$  are not known. By contrast, the mixed sandwich complex  $\text{Rb}^+(\text{18C6})(\text{12C4})\text{Na}^-$  is well coordinated by the 18-crown-6 and 12-crown-4 molecules. The  $\text{Rb}^+$  ion resides in the cavity formed between the 18-crown-6 and 12-crown-4. No solvent molecule or cation-anion ion pair is needed for coordination.

$\text{Rb}^+(\text{18C6})(\text{12C4})\text{Rb}^-$  is isostructural with  $\text{Rb}^+(\text{18C6})(\text{12C4})\text{Na}^-$ . One of its 'parent' compounds,  $\text{Rb}^+(\text{18C6})\text{Rb}^-$  has cation-anion ion pairs to better coordinate the  $\text{Rb}^+$  while the other 'parent' compound,  $\text{Rb}^+(\text{12C4})_2\text{Rb}^-$ , has not been synthesized.

Two features of these two mixed sandwich complexes increase the interest in their study. First, is the pronounced green color of  $\text{Rb}^+(\text{18C6})(\text{12C4})\text{Na}^-$  which prompted the study of its optical spectrum. Second, solid state  $^{87}\text{Rb}$  NMR spectra of the two compounds showed that the NMR line shapes of the  $\text{Rb}^+$  cations in both compounds are very similar and their line widths are very narrow compared to those of other  $\text{Rb}^+$  alkalides. The  $^{23}\text{Na}$  NMR spectrum of  $\text{Rb}^+(\text{18C6})(\text{12C4})\text{Na}^-$  is shown in Figure 2-25. This spectrum has a single  $^{23}\text{Na}$  NMR peak at -61.24ppm, indicating that

i  
c  
s  
w  
c  
R  
v  
a  
p  
c  
s  
to  
R  
o  
st  
b  
er  
or  
N  
in  
al  
Fi  
pa  
te  
ca  
qu  
nu

it is indeed a sodide although this compound appeared to be green in color. Figure 2-26 shows the  $^{87}\text{Rb}$  NMR spectra obtained by the solid state spin-echo technique for both compounds. The half-height line width is less than 200ppm for  $\text{Rb}^+$  in both mixed sandwich compounds in contrast to values of about 1000ppm for  $\text{Rb}^+$  cations in  $\text{Rb}^+(\text{18C6})\text{Na}^-(\text{MeNH}_2)$  and  $\text{Rb}^+(\text{18C6})\text{Rb}^-$ [49]. The chemical shift value of  $\text{Rb}^-$  in  $\text{Rb}^+(\text{18C6})(\text{12C4})\text{Rb}^-$  is -203ppm, a typical value for an isolated  $\text{Rb}^-$  in alkalides, while that of  $\text{Rb}^-$  in  $\text{Rb}^+(\text{18C6})\text{Rb}^-$  is paramagnetically shifted about 70ppm. It was suggested that  $\text{Rb}^+$  cations in  $\text{Rb}^+(\text{18C6})\text{Rb}^-$  or  $\text{Rb}^+(\text{18C6})\text{Na}^-(\text{MeNH}_2)$  are in a very non-symmetric environment, and are strongly coupled to  $\text{Rb}^-$  or  $\text{Na}^-$  due to the cation-anion ion pairs. In addition, the paramagnetic shift of  $\text{Rb}^-$  in  $\text{Rb}^+(\text{18C6})\text{Rb}^-$  was suggested to be caused by some degree of overlap of the p and d orbitals on the anion with its surroundings[49]. By contrast to these compounds,  $\text{Rb}^+$  cations in both mixed sandwich compounds sit in a more symmetric environment and cations and anions are well isolated from each other so that the dominant second order quadrupolar broadened NMR lines of  $\text{Rb}^+$  are quite narrow and NMR peaks of the anions are in the typical chemical shift value ranges for the  $\text{Rb}^-$  and  $\text{Na}^-$  in alkalides. It is interesting to see that the NMR line shapes, shown in Figure 2-27 and Figure 2-28, of  $\text{Rb}^+$  in both compounds show a pattern of decreasing asymmetry parameter,  $\eta$ , with increasing temperature, indicating an approach to axial symmetry. This pattern can be compared to the computer simulated static second order quadrupolar line shapes for the central transition of a quadrupolar nucleus in Figure 2-29[9]. The line shape change with temperature

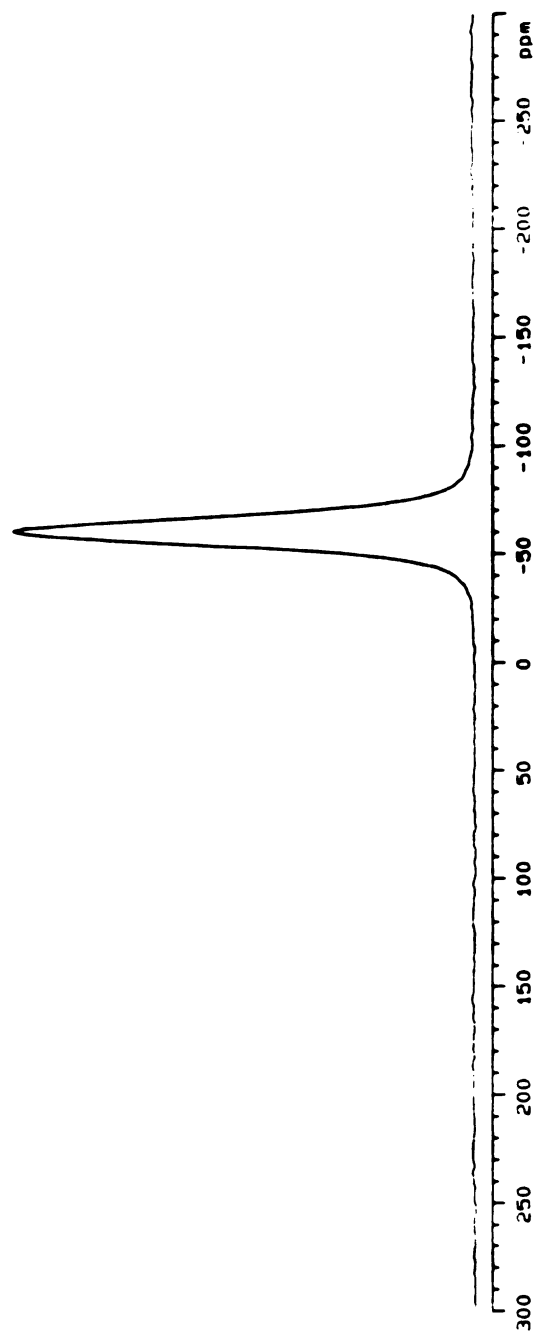


Figure 2-25.  $^{23}\text{Na}$  static NMR spectrum of  $\text{Rb}^+(18\text{C}6)(12\text{C}4)\text{Na}^-$  at  $-60^\circ\text{C}$ .

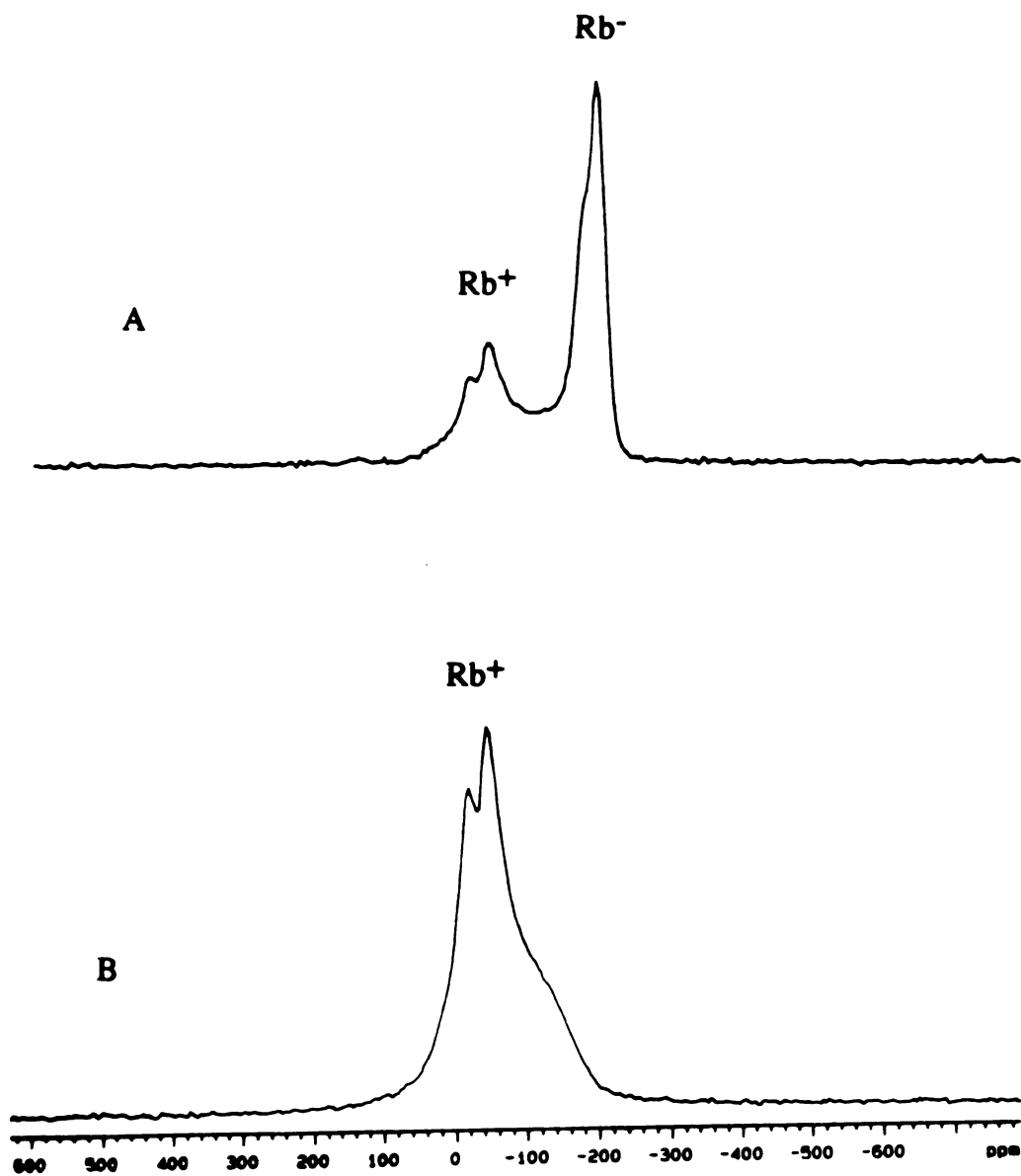
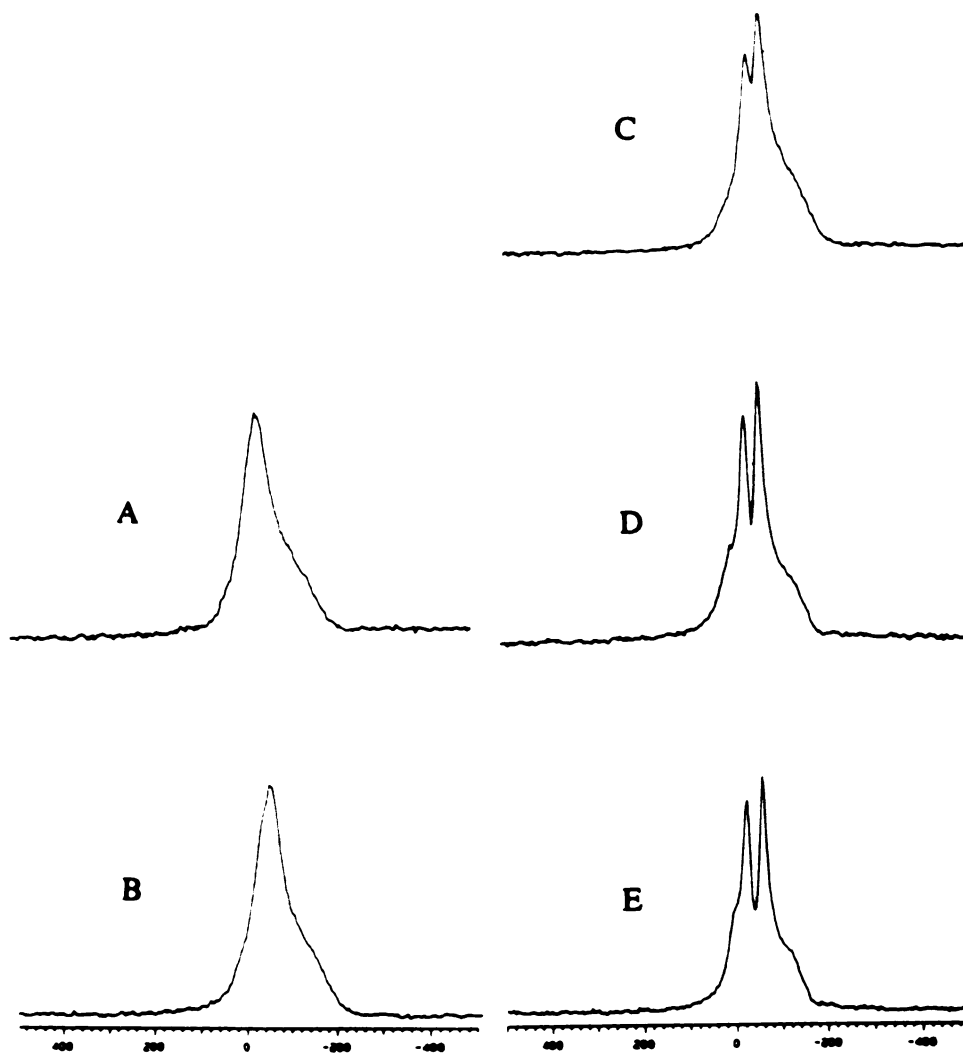


Figure 2-26.  $^{87}\text{Rb}$  NMR spectra of A)  $\text{Rb}^+(18\text{C}6)(12\text{C}4)\text{Rb}^-$  and B)  $\text{Rb}^+(18\text{C}6)(12\text{C}4)\text{Na}^-$ , obtained with a solid state spin-echo pulse sequence. Note that NMR peaks for both  $\text{Rb}^+$  and  $\text{Rb}^-$  in  $\text{Rb}^+(18\text{C}6)(12\text{C}4)\text{Rb}^-$  were observed.

s  
v  
i  
t  
a  
c  
e  
  
F  
3  
F  
f  
R  
r  
s  
R  
g  
th  
c  
R  
a  
w  
ra  
as  
N  
se  
C

suggests that as the temperature increases, thermal motion of vibration or even hopping[61] of the crown ethers which are locked in position at low temperature in the crystal also increases. The thermal motion is eventually so fast at higher temperature that the asymmetry parameter is reduced greatly, indicating that the  $\text{Rb}^+$  cations are approaching a thermally-averaged axially-symmetric environment.

The optical absorption spectra of solvent-evaporated films of  $\text{Rb}^+(\text{18C6})(\text{12C4})\text{Na}^-$  and  $\text{Rb}^+(\text{18C6})(\text{12C4})\text{Rb}^-$  are shown in Figure 2-30 and Figure 2-31. In general,  $\text{Na}^-$  in sodides has a single absorption peak at 640nm which is attributed to the electron transition of  $\text{Na}^-$  from  $3s^2$  to  $3s3p$ . By contrast, the absorption spectrum of  $\text{Rb}^+(\text{18C6})(\text{12C4})\text{Na}^-$  shows two peaks, at 550nm and 780nm respectively, one red-shifted by about 140nm and the other blue shifted by 90nm from the usual position. These spectra explain why  $\text{Rb}^+(\text{18C6})(\text{12C4})\text{Na}^-$  has a beautiful green color while other sodides generally are shiny brown, golden or reddish in color. The origin of these shifts is not known. It should be noted that the similar compound,  $\text{K}^+(\text{18C6})(\text{12C4})\text{Na}^-$ , which is isostructural with  $\text{Rb}^+(\text{18C6})(\text{12C4})\text{Na}^-$ , is also green in color and has a similar optical absorption spectrum[62]. Another compound,  $\text{Cs}^+(\text{18C6})(\text{12C4})\text{Na}^-$  which can be synthesized in  $\text{MeNH}_2$  solvent with exact 1:1 molar ratio of 18-crown-6 to 12-crown-4, also appears to be green in color as a 'wet' film, but it decomplexes when the solvent is removed. Nevertheless, sodides made with  $\text{M-18C6-12C4}$  ( $\text{M}=\text{Cs}^+$ ,  $\text{Rb}^+$ , and  $\text{K}^+$ ) seem to be green in color, while their 'parent' compounds,  $\text{Cs}^+(\text{18C6})_2\text{Na}^-$ ,  $\text{Rb}^+(\text{18C6})\text{Na}^-(\text{MeNH}_2)$ , and  $\text{K}^+(\text{18C6})\text{Na}^-(\text{MeNH}_2)_2$  or



**Figure 2-27.** Temperature dependence of the NMR line shapes of the  $\text{Rb}^+$  ions in  $\text{Rb}^+(\text{18C6})(\text{12C4})\text{Na}^-$ . A)  $-100^\circ\text{C}$ ; B)  $-80^\circ\text{C}$ ; C)  $-60^\circ\text{C}$ ; D)  $-40^\circ\text{C}$ ; and E)  $-20^\circ\text{C}$ .

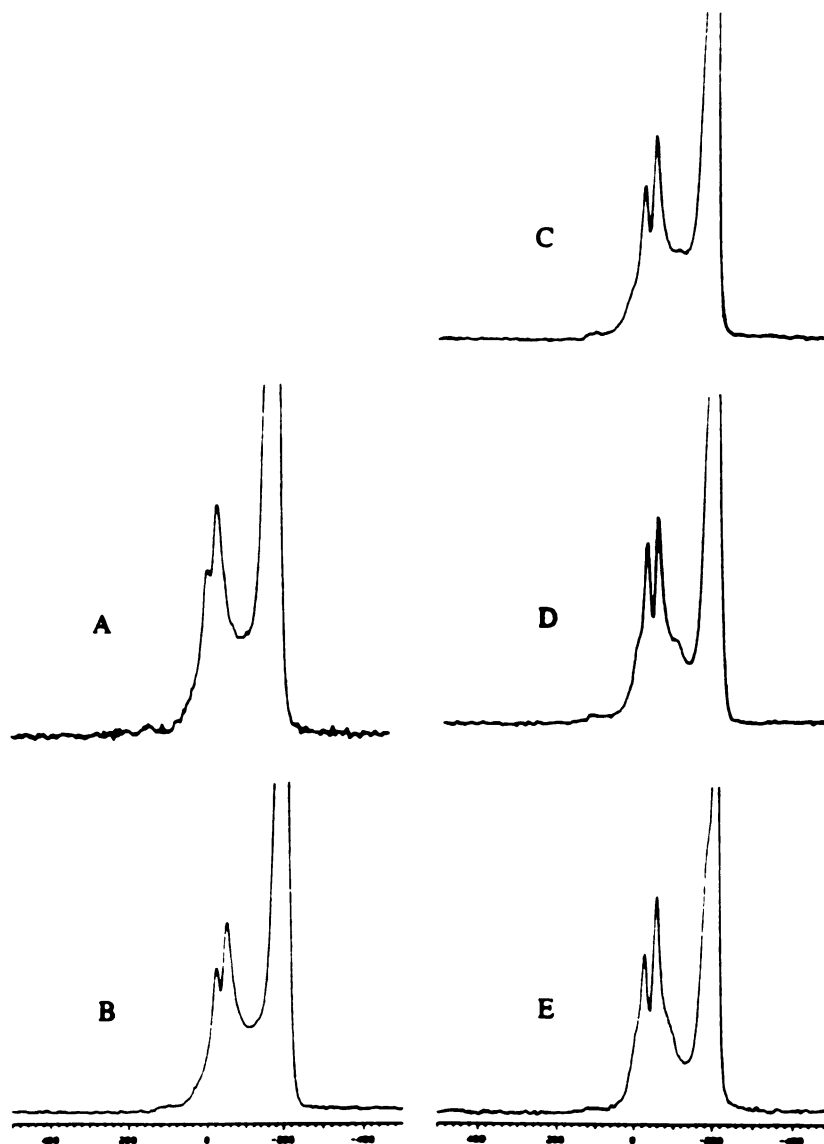


**Figure 2-28.** Temperature dependence of the NMR line shapes of the  $\text{Rb}^+$  ions in  $\text{Rb}^+(\text{18C6})(\text{12C4})\text{Rb}^-$ . A)  $-100^\circ\text{C}$ ; B)  $-80^\circ\text{C}$ ; C)  $-60^\circ\text{C}$ ; D)  $-40^\circ\text{C}$ ; and E)  $-20^\circ\text{C}$ .

Fi

lin

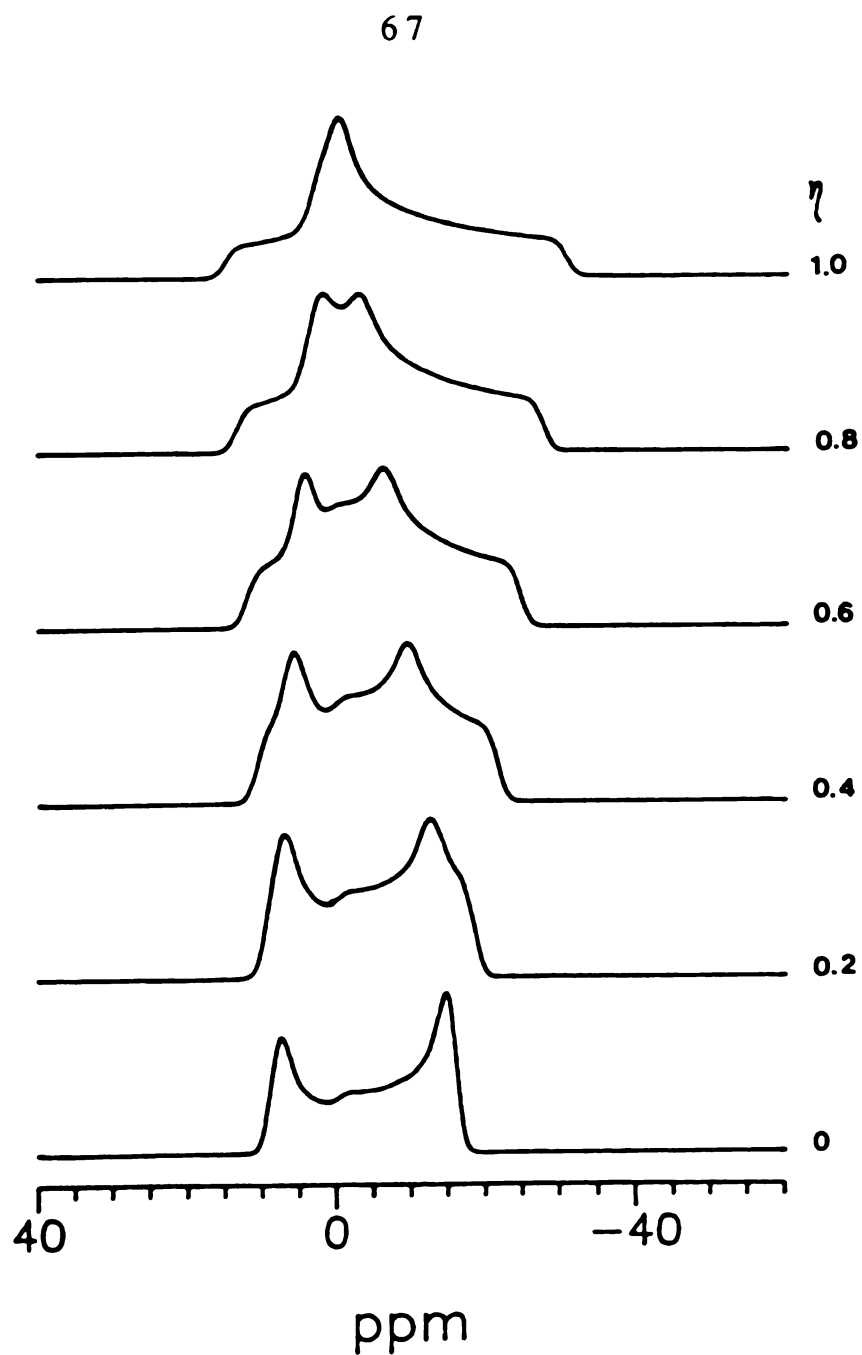


**Figure 2-29. Computer simulated static second order quadrupolar line shapes for the central transition of a quadrupolar nucleus.**

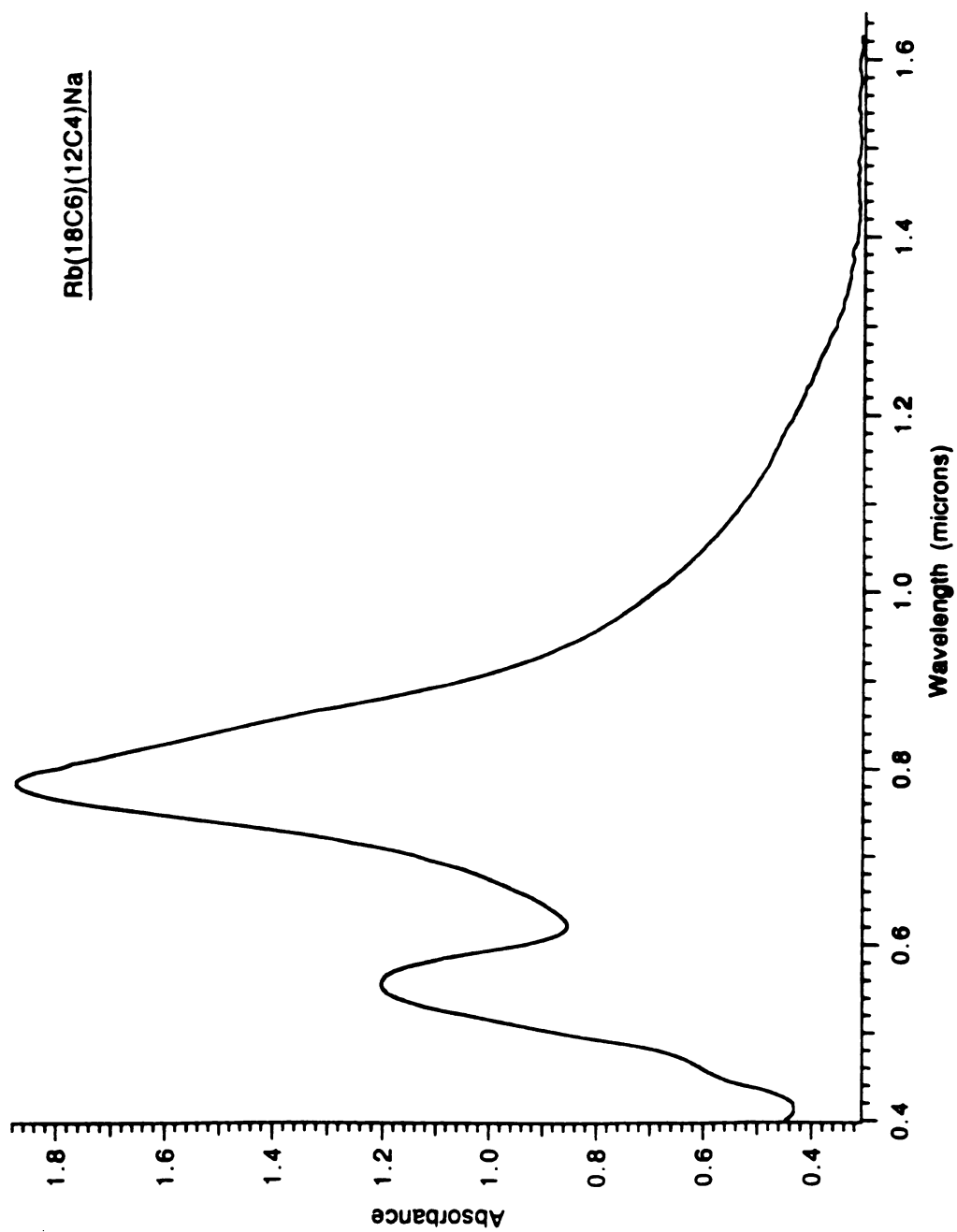


Figure 2-30. Optical absorption spectrum of a thin film of  $\text{Rb}^+(18\text{C}6)(12\text{C}4)\text{Na}^-$  at  $-60^\circ\text{C}$ , prepared by rapid evaporation of the methylamine solvent.

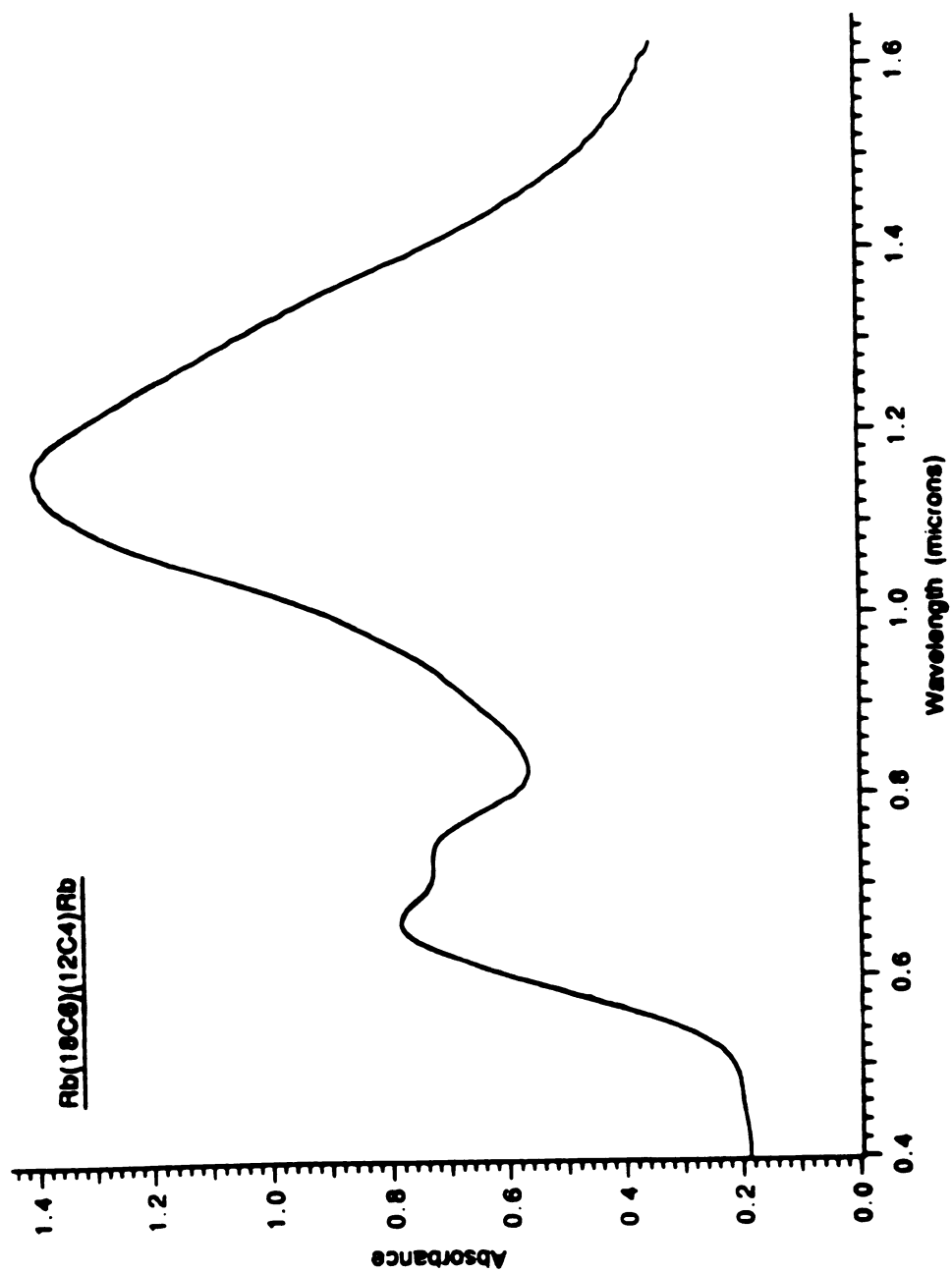


Figure 2-31. Optical absorption spectrum of a thin film of  $\text{Rb}^+(\text{18C6})(\text{12C4})\text{Rb}^-$  at  $-60^\circ\text{C}$ , prepared by rapid evaporation of the methyllamine solvent.

another mixed sandwich compound  $\text{Cs}^+(18\text{C}6)(15\text{C}5)\text{Na}^-$  are reddish or golden in color. The optical absorption spectrum of  $\text{Rb}^+(18\text{C}6)(12\text{C}4)\text{Rb}^-$  has three absorption peaks at 660, 750, and 1150nm respectively. It is, however, unclear what causes these absorption peaks.

o  
2  
f  
th  
e  
c  
h  
sa  
fo  
in

## CHAPTER 3. SOLUTION NMR STUDIES OF COMPLEXED Cs<sup>+</sup> IONS WITH MIXED CROWN ETHERS

### I. Introduction

Since the macrocyclic crown ethers are capable of forming stable and selective complexes with alkali and alkaline earth metal ions[56], the studies of these complexants and their complexes have become an important research area in science. During the past two decades, one of the most exciting results from the studies of crown ethers is the discovery of two new classes of compounds, the alkalides and electrides. In addition, intensive efforts have been undertaken to understand the factors that control the thermodynamic and kinetic stability and the selectivity of these complexes[63-66].

One of the interesting features of crown ethers, as two dimensional macrocyclic complexants, is their ability to form 2:1(complexant to metal) sandwich complexes. Evidence for the formation of such sandwich complexes both in solution[67-69] and in the solid state[70-71] has been reported. Recently, five alkalides, one electride, and one model salt with mixed crown ethers as complexants have been synthesized, and their crystal structures have been determined[32]. After the discovery of these mixed sandwich compounds, it was of interest to study the possibility of the formation of such mixed sandwich complexes with alkali metal ions in solution. It was also of interest to study the stability of the mixed

o  
h  
c  
i  
e  
u  
w  
fr  
el

sandwich complexes and their 'parent' compounds in solution. Information on the relative stabilities of these complexes may be useful as a guideline for the synthesis of other mixed sandwich alkalides and electrides.

The use of nuclear magnetic resonance has long been popular in the studies of complexation in electrolyte solutions because of the presence of extremely rapid and generally random molecular motions. These molecular motions can result in narrow resonance lines, even for nuclei with quadrupole moments. Moreover, the resonance frequencies of metal ions are very sensitive to their chemical environment. Therefore, ion-ion, ion-complexant, and ion-solvent interactions can be easily studied by NMR techniques.

## II. Experimental

The solution NMR studies were done in collaboration with Professor Mojtaba Shamsipur during his sabbatical leave from Shiraz University, Iran.

12-crown-4, 15-crown-5, 18-crown-6, and HMHCY were obtained from Aldrich and all complexants were purified and stored in a He filled dry-box for use in the synthesis of alkalides and electrides. These complexants were removed from the dry-box and used for solution NMR studies without further purification. CsSCN was obtained from Pfaltz and Bauer and nitromethane was obtained from EM Science. They were purified and dried as described elsewhere[72-74].

$^{133}\text{Cs}$  NMR measurements were carried out on a Varian VXR-300 NMR spectrometer equipped with a variable temperature controller.

All chemical shifts were measured at  $25.0 \pm 0.1^\circ\text{C}$  and were calibrated with 0.5M CsBr in  $\text{D}_2\text{O}$  as an external reference during measurement. However, all data reported in this thesis are ultimately referenced to the infinitely dilute  $\text{Cs}^+$  ion in water at  $25^\circ\text{C}$ . The chemical shift of the  $\text{Cs}^+$  ion at infinite dilution was obtained by extrapolation of plots of the chemical shift vs. concentration. All data are also corrected for differences in bulk diamagnetic susceptibility between sample and reference according to the following equation[75]

$$\delta_{\text{corr}} = \delta_{\text{obs}} + \frac{4\pi}{3} (\chi_{\text{ref}} - \chi_{\text{sample}}) \quad (3-1)$$

where  $\chi_{\text{ref}}$  and  $\chi_{\text{sample}}$  are the volumetric susceptibility of the reference and sample solvents, respectively and  $\delta_{\text{obs}}$  and  $\delta_{\text{corr}}$  are the observed and corrected chemical shifts, respectively.

The formation constants of ion pairs and complexes were obtained by computer fitting of the experimental data using the appropriate equations and the nonlinear least-squares KINFIT program[76]. Some of the related equations and computer subroutines have been described in detail elsewhere[71, 77-78].

### III. Results and Discussion

#### III.A. The Ion-Pairing Formation Constants of Cs<sup>+</sup> Ion in Nitromethane Solvent

It should be noted that cesium salts may form ion pairs in solvents with low dielectric constants or low donor ability in concentrated solutions. The nitromethane solvent used in this study has an intermediate value of the dielectric constant(36.87) and a low value of the donor number(2.7)[79]. Naturally, it was important to determine the extent of ionic association of CsSCN in nitromethane in order to evaluate the complexation reactions of Cs<sup>+</sup> ion with crown ethers. For this purpose, the concentration dependence of the <sup>133</sup>Cs chemical shift as a function of the salt concentration was studied for Cs<sup>+</sup>SCN<sup>-</sup>, Cs<sup>+</sup>(18C6)SCN<sup>-</sup>, and Cs<sup>+</sup>(18C6)<sub>2</sub>SCN<sup>-</sup>. The results are given in Table 3-1 and shown in Figure 3-1.

The ion-pairing constants of these compounds in nitromethane were calculated based on the idea that the exchange between the free solvated cesium ion and the ion pair is fast on the NMR time scale; consequently, only one resonance signal is observed.

For CsSCN, the ion-pairing reaction which takes place in nitromethane may be represented by:



where  $K_{ip}$  is the ion pair formation constant of Cs<sup>+</sup>SCN<sup>-</sup>. The observed chemical shift is given by the expression[80],

Table 3-1.  $^{133}\text{Cs}$  Chemical Shifts of Cesium Salt Solution of  $\text{MeNO}_2$  at  $25^\circ\text{C}$ .

$\text{CsSCN}$		$\text{Cs(18C6)SCN}$		$\text{Cs(18C6)}_2\text{SCN}$	
Conc. (M)	$\delta\text{ppm}$	Conc. (M)	$\delta\text{ppm}$	Conc. (M)	$\delta\text{ppm}$
0.001	-58.27	0.001	-29.27	0.0005	-23.60
0.003	-57.05	0.002	-27.13	0.001	-21.78
0.005	-56.53	0.003	-25.61	0.002	-20.53
0.010	-54.91	0.005	-24.27	0.003	-20.18
0.020	-52.62	0.008	-23.35	0.005	-19.67
0.030	-50.91	0.010	-22.69	0.008	-19.25
0.040	-50.12	0.011	-22.31	0.010	-19.10
		0.015	-21.55	0.015	-18.83
		0.020	-20.74	0.020	-18.66
		0.030	-19.64	0.030	-18.39
		0.040	-18.81	0.040	-18.23

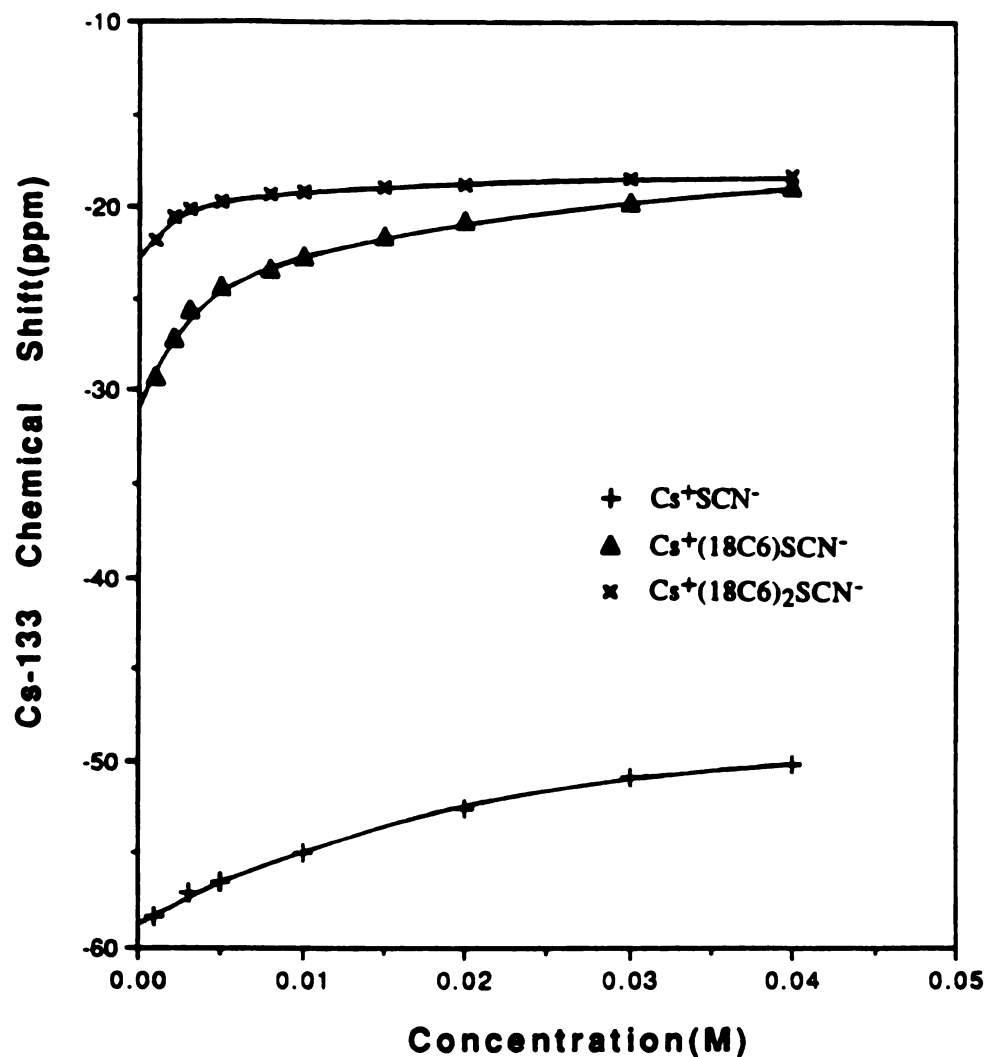


Figure 3-1. Concentration dependence of the  $^{133}\text{Cs}$  chemical shifts of cesium compounds in nitromethane at 25°C. The solid lines are least-squares plots, obtained by simultaneous multiple data set fitting of all three data sets with the KINFIT program.

$$\delta_{\text{obs}} = X_f \delta_f + X_{\text{ip}} \delta_{\text{ip}} = X_f \delta_f + (1 - X_f) \delta_{\text{ip}} \quad (3-2)$$

where  $\delta_f$  and  $\delta_{\text{ip}}$  are the chemical shifts of the free and ion-paired  $\text{Cs}^+$  ion respectively and  $X_f$  and  $X_{\text{ip}}$  are the corresponding relative mole fractions of the two cesium species. Let  $C_f^{\text{M}}$  be the concentration of the free  $\text{Cs}^+$  ion and  $C_t^{\text{M}}$  be the total concentration of  $\text{CsSCN}$ . Obviously,

$$X_f = C_f^{\text{M}}/C_t^{\text{M}} \quad (3-3)$$

Combining Equations (3-2) and (3-3), Equation (3-4) can be obtained as

$$\delta_{\text{obs}} = (C_f^{\text{M}}/C_t^{\text{M}})(\delta_f - \delta_{\text{ip}}) + \delta_{\text{ip}} \quad (3-4)$$

The ion pair formation constant is

$$\begin{aligned} K_{\text{ip}} &= K_c / \gamma_{\pm}^2 = [\text{Cs}^+ \text{SCN}^-] / [\text{Cs}^+][\text{SCN}^-] \gamma_{\pm}^2 \\ &= (C_t^{\text{M}} - C_f^{\text{M}}) / (C_f^{\text{M}})^2 \gamma_{\pm}^2 \end{aligned} \quad (3-5)$$

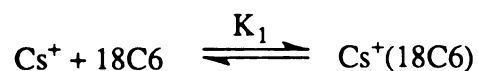
where  $K_c$  is the concentration equilibrium constant. Substituting Equation (3-5) into Equation (3-2) gives

$$\delta_{\text{obs}} = [-1 + (1 + 4K_{\text{ip}} \gamma_{\pm}^2 C_t^{\text{M}})^{1/2}] (\delta_f - \delta_{\text{ip}}) / 2K_{\text{ip}} \gamma_{\pm}^2 C_t^{\text{M}} + \delta_{\text{ip}} \quad (3-6)$$

This equation relates the observed chemical shifts to the total concentration of  $\text{CsSCN}$  salt ( $C_t^{\text{M}}$ ), the chemical shift of the free  $\text{Cs}^+$

ion( $\delta_f$ ), the chemical shift of the ion-paired  $\text{Cs}^+(\delta_{ip})$ , the mean activity coefficient  $\gamma_{\pm}$  and the ion pair formation constant  $K_{ip}$ . The values of  $C_t^M$  and  $\delta_f$  are known and the value of  $\gamma_{\pm}$  can be calculated using the Debye-Huckel Equation. The values of  $\delta_{ip}$  and  $K_{ip}$  can be obtained with the help of the non-linear least-squares curve-fitting program KINFIT. In fact,  $\delta_f$  can also be obtained by KINFIT fitting.

For  $\text{Cs}^+(18\text{C6})\text{SCN}^-$ , the reactions may be represented by:



where  $K_1$  is the formation constant of complexed  $\text{Cs}^+(18\text{C6})$  and  $K_{ip}'$  is the ion pair formation constant of  $\text{Cs}^+(18\text{C6})\text{SCN}^-$ .  $K_1$ ,  $K_{ip}$ , and  $K_{ip}'$  can be expressed as

$$K_1 = [\text{Cs}^+(18\text{C6})]/[\text{Cs}^+][18\text{C6}] \quad (3-7)$$

$$K_{ip} \gamma_{\pm}^2 = K_c = [\text{Cs}^+\text{SCN}^-]/[\text{Cs}^+][\text{SCN}^-] \quad (3-8)$$

$$K_{ip}' \gamma_{\pm}^2 = K_c' = [\text{Cs}^+(18\text{C6})\text{SCN}^-]/[\text{Cs}^+(18\text{C6})][\text{SCN}^-] \quad (3-9)$$

Since the total concentration of the  $\text{Cs}^+$  ion,  $\text{SCN}^-$  ion, and 18-crown-6 molecule in the solution are the same, let  $C_t$  represent the total concentration,

$$C_t = [Cs^+] + [Cs^+SCN^-] + [Cs^+(18C6)] + [Cs^+(18C6)SCN^-] \quad (3-10)$$

$$C_t = [SCN^-] + [Cs^+SCN^-] + [Cs^+(18C6)SCN^-] \quad (3-11)$$

$$C_t = [18C6] + [Cs^+(18C6)] + [Cs^+(18C6)SCN^-] \quad (3-12)$$

From Equation (3-7) to (3-12), there are six independent equations. There are also six independent variables of  $[Cs^+]$ ,  $[Cs^+SCN^-]$ ,  $[Cs^+(18C6)]$ ,  $[Cs^+(18C6)SCN^-]$ ,  $[SCN^-]$ , and  $[18C6]$ . Therefore, any of these variables can be expressed as a function of  $K_1$ ,  $K_c$ ,  $K_c'$ , and  $C_t$ . For example,  $[Cs^+(18C6)]$  can be expressed as

$$\begin{aligned} & K_c'^2[Cs^+(18C6)]^4 + (K_1K_c' + K_c'^2 + K_cK_c'^2) [Cs^+(18C6)]^3 \\ & + (K_1 - K_1K_c'C_t - 2K_cK_c' - K_c'C_t) [Cs^+(18C6)]^2 \\ & - (2K_1C_t + K_c) [Cs^+(18C6)] + K_1C_t^2 = 0 \end{aligned} \quad (3-13)$$

Since the observed chemical shift is

$$\begin{aligned} \delta_{obs} = & X_{Cs^+} \delta_{Cs^+} + X_{Cs^+SCN^-} \delta_{Cs^+SCN^-} + X_{Cs^+(18C6)} \delta_{Cs^+(18C6)} \\ & + X_{Cs^+(18C6)SCN^-} \delta_{Cs^+(18C6)SCN^-} \end{aligned} \quad (3-14)$$

where  $X_{Cs^+} = [Cs^+]/C_t$ ,  $X_{Cs^+SCN^-} = [Cs^+SCN^-]/C_t$ ,  $X_{Cs^+(18C6)} = [Cs^+(18C6)]/C_t$ , and  $X_{Cs^+(18C6)SCN^-} = [Cs^+(18C6)SCN^-]/C_t$ , to fit the

calculated results with the experimental data, an expression for the relative mole fractions of all four species in terms of  $K_1$ ,  $K_c$ ,  $K_c'$ , and  $C_t$  is demanded. However, Equation (3-13) is a fourth order one for  $[Cs^+(18C6)]$ . In order to avoid the difficulty of solving this high order equation, reasonable simplification must be made. Obviously, complexed  $Cs^+(18C6)$  is a strong complex, and its formation constant,  $K_1$ , is much larger than  $K_c$  and  $K_c'$ . Therefore, the relation between  $[Cs^+(18C6)]$  and  $[18C6]$  and  $[Cs^+]$  can be expressed as

$$[Cs^+(18C6)] \gg [18C6] \geq [Cs^+] \quad (3-15)$$

From Equations (3-10) and (3-11),

$$[SCN^-] = [Cs^+] + [Cs^+(18C6)] \quad (3-16)$$

So that with (3-15)

$$[SCN^-] \approx [Cs^+(18C6)] \quad (3-17)$$

Using (3-15) and (3-17) and combining (3-9) and (3-12), equation (3-18) can be obtained as

$$\begin{aligned} C_t &\approx [Cs^+(18C6)] + [Cs^+(18C6)SCN^-] \\ &= [Cs^+(18C6)] + K_c'[Cs^+(18C6)][SCN^-] \\ &= [Cs^+(18C6)] + K_c'[Cs^+(18C6)]^2 \end{aligned} \quad (3-18)$$

or 
$$K_c' [Cs^+(18C6)]^2 + [Cs^+(18C6)] - C_t = 0 \quad (3-19)$$

Equation (3-19) is a quadratic equation for  $[Cs^+(18C6)]$ . Solving this equation for  $[Cs^+(18C6)]$  gives

$$[Cs^+(18C6)] = \{ -1 \pm (1+4C_tK_c')^{1/2} \} / 2K_c' \quad (3-20)$$

Since physically  $[Cs^+(18C6)]$  cannot be negative, only the positive root is chosen. Therefore,

$$[Cs^+(18C6)] = \{ -1 + (1+4C_tK_c')^{1/2} \} / 2K_c' \quad (3-21)$$

Then,

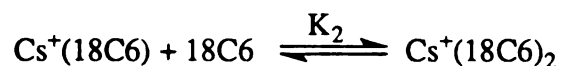
$$Cs^+(18C6)SCN^- = K_c' [Cs^+(18C6)]^2 \quad (3-22)$$

$$[Cs^+] = \{ [Cs^+(18C6)] / K_1 (1 + K_c [Cs^+(18C6)]) \}^{1/2} \quad (3-23)$$

$$[Cs^+SCN^-] = K_c [Cs^+(18C6)] [Cs^+] \quad (3-24)$$

Now all four species are expressed in terms of  $K_1$ ,  $K_c$ ,  $K_c'$ , and  $C_t$ . Note, however, that  $K_c$  and  $K_c'$  are not independent of concentration because of the concentration dependence of  $\gamma_{\pm}$ . This effect was accounted for at each concentration by using  $K_{ip}$  and  $K_{ip}'$  as concentration independent parameters and the mean activity coefficient  $\gamma_{\pm}$ . Therefore,  $K_c$  and  $K_c'$  can be replaced with  $K_{ip}$ ,  $K_{ip}'$ , and  $\gamma_{\pm}$ . The computer fit of the data with Equation (3-14) can give the values of  $K_1$ ,  $K_{ip}$ , and  $K_{ip}'$ .

The concentration dependence of  $^{133}\text{Cs}$  chemical shift for  $\text{Cs}^+(\text{18C6})_2\text{SCN}^-$  can be obtained in a similar way. For  $\text{Cs}^+(\text{18C6})_2\text{SCN}^-$ ,  $\text{Cs}^+(\text{18C6})$  can be considered as a very strong complexed ion and no free  $\text{Cs}^+$  ion exists in the solution. Therefore, the reactions may be expressed as



where  $K_2$  is the second formation constant of complexed  $\text{Cs}^+(\text{18C6})_2$  and  $K_{ip}''$  is the ion pair formation constant of  $\text{Cs}^+(\text{18C6})_2\text{SCN}^-$ . The expression of  $K_{ip}'$  can be found from Equation (3-9).  $K_2$  and  $K_{ip}''$  can be expressed as

$$K_2 = [\text{Cs}^+(\text{18C6})_2]/[\text{18C6}][\text{Cs}^+(\text{18C6})] \quad (3-25)$$

$$K_{ip}''\gamma_{\pm}^2 = K_c'' = [\text{Cs}^+(\text{18C6})_2\text{SCN}^-]/[\text{SCN}^-][\text{Cs}^+(\text{18C6})_2] \quad (3-26)$$

Material balance gives

$$\begin{aligned} C_i' &= [\text{Cs}^+(\text{18C6})] + [\text{Cs}^+(\text{18C6})\text{SCN}^-] + [\text{Cs}^+(\text{18C6})_2] \\ &\quad + [\text{Cs}^+(\text{18C6})_2\text{SCN}^-] \end{aligned} \quad (3-27)$$

$$\begin{aligned}
2C_t' &= [18C6] + [Cs^+(18C6)] + [Cs^+(18C6)SCN^-] \\
&+ 2[Cs^+(18C6)_2] + 2[Cs^+(18C6)_2SCN^-]
\end{aligned} \tag{3-28}$$

$$C_t' = [SCN^-] + [Cs^+(18C6)SCN^-] + [Cs^+(18C6)_2SCN^-] \tag{3-29}$$

where  $C_t'$  is the total concentration of the  $Cs^+$  or  $SCN^-$  ion in the solution. Similarly, all four species,  $[Cs^+(18C6)]$ ,  $[Cs^+(18C6)SCN^-]$ ,  $[Cs^+(18C6)_2]$ , and  $[Cs^+(18C6)_2SCN^-]$ , can be expressed in terms of  $K_2$ ,  $K_{ip}'$ ,  $K_{ip}''$ ,  $\gamma_{\pm}$ , and  $C_t'$ . The observed chemical shift is

$$\begin{aligned}
\delta_{obs} &= X_{Cs^+(18C6)} \delta_{Cs^+(18C6)} + X_{Cs^+(18C6)SCN^-} \delta_{Cs^+(18C6)SCN^-} \\
&+ X_{Cs^+(18C6)_2} \delta_{Cs^+(18C6)_2} \\
&+ X_{Cs^+(18C6)_2SCN^-} \delta_{Cs^+(18C6)_2SCN^-}
\end{aligned} \tag{3-30}$$

where  $X_{Cs^+(18C6)} = [Cs^+(18C6)]/C_t'$ ,  $X_{Cs^+(18C6)SCN^-} = [Cs^+(18C6)SCN^-]/C_t'$ ,  $X_{Cs^+(18C6)_2} = [Cs^+(18C6)_2]/C_t'$ , and  $X_{Cs^+(18C6)_2SCN^-} = [Cs^+(18C6)_2SCN^-]/C_t'$ . The computer fit of the data with Equation (3-30) gives the values of  $K_2$ ,  $K_{ip}'$ , and  $K_{ip}''$ . Because  $K_{ip}$  and  $K_{ip}'$  are common parameters for  $Cs^+SCN^-$ ,  $Cs^+(18C6)SCN^-$ , and  $Cs^+(18C6)_2SCN^-$ , multiple data set fitting of the data of the three compounds with Equations (3-6), (3-14), and (3-30) were carried out by using the KINFIT program. The subroutine program for the multiple data set fitting is given in Appendix B. The resulting ion pair formation constants for all three

compounds are listed in Table 3-2 along with their complexation formation constants.

These results show that the formation constants of the complexes are much larger than the ion-pairing constants, indicating that complexation is the major cause of the variation of the chemical shift when 18-crown-6 molecule is involved in the complexation reactions.

Table 3-2. Ion Pair and Complexation Formation Constants of Cesium Compounds in Nitromethane at 25°C.

Compound	$K_{ip}^*$	$K_1$	$K_2$
CsSCN	$(2.2 \pm 1.5) \times 10$	--	--
$Cs^+(18C6)SCN^-$	$(4.5 \pm 0.1) \times 10$	$(1.7 \pm 0.2) \times 10^5$	--
$Cs^+(18C6)_2SCN^-$	$(1.9 \pm 0.5) \times 10$	$(1.7 \pm 0.2) \times 10^5$	$(1.0 \pm 0.3) \times 10^3$

\*  $K_{ip}$  represents  $K_{ip}$ ,  $K_{ip}'$ , or  $K_{ip}''$ .

### III.B. Formation Constants of Cesium Thiocyanate Complexes with Crown Ethers in Nitromethane

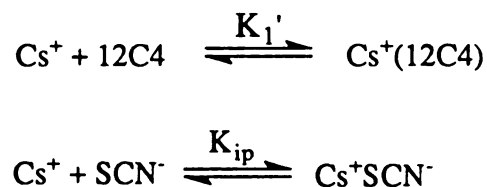
It is well known that the  $Cs^+$  ion is the least solvated among the alkali metal ions because of its large size and low charge density and that nitromethane is a very poor solvating solvent for ions since it has a low donor number(2.7) in spite of the rather large dielectric constant(36.87). Consequently, ion pairing and complexation reactions are important competitors for solvation in this solvent.

In a solution of CsSCN and crown ethers, there may exist crown ether molecules, free  $\text{Cs}^+$  and  $\text{SCN}^-$  ions, ion-paired  $\text{Cs}^+$  and  $\text{SCN}^-$  ions, and complexed  $\text{Cs}^+$  ions. When exchange between the free and complexed  $\text{Cs}^+$  ions is fast on the NMR time scale, only a population averaged chemical shift is observed.

$$\delta_{\text{obs}} = X_f \delta_f + X_{\text{ip}} \delta_{\text{ip}} + X_c \delta_c \quad (3-31)$$

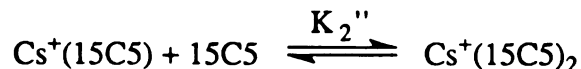
In the above equation,  $\delta_{\text{obs}}$  is the observed chemical shift.  $X_f$ ,  $X_{\text{ip}}$ , and  $X_c$  are the relative mole fractions, and  $\delta_f$ ,  $\delta_{\text{ip}}$ , and  $\delta_c$  are the chemical shifts for free  $\text{Cs}^+$ , ion-paired  $\text{Cs}^+$  and complexed  $\text{Cs}^+$  ions, respectively.

Complexed  $\text{Cs}^+(12\text{C}4)$  was treated as a one step complexation reaction and ion-pairing formation was also considered because of the mismatch of sizes between  $\text{Cs}^+$  ion and 12-crown-4 molecule and the weak complexation ability of 12-crown-4. The equilibrium equations may be represented by



where  $K_1'$  is the formation constant of complexed  $\text{Cs}^+(12\text{C}4)$ .

For complexed  $\text{Cs}^+(15\text{C}5)_2$ , a two step complexation reaction treatment was adopted and the ion pairing reaction was also considered. The reaction equilibria can be expressed as



In the above equations,  $K_1''$  and  $K_2''$  are the first and second formation constants of  $\text{Cs}^+(15\text{C5})_2$ , respectively, and  $k_{ip}$  is the ion pair formation constant of  $\text{Cs}^+(15\text{C5})\text{SCN}^-$ .

Complexed  $\text{Cs}^+(18\text{C6})_2$  was also considered as a two step complexation reaction with a possible ion pairing reaction,



Since the results given in Table 3-2 shows that the first-step complexation is very strong, it was assumed that the second-step complexation takes place only after the first-step complexation has been completed. Therefore, this two step complexation reaction was treated as two single step complexation reactions.

From the data list in Table 3-3 and plotted in Figure 3-2, it is clear that the subsequent reaction of  $\text{Cs}^+$  ion with 18-crown-6

Table 3-3. Mole Ratio Studies of Crown Ether Complexes with CsSCN in MeNO<sub>2</sub> Solvent by <sup>133</sup>Cs NMR at 25°C. [CsSCN]<sub>T</sub>=0.005M.

<u>[18C6]</u>		<u>[15C5]</u>		<u>[12C4]</u>	
[Cs <sup>+</sup> ]	δppm	[Cs <sup>+</sup> ]	δppm	[Cs <sup>+</sup> ]	δppm
0.0	-56.88	0.0	-56.88	0.0	-56.88
0.2	-50.50	0.4	-51.05	0.4	-55.94
0.4	-45.19	0.6	-48.68	0.6	-55.84
0.6	-37.11	0.8	-45.43	0.8	-55.47
0.8	-31.49	1.0	-42.86	1.0	-55.12
1.0	-26.09	1.2	-40.83	1.2	-54.83
1.2	-23.51	1.6	-37.73	1.6	-54.26
1.4	-21.61	1.8	-36.22	1.8	-53.98
1.6	-20.61	2.0	-35.75	2.0	-53.77
1.8	-20.09	2.4	-33.75	2.4	-53.33
2.0	-19.88	3.0	-31.69	3.0	-52.85
2.4	-19.71	4.0	-28.52	4.0	-51.92
3.0	-19.56	5.0	-26.07	5.0	-51.25
4.0	-19.22	6.0	-24.37	6.0	-50.70
5.0	-19.23	8.0	-21.00	8.0	-49.74
6.0	-19.12	0.0	-18.51	10.0	-48.95
8.0	-19.03	12.0	-16.79		
10.0	-18.72	15.0	-14.53		
		18.0	-13.03		
		20.0	-12.28		

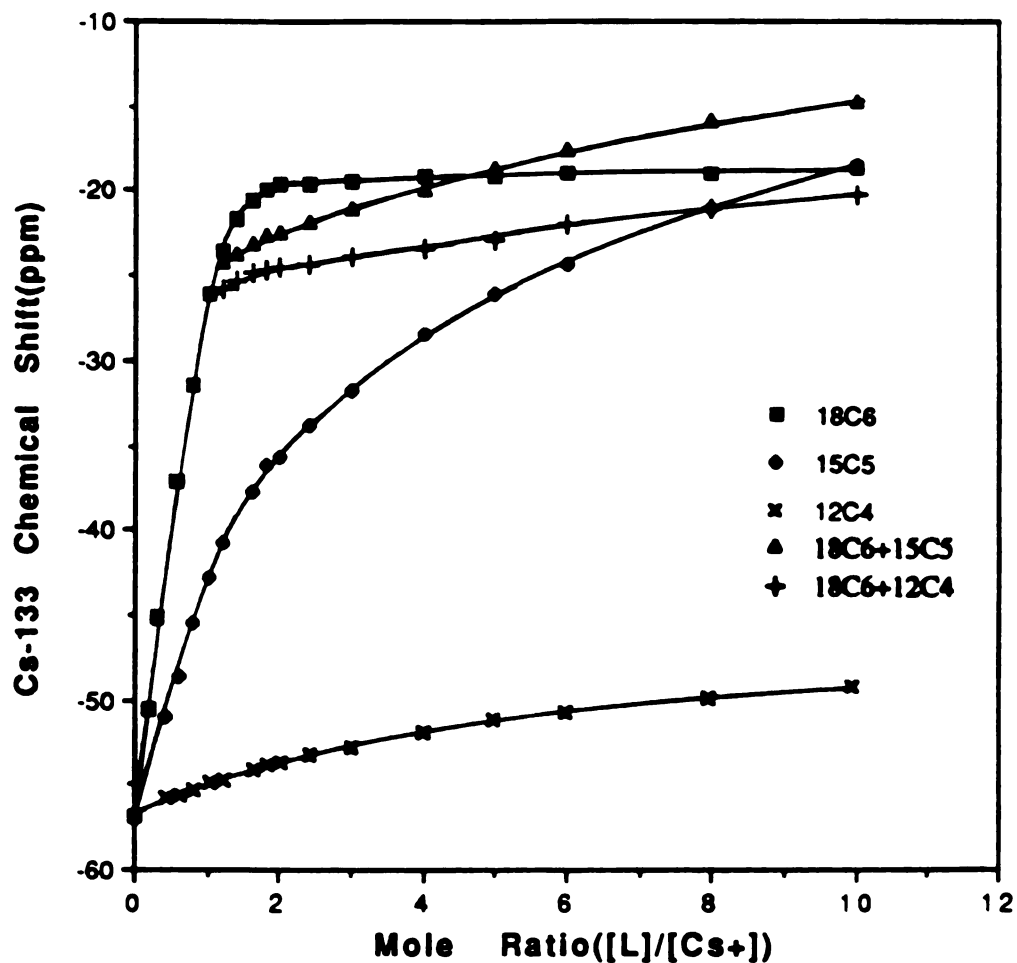


Figure 3-2.  $^{133}\text{Cs}$  chemical shifts vs.  $[\text{L}]/[\text{Cs}^+]$  mole ratio in nitromethane at  $25^\circ\text{C}$ . L = 18-crown-6, 15-crown-5, or 12-crown-4. The solid lines are least-squares plots.

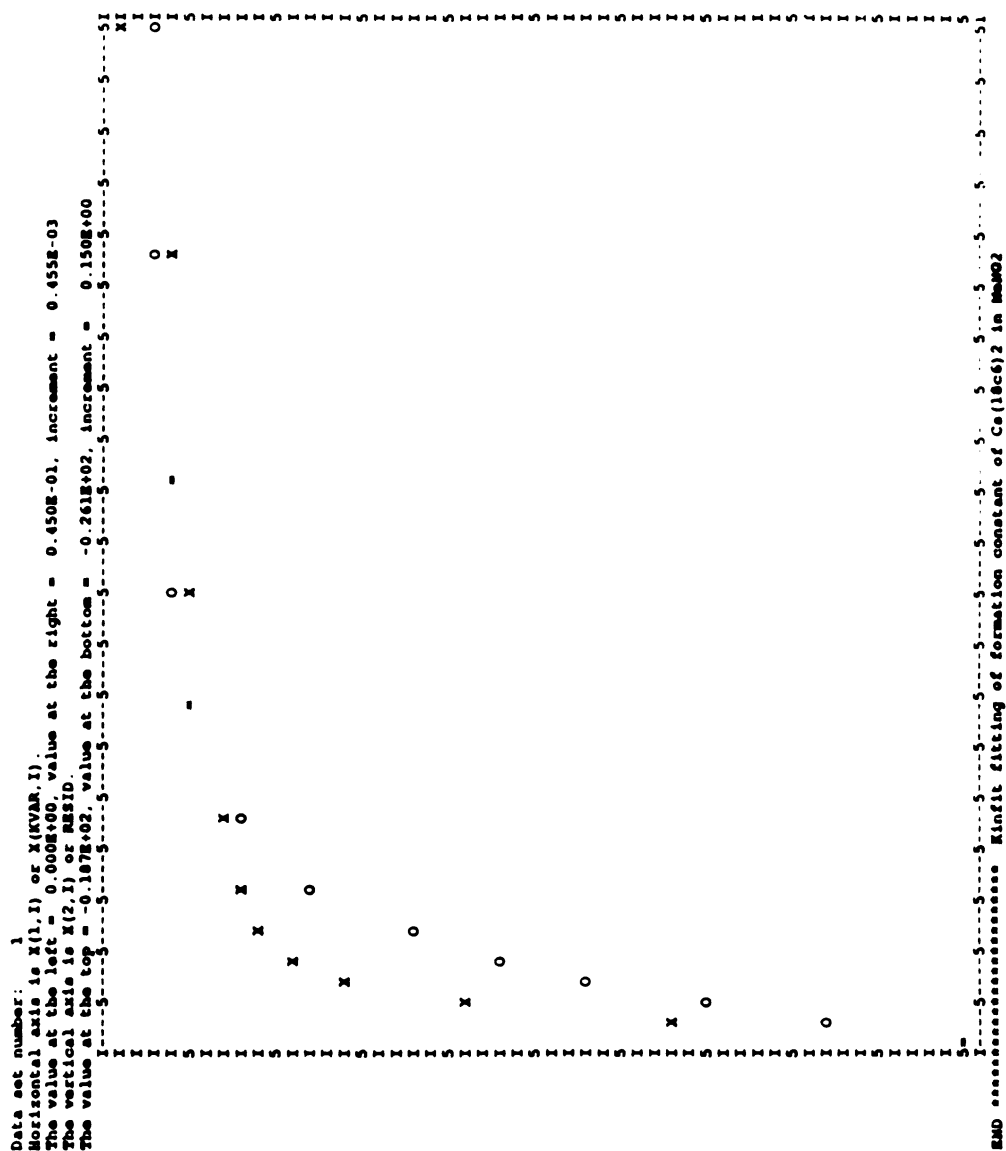


Figure 3-3. Nonlinear least-squares curve fitting of the chemical shift  $\nu_s$ .  
 $[18C6]/[Cs^+]$  mole ratio without the model of the intermediate  $(Cs^+)_2(18C6)_3$ .

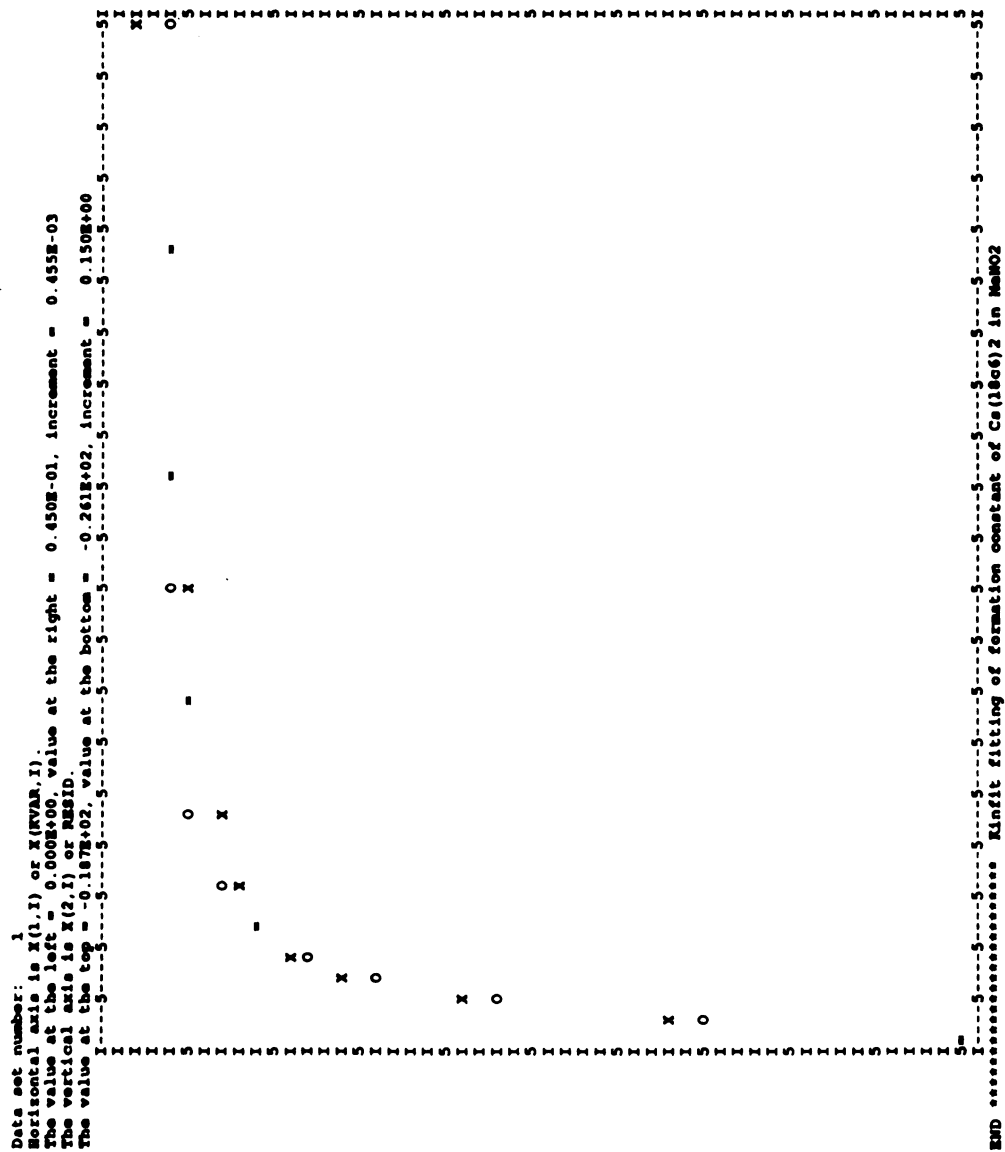
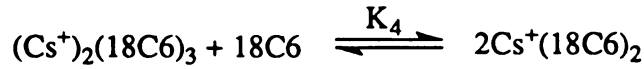


Figure 3-4. Nonlinear least-squares curve fitting of the chemical shift vs.  $[18C6]/[Cs^+]$  mole ratio with the model of the intermediate  $(Cs^+)_2(18C6)_3$ .

molecule forms a sandwich complex of  $\text{Cs}^+(\text{18C6})_2$ . But the plot also shows that there is a sharp slope between mole ratio  $[\text{18C6}]/[\text{Cs}^+]=1$  and 2, and the KINFIT fitting gives a rather different curve from the experimental data in this region, as shown in Figure 3-3. This indicates that it may form a club sandwich complex ( $\text{18C6}:\text{Cs}^+=3:2$ ) in this region. In order to discriminate a sandwich complex (2:1) from a club sandwich complex, a substitute reaction equilibrium model was used to fit the data with the KINFIT program for the possible formation of club sandwich complex in  $[\text{18C6}]/[\text{Cs}^+]$  mole ratio range from 1 to 2. The model is presented as follows:



where  $K_3 = [(\text{Cs}^+)_2(\text{18C6})_3]/[\text{18C6}][\text{Cs}^+(\text{18C6})]^2$  (3-32)

$$K_4 = [\text{Cs}^+(\text{18C6})_2]^2/[\text{18C6}][(\text{Cs}^+)_2(\text{18C6})_3]$$
 (3-33)

In the above reaction equilibrium model, complexed  $\text{Cs}^+(\text{18C6})$  was treated as starting material. Therefore, material balance gives

$$C_M^t = [\text{Cs}^+(\text{18C6})] + [\text{Cs}^+(\text{18C6})_2] + 2[(\text{Cs}^+)_2(\text{18C6})_3]$$
 (3-34)

$$C_L^t = [\text{18C6}] + [\text{Cs}^+(\text{18C6})_2] + [(\text{Cs}^+)_2(\text{18C6})_3]$$
 (3-35)

where  $C_M^t$  and  $C_L^t$  are the total concentration of the  $Cs^+$  ion and 18-crown-6 molecule in the solution. The observed chemical shift can be represented by

$$\begin{aligned} \delta_{obs} = & X_{Cs^+(18C6)} \delta_{Cs^+(18C6)} + X_{Cs^+(18C6)_2} \delta_{Cs^+(18C6)_2} \\ & + X_{(Cs^+)_2(18C6)_3} \delta_{(Cs^+)_2(18C6)_3} \end{aligned} \quad (3-36)$$

with  $X_{Cs^+(18C6)} = [Cs^+(18C6)]/C_M^t$ ,  $X_{Cs^+(18C6)_2} = [Cs^+(18C6)_2]/C_M^t$ , and  $X_{(Cs^+)_2(18C6)_3} = [(Cs^+)_2(18C6)_3]/C_M^t$ . An expression for the relative mole fractions of all three species in terms of  $C_M^t$ ,  $C_L^t$ ,  $K_3$ , and  $K_4$  is required in order to carry out the computer fit with the experimental data. From Equation (3-32) to (3-35), equation (3-37) can be obtained as

$$\begin{aligned} & K_3[Cs^+(18C6)]^3 + \{2K_3C_L^t - K_3C_M^t + (K_3K_4)^{1/2}\} [Cs^+(18C6)]^2 \\ & + \{1 + C_L^t(K_3K_4)^{1/2} - C_M^t(K_3K_4)^{1/2}\} [Cs^+(18C6)] - C_M^t/K_3 = 0 \end{aligned} \quad (3-37)$$

Cubic Equation (3-37) can be solved for  $[Cs^+(18C6)]$  in terms of  $C_M^t$ ,  $C_L^t$ ,  $K_3$ , and  $K_4$ .  $[Cs^+(18C6)_2]$  and  $[(Cs^+)_2(18C6)_3]$  can then be obtained in terms of  $C_M^t$ ,  $C_L^t$ ,  $K_3$ ,  $K_4$  and  $[Cs^+(18C6)]$ . Therefore, a computer fit of the data with Equation (3-36) can give the values of  $K_3$  and  $K_4$ . Combining Equations (3-32) and (3-33), Equation (3-25) can also be obtained as

$$(K_3K_4)^{1/2} = K_2 = [\text{Cs}^+(\text{18C6})_2]/[\text{18C6}][\text{Cs}^+(\text{18C6})]$$

The subroutine program used to solve Equation (3-37) and to fit the calculated results with the experimental data is given in Appendix C. The KINFIT fitting of the data based on the formation of the club sandwich complex gives a much smaller standard deviation and the fit is much better as shown in Figure 3-4. The formation constants obtained from the fitting are  $K_2 = (9.3 \pm 1.2) \times 10^2$ ,  $K_3 = (7.1 \pm 0.2) \times 10^3$ , and  $K_4 = (1.2 \pm 0.3) \times 10^2$ . From the fitting results, it may be suggested that after complete formation of a 1:1 complex of  $\text{Cs}^+(\text{18C6})$ , the intermediate club sandwich complex is favored between mole ratio  $[\text{18C6}]/[\text{Cs}^+] = 1$  and 2 because nitromethane is a poor solvating solvent and ion pair formation of  $\text{Cs}^+(\text{18C6})\text{SCN}^-$  is weak. When the mole ratio of  $[\text{18C6}]/[\text{Cs}^+]$  increases, the 2:1 sandwich complex,  $\text{Cs}^+(\text{18C6})_2$ , is formed.

The formation constants for complexed  $\text{Cs}^+(\text{12C4})$ ,  $\text{Cs}^+(\text{15C5})_2$ , and  $\text{Cs}^+(\text{18C6})_2$  are listed in Table 3-4. These results clearly show that  $K_1$  for the complexation of  $\text{Cs}^+$  with 18C6 is much larger than  $K_2$ , but that  $K_2$  is also large, indicating that complexed  $\text{Cs}^+(\text{18C6})_2$  is very stable in nitromethane. In addition, both  $K_1$  and  $K_2$  of complexed  $\text{Cs}^+(\text{18C6})_2$  ion are much larger than those of complexed  $\text{Cs}^+(\text{15C5})_2$ , presumably because the cavity size of the 18-crown-6 molecule provides a much better fit for the  $\text{Cs}^+$  ion.

It is interesting to note that the  $K_1$  and  $K_2$  values of complexed  $\text{Cs}^+(\text{18C6})_2$  in Table 3-4 are close to those in Table 3-2, although those values from Table 3-2 were obtained by the computer fitting

of

w

13

ec

cc

—

—

\*

\*

II

s

w

a

re

of the data of  $^{133}\text{Cs}$  chemical shift vs. concentration of the complex while the values from Table 3-4 were obtained from the data for the  $^{133}\text{Cs}$  chemical shift vs.  $[\text{18C6}]/[\text{Cs}^+]$  mole ratio. This indicates that the equilibrium equations of complexation reactions used for the computer fitting are at least internally consistent.

Table 3-4. Formation Constants for  $\text{Cs}^+$ -Crown Ether Complexes in Nitromethane Solvent at  $25^\circ\text{C}$ .

Complexed Ions	$K_1^*$	$K_2^{**}$
$\text{Cs}^+(\text{12C4})$	$(3.6 \pm 0.1) \times 10^3$	--
$\text{Cs}^+(\text{15C5})_2$	$(2.2 \pm 1.2) \times 10^3$	$(3.0 \pm 0.2) \times 10^3$
$\text{Cs}^+(\text{18C6})_2$	$(1.6 \pm 0.2) \times 10^5$	$(9.3 \pm 1.2) \times 10^2$

\*  $K_1$  represents  $K_1'$ ,  $K_1''$ , or  $K_1$ .

\*\*  $K_2$  represents  $K_2''$  or  $K_2$ .

### III.C. Formation Constants of Mixed Sandwich Complexes

In order to examine the possibility of formation of mixed sandwich complexes of the  $\text{Cs}^+$  ion, either 15-crown-5 or 12-crown-4 was added to the solution in which the  $[\text{18C6}]/[\text{Cs}^+]$  mole ratio was already maintained at a value of one. The two resulting complexation reactions and the ion pair formation reaction may be represented by

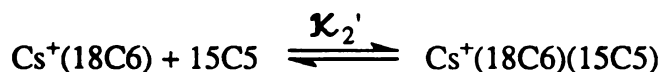
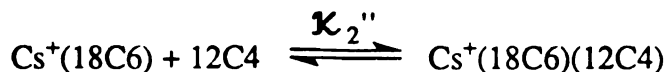


Table 3-5. Mole Ratio Studies of Mixed Sandwich Complexes with CsSCN in MeNO<sub>2</sub> Solvent by <sup>133</sup>Cs NMR at 25°C. [CsSCN]<sub>T</sub>=0.005M.

[18C6]=0.005M		[18C6]=0.01M		[18C6]=0.005M	
<u>[15C5]</u>		<u>[15C5]</u>		<u>[12C4]</u>	
[Cs <sup>+</sup> ]	δppm	[Cs <sup>+</sup> ]	δppm	[Cs <sup>+</sup> ]	δppm
0.0	-26.09	0.0	-19.69	0.0	-26.09
0.2	-24.22	0.4	-18.86	0.2	-25.74
0.4	-23.71	0.8	-18.54	0.4	-25.31
0.6	-23.08	1.0	-18.43	0.6	-24.97
0.8	-22.68	1.4	-18.08	0.8	-24.70
1.0	-22.47	2.0	-17.46	1.0	-24.57
1.4	-21.77	3.0	-16.66	1.4	-24.45
2.0	-21.08	4.0	-15.78	2.0	-24.03
3.0	-19.87	6.0	-14.42	3.0	-23.33
4.0	-18.66	8.0	-13.26	4.0	-22.92
5.0	-17.64	10.0	-12.52	5.0	-21.94
7.0	-15.95	13.0	-12.21	7.0	-21.07
9.0	-14.77	16.0	-12.09	9.0	-20.22
10.0	-14.25	20.0	-11.90		
13.0	-13.72	25.0	-11.75		
16.0	-13.22	30.0	-11.61		
20.0	-12.93	35.0	-11.57		
25.0	-12.57	40.0	-11.47		
30.0	-12.36				
35.0	-12.23				
40.0	-12.04				



The results are given in Table 3-5 and in Figure 3-2. The plots in Figure 3-2 show a gradual paramagnetic shift upon addition of 15-crown-5 or 12-crown-4, clearly indicating the formation of mixed sandwich complexes of  $\text{Cs}^+(18\text{C}6)(15\text{C}5)$  and  $\text{Cs}^+(18\text{C}6)(12\text{C}4)$  in nitromethane solution. A third possible complexation reaction was also investigated by addition of 15-crown-5 to a solution with the  $[18\text{C}6]/[\text{Cs}^+]$  mole ratio of two in order to determine directly whether complexed  $\text{Cs}^+(18\text{C}6)_2$  or  $\text{Cs}^+(18\text{C}6)(15\text{C}5)$  ion is more stable. This reaction equation may be expressed as



The formation constants of the two mixed sandwich complexes obtained from computer fitting of the data with the KINFIT program are listed in Table 3-6. It was found from all formation constants that the overall stability of the sandwich complexes varies in the order  $\text{Cs}^+(18\text{C}6)_2 > \text{Cs}^+(18\text{C}6)(15\text{C}5) > \text{Cs}^+(18\text{C}6)(12\text{C}4) > \text{Cs}^+(15\text{C}5)_2 > \text{Cs}^+(12\text{C}4)_2$ . This order nicely reflects the decrease of the oxygen number in crown ethers and the sizes of the crown ether molecules. Because the size of the  $\text{Cs}^+$  ion (3.38 Å) [58, 81] is larger than the cavity of all three crown ethers, observation of the above correlation

is  
 $\text{Cs}^+$   
despi  
atoms  
of the  
cavity  
molec  
 $\text{Cs}^+$   
is exp  
a K v  
more

Tabl

---

C  
C  
C  
C  
C  
C  
C

---

\* $\chi_2$  r

Th  
[HMHCY

is not surprising. However, the overall stability of the  $\text{Cs}^+(\text{18C6})(\text{12C4})$  complex is much higher than that of  $\text{Cs}^+(\text{15C5})_2$ , despite the equal number of donating oxygen atoms (10 oxygen atoms) involved in the complex formation. This is probably because of the much better coordination condition of  $\text{Cs}^+$  ion inside the larger cavity of 18-crown-6 molecule than that of the smaller 15-crown-5 molecule. Since the complexed  $\text{Cs}^+(\text{18C6})_2$  ion is more stable than  $\text{Cs}^+(\text{18C6})(\text{15C5})$ , a very small  $K$  value for the third reaction equation is expected. In fact, computer fitting with the data in table 3-5 gives a  $K$  value of 0.3, indicating that the complex of  $\text{Cs}^+(\text{18C6})_2$  is indeed more stable than that of  $\text{Cs}^+(\text{18C6})(\text{15C5})$ .

Table 3-6. Formation Constants for  $\text{Cs}^+$  Ion Complexes with Mixed Crown Ethers in Nitromethane Solvent at 25°C.

Complexed Ions	$K_1$	$K_2^*$
$\text{Cs}^+(\text{18C6})(\text{12C4})$	$(1.6 \pm 0.2) \times 10^5$	$(2.1 \pm 0.4) \times 10$
$\text{Cs}^+(\text{18C6})(\text{15C5})$	$(1.6 \pm 0.2) \times 10^5$	$(6.7 \pm 0.3) \times 10$
$\text{Cs}^+(\text{HMHCY})(\text{12C4})$	$>10^5$	$(3.7 \pm 1.8) \times 10^3$
$\text{Cs}^+(\text{HMHCY})(\text{15C5})$	$>10^5$	$(7.9 \pm 1.5) \times 10^3$
$\text{Cs}^+(\text{HMHCY})_2$	$>10^5$	$(1.6 \pm 0.1) \times 10^3$

\*  $K_2$  represents the  $K_2'$ ,  $K_2''$ , or  $K_2'''$ .

The variation of the  $^{133}\text{Cs}$  chemical shifts as a function of the  $[\text{HMHCY}]/[\text{Cs}^+]$ ,  $[\text{15C5}]/[\text{Cs}^+(\text{HMHCY})]$ , and  $[\text{12C4}]/[\text{Cs}^+(\text{HMHCY})]$  mole

**Table 3-7. Mole Ratio Studies of Mixed Sandwich Complexes with CsSCN in MeNO<sub>2</sub> Solvent by <sup>133</sup>Cs NMR at 25°C. [CsSCN]<sub>T</sub>=0.005M.**

		[HMH CY]=0.005M		[HMH CY]=0.005M	
<u>[HMH CY]</u>		<u>[<sup>15</sup>C5]</u>		<u>[<sup>12</sup>C4]</u>	
[Cs <sup>+</sup> ]	δppm	[Cs <sup>+</sup> ]	δppm	[Cs <sup>+</sup> ]	δppm
1.0	9.90	0.0	9.90	0.0	9.90
1.2	16.33	0.2	3.82	0.2	6.42
1.4	21.06	0.4	-1.28	0.4	3.90
1.6	25.39	0.6	-6.24	0.6	1.89
1.8	28.30	0.8	-11.09	0.8	-0.21
2.0	31.16	1.0	-14.28	1.0	-1.61
2.4	34.47	1.4	-15.96	1.4	-2.60
3.0	36.82	2.0	-16.77	2.0	-3.02
4.0	37.41	3.0	-17.24	3.0	-3.26
5.0	37.81	4.0	-17.03	4.0	-2.95
7.0	38.26	5.0	-17.33	5.0	-3.20
8.0	38.37	7.0	-17.40	7.0	-3.51
10.0	38.62	9.0	-17.38	9.0	-3.37

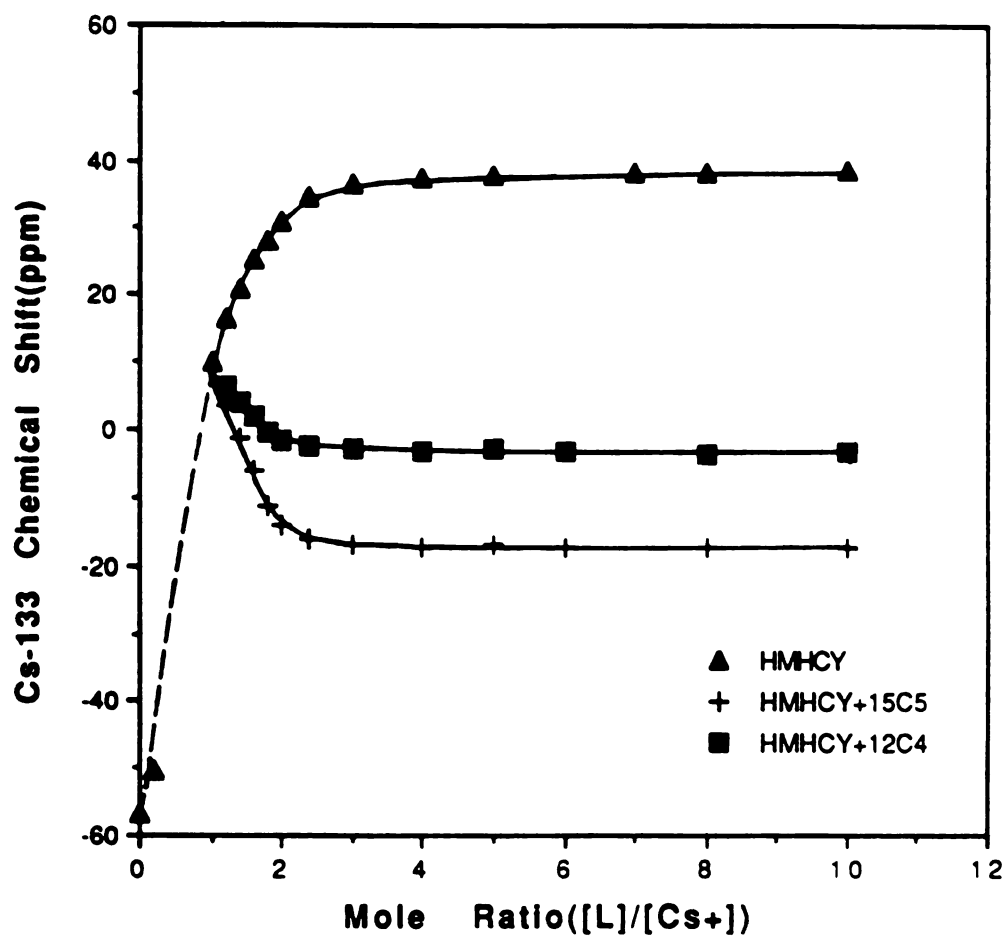
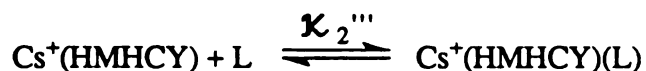


Figure 3-5.  $^{133}\text{Cs}$  chemical shifts vs.  $[\text{L}]/[\text{Cs}^+]$  mole ratio in nitromethane at  $25^\circ\text{C}$ .  $\text{L} = \text{HMHCY}$ , 15-crown-5, or 12-crown-4. The solid lines are least-squares plots.

ratios in nitromethane is given in Table 3-7 and shown in Figure 3-5. It is interesting to note that, between  $[\text{HMHCY}]/[\text{Cs}^+]$  mole ratio of zero and one, two broad  $^{133}\text{Cs}$  peaks were observed and the corresponding chemical shift values could not be measured accurately. Nevertheless, these broad peaks indicate the existence of a rather slow exchange between the free and complexed  $\text{Cs}^+$  ions, and the formation of a very stable 1:1 complexed  $\text{Cs}^+(\text{HMHCY})$  ion. However, after the mole ratio of one, only one population-averaged broad NMR peak was observed and this peak showed a paramagnetic shift upon further addition of HMHCY. The plot in Figure 3-5 also shows that the  $^{133}\text{Cs}$  chemical shift starts to level off at a  $[\text{HMHCY}]/[\text{Cs}^+]$  mole ratio of about two. This behavior is clearly indicative of the formation of a stable 2:1 sandwich complex of  $\text{Cs}^+(\text{HMHCY})_2$  in nitromethane solution.

The formation of mixed sandwich complexes of  $\text{Cs}^+$  ion with HMHCY and crown ethers was investigated by the addition of either 15-crown-5 or 12-crown-4 to the nitromethane solution with a  $[\text{HMHCY}]/[\text{Cs}^+]$  mole ratio of one. In these cases, the  $^{133}\text{Cs}$  peak shifts diamagnetically upon addition of the crown ethers, and tends to level off at mole ratio of about two as shown in Figure 3-5, indicating the formation of mixed sandwich complexes of  $\text{Cs}^+(\text{HMHCY})(15\text{C}5)$  and  $\text{Cs}^+(\text{HMHCY})(12\text{C}4)$  respectively.

All three 2:1 complexation reactions involving the HMHCY 1:1 complex may be expressed by the one step reaction equation,



where L represents the complexant, HMHCY, 15-crown-5 or 12-crown-4. Computer fittings of the data with the KINFIT program were carried out in order to evaluate the  $\mathcal{K}_2'''$  values of the three 2:1 complexes and the results are included in Table 3-6. These results show that the  $\mathcal{K}_2'''$  values of complexed  $\text{Cs}^+$  ions varies in the order  $\text{Cs}^+(\text{HMHCY})(15\text{C}5) > \text{Cs}^+(\text{HMHCY})(12\text{C}4) > \text{Cs}^+(\text{HMHCY})_2$ . In contrast to the  $\text{Cs}^+$ -18C6 sandwich complexes, the complexed  $\text{Cs}^+(\text{HMHCY})_2$  is the least stable 2:1 complex in the series, probably due to the existence of the six bulky  $-\text{CH}_3$  groups on the nitrogen atoms of the macrocyclic ring. These methyl groups can prevent the convenient approach of the second HMHCY molecule to the previously complexed  $\text{Cs}^+$  ion. On the other hand, a smaller molecule, such as 15-crown-5 can better cap the bowl-shaped 1:1 complex of  $\text{Cs}^+(\text{HMHCY})$  without considerable spatial interference, giving a very stable mixed sandwich complex. The small size and lower coordination number of the 12-crown-4 molecule gives a relatively weaker mixed sandwich complex of  $\text{Cs}^+(\text{HMHCY})(12\text{C}4)$ , but it is still more stable than the complex of  $\text{Cs}^+(\text{HMHCY})_2$ . It is interesting to note that, in the solid state, no alkali or electride could be made that contained 2:1 complexes, such as  $\text{Cs}^+(\text{HMHCY})(12\text{C}4)$ ,  $\text{Cs}^+(\text{HMHCY})(15\text{C}5)$ , or  $\text{Cs}^+(\text{HMHCY})_2$ . The only compound prepared was  $\text{Cs}^+(\text{HMHCY})\text{Na}^-$  which has a cation-anion contact ion pair to coordinate the  $\text{Cs}^+$  ion[55]. Therefore, the existence of the 2:1 complexes and their large  $\mathcal{K}_2'''$  values in nitromethane can be attributed to the very poor solvation power of nitromethane and the weak ion pair formation between  $\text{Cs}^+$  and  $\text{SCN}^-$  ions.

Comparison of the  $K_2$  values shows that, while the second step formation constants are about the same for complexed  $\text{Cs}^+(\text{18C6})_2$  and  $\text{Cs}^+(\text{HMHCY})_2$  ions, the  $K_2$  values for complexed  $\text{Cs}^+(\text{HMHCY})(\text{15C5})$  and  $\text{Cs}^+(\text{HMHCY})(\text{12C4})$  ions are much larger than those of the  $\text{Cs}^+(\text{18C6})(\text{15C5})$  and  $\text{Cs}^+(\text{18C6})(\text{12C4})$  complexes. According to the crystal structure of  $\text{Cs}^+(\text{HMHCY})\text{Na}^-$  [55], the configuration of the HMHCY molecule is a rigid hemisphere or bowl-shaped structure. In this structure, one side of the HMHCY molecule is completely surrounded by the hydrogen atoms on the HMHCY ring and the  $\text{Cs}^+$  ion sits inside the hemisphere and is coordinated to all six nitrogen atoms of the HMHCY molecule. The  $\text{Na}^-$  anion also forms a cation-anion contact ion pair with the  $\text{Cs}^+$  ion, directly from the open side. In solution, the complexed  $\text{Cs}^+(\text{HMHCY})$  ion probably has the same structure and a 15-crown-5 molecule can easily cover the open side of the hemisphere to form a three-dimensional cavity. In this conformation, there is no open space for the penetration of the solvent molecule or the counter-anion,  $\text{SCN}^-$ , toward the  $\text{Cs}^+$  cation and the complex can be very stable, especially when the solvent is a very poor solvated solvent and the ion-pairing is weak.

In contrast to HMHCY, 18-crown-6 has a two-dimensional cavity and the  $\text{Cs}^+$  ion can only partially fit inside the cavity because of the larger size of the cation. If the complexed  $\text{Cs}^+(\text{18C6})$  is covered by a 15-crown-5 or 12-crown-4 molecule, there is still some open space so that the complexed  $\text{Cs}^+$  ion remains exposed to the solvent molecules. Therefore, complexed  $\text{Cs}^+(\text{HMHCY})(\text{15C5})$  and  $\text{Cs}^+(\text{HMHCY})(\text{12C4})$  ions are expected to be more stable than complexed  $\text{Cs}^+(\text{18C6})(\text{15C5})$  and  $\text{Cs}^+(\text{18C6})(\text{12C4})$ .

# CHAPTER 4. SINGLE-CRYSTAL $^{133}\text{Cs}$ NMR STUDY OF $\text{Cs}^+(\text{18C6})_2\text{e}^-$

## I. Introduction

The nuclear spin Hamiltonian can be expressed in the following tabular form:

Term	Coupling of nuclear spins with
$\mathcal{H} = \mathcal{H}_Z$	external static magnetic fields
$+\mathcal{H}_{\text{rf}}$	external rf magnetic fields
$+\mathcal{H}_{\text{CS}}$	induced magnetic fields originating from orbital motions of electrons
$+\mathcal{H}_Q$	electric field gradients
$+\mathcal{H}_{\text{SR}}$	magnetic moment associated with the molecular angular momentum
$+\mathcal{H}_D$	each other, directly through their dipole moments
$+\mathcal{H}_J$	each other, indirectly via electron spins

where  $\mathcal{H}_Z$  and  $\mathcal{H}_{\text{rf}}$  are Hamiltonians from external magnetic fields which are much larger than internal fields and can be controlled by experiments. Detailed descriptions of each term can be found from many books[82-85]. For  $^{133}\text{Cs}$  NMR studies of  $\text{Cs}^+(\text{18C6})_2\text{e}^-$ , quadrupolar coupling and chemical shielding interaction are the two most important terms among the internal Hamiltonians. Therefore,

the total Hamiltonian,  $\mathcal{H}$ , which governs the NMR spectrum of a quadrupolar nucleus of Cs, may be expressed by

$$\mathcal{H} = \mathcal{H}_Z + \mathcal{H}_{CS} + \mathcal{H}_Q \quad (4-1)$$

where Z, CS, and Q represent the Zeeman, chemical shielding and quadrupolar interactions, respectively. The dominant Zeeman term is from the interaction between the nuclear magnetic moment and the applied magnetic field. The terms  $\mathcal{H}_{CS}$  and  $\mathcal{H}_Q$  can be treated as perturbations and are sensitive to the electronic environment around the nucleus. The dipolar term  $\mathcal{H}_D$ , while smaller, causes broadening and 'smoothing' of the spectra.

The chemical shielding interaction results from the motion of electrons around a nucleus induced by the applied external magnetic field,  $B_0$ . The local magnetic fields induced by this motion change the total field experienced by the nucleus. The chemical shielding Hamiltonian, therefore, can be expressed as

$$\mathcal{H}_{CS} = \gamma \mathbf{I} \cdot \boldsymbol{\sigma} \cdot \mathbf{B}_0 \quad (4-2)$$

where  $\gamma$  is the magnetogyric ratio of the nucleus and  $\mathbf{I}$  and  $\boldsymbol{\sigma}$  are the nuclear spin angular momentum vector and the chemical shielding tensor, respectively. This tensor describes the three-dimensional nature of the electronic shielding of the nucleus. The shielding usually varies with the orientation of a crystal or molecule in the magnetic field. In its principal-axis system(PAS), the diagonalized tensor is described by three orthogonal principal components,  $\sigma_{11}$ ,  $\sigma_{22}$ ,

and  $\sigma_{33}$ , with, by convention,  $\sigma_{11} \leq \sigma_{22} \leq \sigma_{33}$ . Three angles are required to describe the chemical shielding PAS with respect to the crystal axis system. The isotropic chemical shielding is given by

$$\sigma_{\text{iso}} = (\sigma_{11} + \sigma_{22} + \sigma_{33})/3 \quad (4-3)$$

A nucleus with nuclear spin quantum number  $I \geq 1$  possess a nuclear quadrupole moment. The nuclear quadrupole coupling is an electrostatic interaction between the nuclear quadrupole moment and the electric field gradient at the nucleus. The quadrupolar Hamiltonian can be expressed as

$$\mathcal{H}_Q = [eQ/2I(2I-1)\hbar] \mathbf{I} \cdot \mathbf{V} \cdot \mathbf{I} \quad (4-4)$$

where  $eQ$  is the nuclear quadrupole moment and  $\mathbf{I}$  and  $\mathbf{V}$  are the nuclear spin angular momentum vector and the quadrupolar tensor, respectively. In the principal-axis system, the principal components of  $\mathbf{V}$  are defined again by convention as  $|V_{33}| \geq |V_{22}| \geq |V_{11}|$  and the electric field gradient tensor is traceless with  $V_{33} + V_{22} + V_{11} = 0$ . Therefore, two parameters, the quadrupolar coupling constant,  $\chi$ , and the asymmetry parameter,  $\eta_Q$ , can completely define the magnitudes of its principal components. The quadrupolar coupling constant and asymmetry parameter are given by

$$\chi = e^2qQ/h \quad (4-5)$$

and 
$$\eta_Q = (V_{11} - V_{22})/V_{33} \quad (4-6)$$

where  $\nu_Q = V_{33}$ . Like the chemical shielding interaction, three angles are also required to define the orientation of the quadrupolar PAS with respect to the crystal axis system.

Because  $^{133}\text{Cs}$  has a small nuclear quadrupole moment, it is sufficient to consider the influence of the quadrupolar interaction on the solid-state NMR spectra by using only first-order perturbation methods. The NMR spectrum that results from magnetically equivalent  $^{133}\text{Cs}$  nuclei in a single crystal that shows the effects of anisotropic chemical shielding and quadrupolar coupling is given by [86]

$$I(\nu) = \sum_{m=-I+1}^{+I} \rho(m)g(\nu-\nu_m) \quad (4-7)$$

where  $\rho(m)$  is the probability of the  $(m \leftrightarrow m-1)$  transition,  $g$  is a line-broadening function, and

$$\begin{aligned} \nu_m = \nu_0 [1 - (\sigma_{11}\sin^2\vartheta \cos^2\phi + \sigma_{22}\sin^2\vartheta \sin^2\phi + \sigma_{33}\cos^2\vartheta)] \\ - (\nu_Q/2)[(3\cos^2\theta - 1) - \eta_Q\sin^2\theta \cos 2\phi](m-1/2) \end{aligned} \quad (4-8)$$

$$\nu_0 = \gamma B_0 / 2\pi \quad (4-9)$$

$$\begin{aligned} \nu_Q &= 3e^2qQ/2I(2I-1)\hbar \\ &= 3\chi/2I(2I-1) \end{aligned} \quad (4-10)$$

The angles  $\vartheta$  and  $\phi$  define the orientation of the PAS of the chemical shielding tensor with respect to the magnetic field, while the angles  $\theta$  and  $\phi$  define the orientation of the PAS of the quadrupolar electric field gradient tensor with respect to the magnetic field.

Since the chemical shielding results in an overall shift of the nuclear spin energy levels, only the quadrupolar interaction determines the splitting between any pair of satellite transitions. For a first order quadrupolar interaction, the central transition is not affected and this central transition depends only on the chemical shielding. Because of these characteristics of a nucleus which has a small quadrupole moment, the quadrupolar and chemical shielding influences on a single-crystal NMR spectrum can easily be separated. The position of the central transition peak and the magnitude of the satellite splitting can be used to determine the chemical shielding and quadrupole coupling, respectively, as a function of the orientation of the single crystal in the magnetic field. From these data one can determine the chemical shielding and quadrupolar tensors.

In general, the frequency of an observed resonance is determined only by the secular contribution, the  $z$  component of a tensor in the laboratory frame. The chemical shielding or quadrupolar tensor, in the reference frame of a cubic box inside of which the crystal is mounted, can be constructed from the angular dependence of the  $z$  component. By a series of unitary transformations, the chemical shielding or quadrupolar tensor can be rotated to its principal axis system in which the tensor is in the diagonal form. Therefore, the eigenvalues of the tensor and the

corresponding eigenvectors, which are the direction cosines with respect to an orthogonalized crystal axis frame, may be obtained in this way. In the crystal frame, the directions of the tensor elements may then be correlated with the molecular structure, which ultimately determines both the magnitude and direction of the tensor elements. The series of transformations required to determine the chemical shielding or quadrupolar tensor in the PAS frame may be expressed as in Figure 4-1[87].

The laboratory system in which data are obtained can be related to the goniometer system by a rotation angle. A cubic box inside of which a single crystal will be placed can be mounted into the goniometer. The coordination between the cubic box and the goniometer is related by simple rotation with a rotating angle of  $90^\circ$ ,  $180^\circ$ , or  $270^\circ$ . The cubic box has an orthogonal coordinate system and this system must be related to the crystal axis system by crystallography because the crystal is randomly mounted inside the cubic box. Finally, matrix diagonalization gives the principal components of the tensor, and the orientation of the tensor in the crystal system.

Although single-crystal NMR studies[86-90] have become more and more popular and have been shown to be a very useful method to extract information about a nucleus of interest, there has been only one such study made of an alkali or electride, that of  $\text{Na}^+(\text{C}_{222})\text{Na}^-$  by J. Kim[46]. The scarcity of such studies is due to the difficulties of crystal growth and sample handling, because these compounds are extremely air- and temperature-sensitive.  $\text{Cs}^+(\text{18C6})_2\text{e}^-$  was selected as a candidate for single-crystal NMR

Laboratory Axis System

$$\Downarrow R(\phi, 90, 90)$$

Goniometer Axis System

$$\Downarrow R(\alpha'', \beta'', \gamma'')$$

Cube Axis System

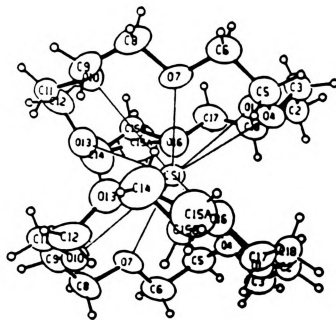
$$\Downarrow R(\alpha', \beta', \gamma')$$

Crystal Axis System

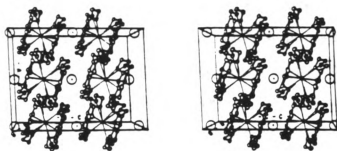
$$\Downarrow R(\alpha, \beta, \gamma)$$

Principal Axis System

**Figure 4-1.** The series of transformations required to determine the **chemical** shielding or quadrupolar tensor in the PAS frame from the **experimental** data obtained in the laboratory frame.



A



B

Figure 4-2. Crystal structure of  $\text{Cs}^+(\text{18C6})_2\text{e}^-$ . A) Single molecule diagram; B) ORTEP stereo packing diagram. The anionic hole centers are indicated by the symbol ⊙.

study for several reasons. First, it is an electride and it is the most stable of the electrides. Second, its crystal structure in the low-temperature phase is known, as shown in Figure 4-2[6]. Third, single crystals of  $\text{Cs}^+(\text{18C6})_2\text{e}^-$  can occasionally be grown large enough to be used for single-crystal NMR studies. Finally, and most importantly, this compound has demonstrated unique physical properties from powder NMR, EPR, conductivity, and magnetic susceptibility studies. Especially relevant to this study, the powder MAS NMR shows that this electride slowly goes through an irreversible transition from a low-temperature phase to a disordered high-temperature phase at about  $-50^\circ\text{C}$ , during which the observed single NMR peak shifts diamagnetically by about 80 ppm[91-92]. For the high-temperature phase, a reversible first order phase transition occurs at about  $-50^\circ\text{C}$ . Above  $-50^\circ\text{C}$ , the MAS NMR spectra show a single peak, but two peaks were observed below  $-50^\circ\text{C}$ , indicating two 'frozen' chemically inequivalent sites for  $\text{Cs}^+$  ions below this temperature. This further indicates that the crystal structure has been changed from the low-temperature phase to high-temperature phase. Although what change occurs in the crystal is not known, a single-crystal  $^{133}\text{Cs}$  NMR study of  $\text{Cs}^+(\text{18C6})_2\text{e}^-$  may be able to ascertain whether  $\text{Cs}^+$  ions in the high-temperature phase are all magnetically equivalent or not above  $-50^\circ\text{C}$ . This study may also indicate how many magnetically inequivalent  $\text{Cs}^+$  ions are present in each of the two chemically inequivalent sites. This information will certainly be useful in understanding the local environment of the  $\text{Cs}^+$  ions in the high-temperature phase and may provide information about changes in the crystal structure.

## II. Experimental

Since electrides are air-sensitive and are thermally unstable at higher temperature, the synthesis and single-crystal growth were carried out at  $-78^{\circ}\text{C}$  after prior evacuation of the cell to  $10^{-5}$  torr. A mixed solvent of dimethyl ether and trimethylamine and a K-cell were used for the synthesis and single-crystal growth. After  $\text{Cs}^{+}(\text{18C6})_2\text{e}^{-}$  had been synthesized, the solvent was slowly evaporated into a liquid nitrogen trap through a series of frits for about seven days. Single crystals as large as  $4\times4\times4\text{ mm}^3$  were obtained. An appropriate single crystal which had the approximate dimensions of  $3\times4\times4\text{ mm}^3$  was selected under a microscope in a dry nitrogen-filled glove bag and then the crystal was mounted into a cubic box, machined from Rexalite polymer. The cubic box with the crystal was then inserted into a supporting frame inside the receiving coil on the NMR probe. Dow Corning vacuum grease was used for crystal mounting.

NMR measurements were carried out at 52.468 MHz with a Varian VXR-400 superconducting NMR spectrometer. A single-pulse sequence was used with pulse width of  $0.7\text{ }\mu\text{s}$ . All  $^{133}\text{Cs}$  spectra were referenced with respect to infinitely dilute aqueous solution of  $\text{Cs}^{+}$  ion. A home-built NMR probe with angle rotating capability was used. Angle rotations were performed in ten-degree intervals with a possible  $\pm 0.1$  degree deviation from the goniometer which has a minimum scale of 0.2 degree. The single-crystal NMR data of  $^{133}\text{Cs}$  in  $\text{Cs}^{+}(\text{18C6})_2\text{e}^{-}$  were collected at about  $-50^{\circ}\text{C}$  and under a nitrogen atmosphere. A precooled nitrogen gas stream kept the sample

temperature at about  $-50^{\circ}\text{C}$ . Although the average temperature seldom differed by more than  $\pm 2^{\circ}\text{C}$  from  $-50^{\circ}\text{C}$ ., excursions of up to about  $\pm 4^{\circ}\text{C}$  sometimes occurred during the 30 hours or so required for a single orientation of the cubic box, since there is no temperature controller in the home-built single-crystal NMR probe. By repeating the measurements with the cubic box turned so that successive rotations could be made about the x, y, and z coordinates of the box, enough data could be obtained to determine the crystal orientation. The orientation of the unit cell axes of the crystal with respect to the cubic box axis system could not be determined independently because of the large size and thermal instability of the crystal. The least-squares KINFIT program and a subroutine program, XTAL[9], were used to fit the data.

### III. Results and Discussion

The low-temperature phase of crystalline  $\text{Cs}^+(\text{18C6})_2\text{e}^-$  belongs to the monoclinic space group  $\text{C2/c}$ . The four  $\text{Cs}^+$  ions in the unit cell lie on special positions on the two-fold axis, with the coordinates (1) 0, y, 1/4; (2) 0, -y, 3/4; (3) 1/2, y+1/2, 1/4; (4) 1/2, -y+1/2, 3/4. Positions (1) and (2) are related by an inversion center as are (3) and (4), while the first pair is related to the second pair by a two-fold screw axis. Therefore, all four  $\text{Cs}^+$  ions are crystallographically equivalent and must have identical isotropic chemical shifts as observed in this laboratory[91-92]. Since (1) and (2) are related by an inversion center, they are magnetically equivalent, as with (3) and (4). Furthermore, the site symmetry constraint due to the two

fold axis indicates that all four  $\text{Cs}^+$  ions in the unit cell of the low-temperature phase are magnetically equivalent. This also has possibly been confirmed[93]. One of the objectives of the present work was to carry out a single-crystal NMR study of the low-temperature phase at low temperatures. Unfortunately, the presence of the disordering transition was not known at the time of this study and the crystal used was warmed to slightly above  $-50^\circ\text{C}$ , so that only single-crystal NMR spectra of the high-temperature phase were obtained. It is clear from the results, however, that the original crystalline orientation was preserved rather than the formation of a random powder.

Two distinct sets of  $^{133}\text{Cs}$  NMR patterns were observed at  $-50^\circ\text{C}$  as shown in Figure 4-3. All seven transitions for one set and five transitions for another one are clearly shown in the lower spectrum, while a total of seven transitions can be observed from the upper spectrum, indicating that the two sites coalesce at this orientation. The crystal was independently rotated around three orthogonal axes, designated as 1, 2, and 3. The orientation plots of half the splitting of the first two satellite transitions for each of the two sites of  $\text{Cs}^+$  versus the angle of rotation about the three orthogonal axes are given in Figure 4-4 and 4-5. Figure 4-6 and 4-7 show the angular dependence of the chemical shifts of the central transitions for both sites. The least-squares KINFIT multiple-data-set fitting of the data from all three orthogonal axes with program XTAL gave the results summarized in Table 4-1. The chemical shifts vary with the orientation of the crystal as expected. Because of the temperature fluctuations during the experiment, the chemical shifts from the

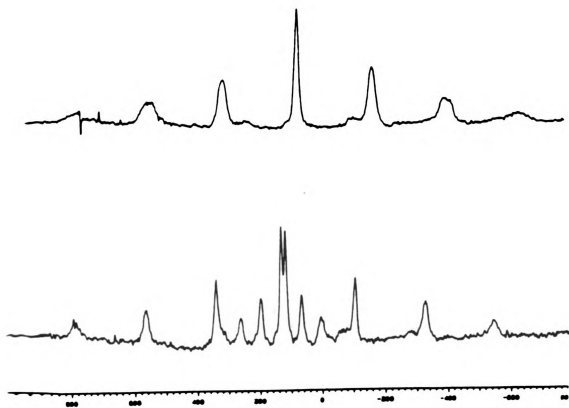


**Figure 4-3.** Single-crystal  $^{133}\text{Cs}$  NMR spectra of the high-temperature phase of  $\text{Cs}^+(\text{18C6})_2\text{e}^-$  at two different orientations at  $\nu_L=52.468\text{MHz}$  and at  $-50^\circ\text{C}$ .

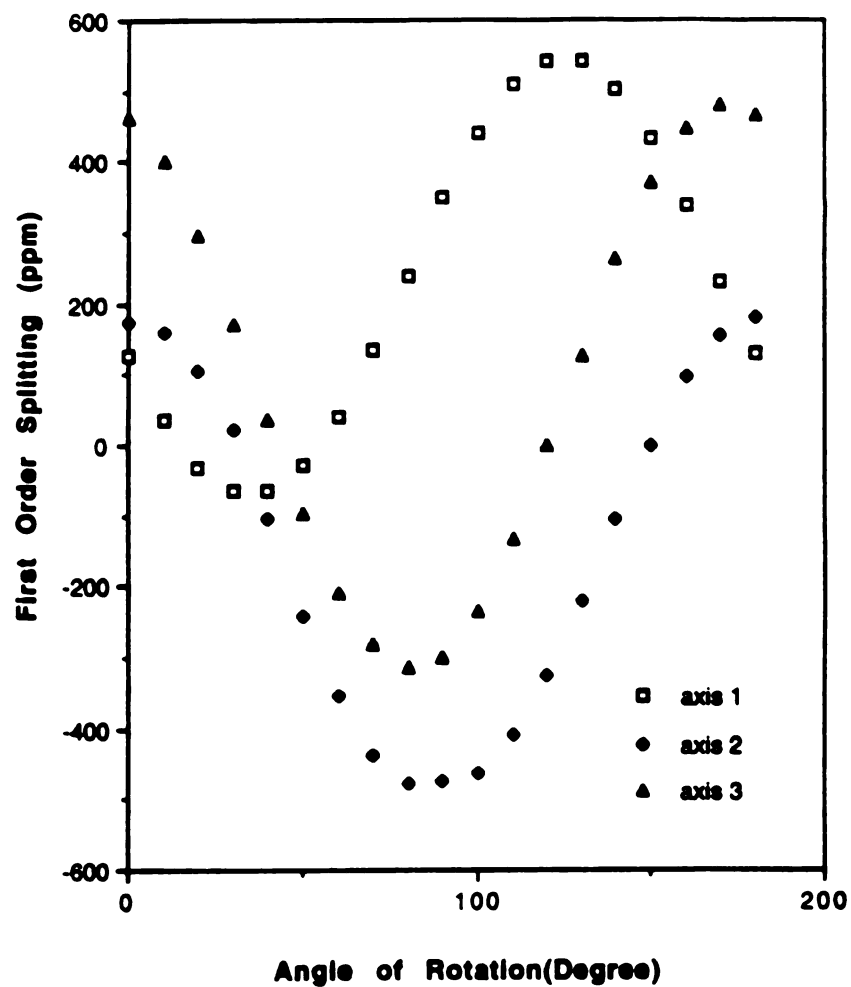


**Figure 4-4.** Angular dependence of half the splitting of the two first satellite transitions of  $\text{Cs}^+$  in site 1 from the high-temperature phase of single crystal  $\text{Cs}^+(\text{18C6})_2\text{e}^-$ .

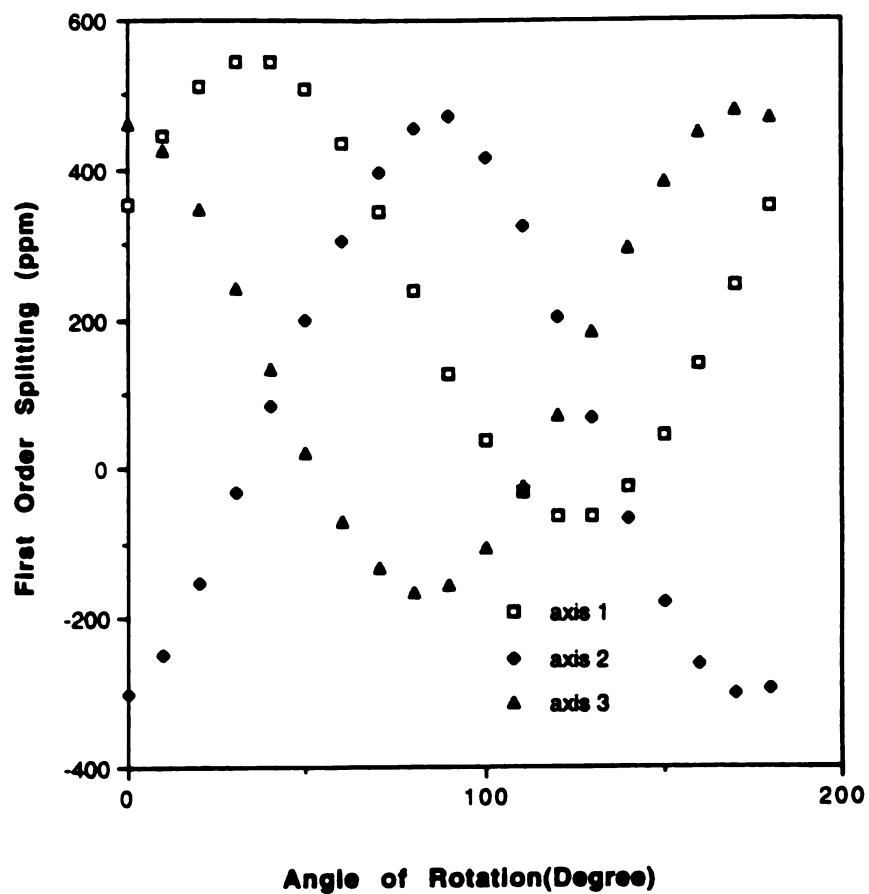


**Figure 4-5.** Angular dependence of half the splitting of the two first satellite transitions of  $\text{Cs}^+$  in site 2 from the high-temperature phase of single crystal  $\text{Cs}^+(\text{18C6})_2\text{e}^-$ .

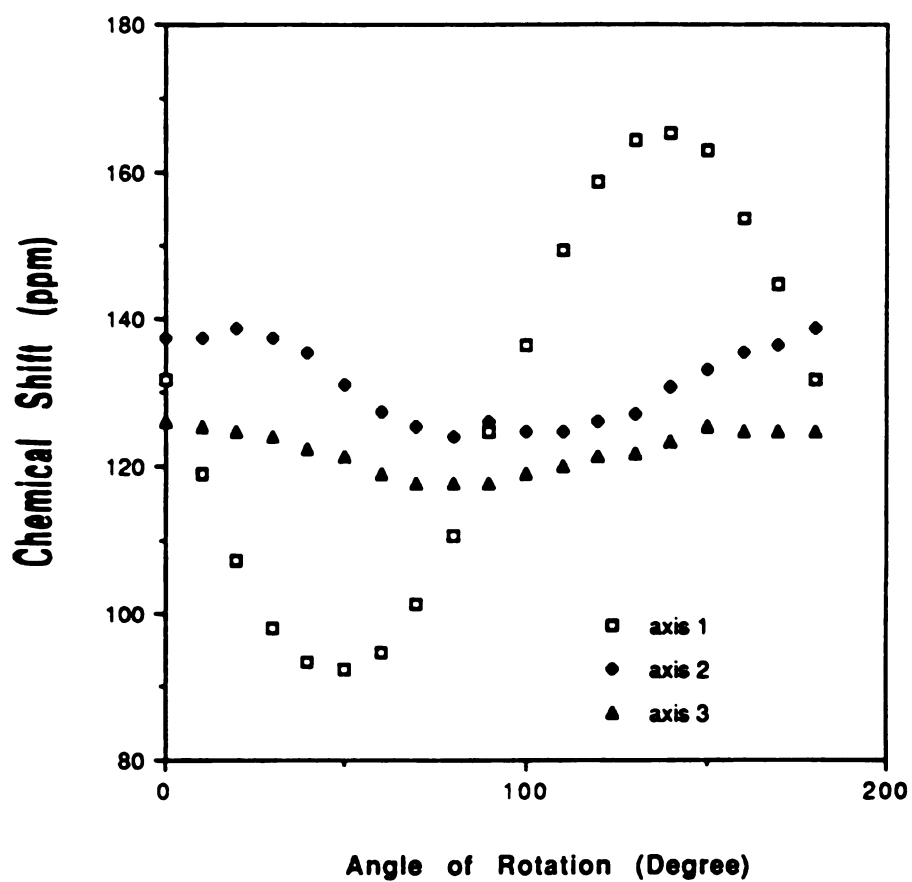


**Figure 4-6.** Angular dependence of the chemical shift of the central transition of  $\text{Cs}^+$  in site 1 from the high-temperature phase of single crystal  $\text{Cs}^+(\text{18C6})_2\text{e}^-$ .

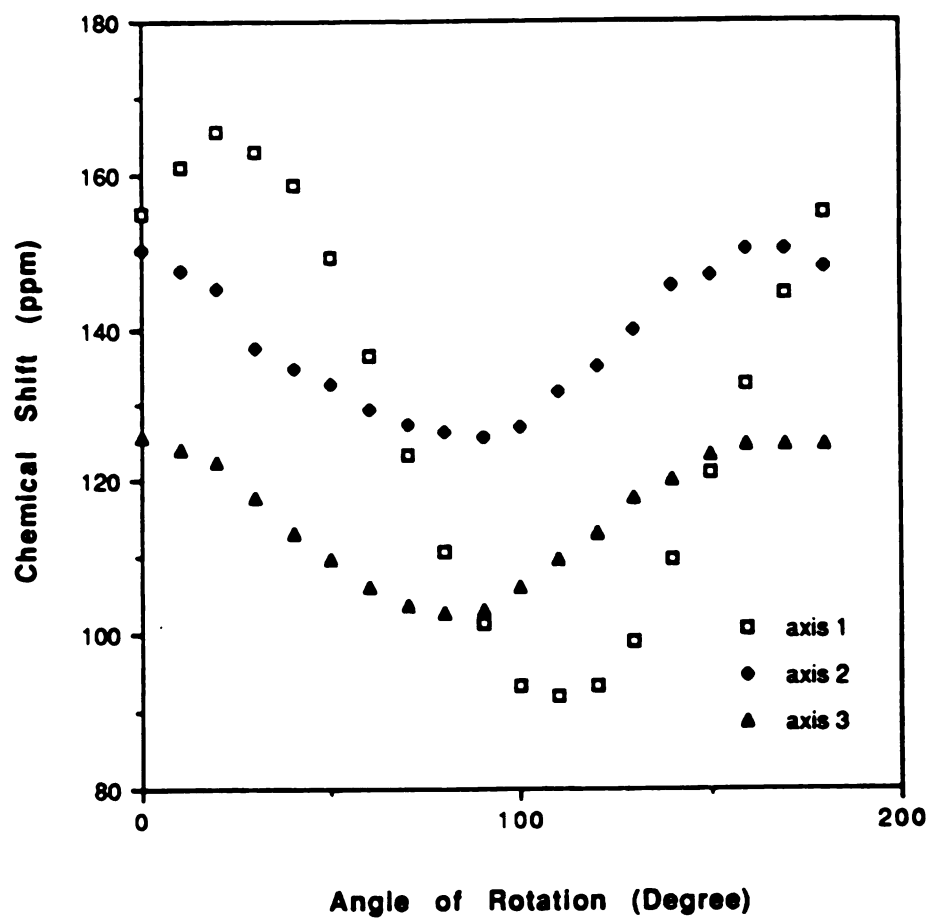


**Figure 4-7.** Angular dependence of the chemical shift of the central transition of  $\text{Cs}^+$  in site 2 from the high-temperature phase of single crystal  $\text{Cs}^+(\text{18C6})_2\text{e}^-$ .

**Table 4-1. Results\* Obtained from a Single-Crystal  $^{133}\text{Cs}$  NMR Study of the High-Temperature Phase of  $\text{Cs}^+(\text{18C6})_2\text{e}^-$  at  $-50^\circ\text{C}$ .**

Site	1	2
$\sigma_{11}$	$92 \pm 5 \text{ ppm}$	$93 \pm 5 \text{ ppm}$
$\sigma_{22}$	$125 \pm 5 \text{ ppm}$	$125 \pm 5 \text{ ppm}$
$\sigma_{33}$	$162 \pm 5 \text{ ppm}$	$165 \pm 5 \text{ ppm}$
QCC	$0.58 \pm 0.04 \text{ MHz}$	$0.57 \pm 0.05 \text{ MHz}$
$\eta_Q$	$0.57 \pm 0.10$	$0.45 \pm 0.07$

\* Results are from simultaneous least-squares KINFIT fitting of all three data sets for each site.

spectra are not as accurate as expected from the instrument specifications. This is because this electride is a paramagnetic compound and its chemical shift is strongly temperature dependent. Nevertheless, an important result was obtained from the central line chemical shifts. The simultaneous presence of both lines for some orientations showed that the isotropic chemical shifts,  $\sigma_{iso}$ , for the two sites are 126 ppm and 128 ppm at  $-50^{\circ}\text{C}$ . Since the two peaks observed at lower temperature by powder MAS measurements have chemical shifts that differ by about 20 ppm, the present result shows that this is only a single type of chemical environment for the two magnetically inequivalent  $\text{Cs}^+$  sites in this higher temperature region of the high-temperature phase.

The quadrupolar coupling constants and the asymmetry parameters for the two sites are  $\text{QCC}=0.58\pm0.04\text{MHz}$  and  $\eta_Q=0.57\pm0.10$ , and  $\text{QCC}=0.57\pm0.05\text{MHz}$  and  $\eta_Q=0.45\pm0.07$ , respectively. The similarity of these values for the two sites as well as the chemical shifts reinforce the assumption that there is only a single average chemical environment for each of the complexed cesium cations in the high-temperature phase at this temperature.

## CHAPTER 5. CONCLUSIONS

Five new alkalides have been synthesized and their crystal structures have been determined. Three of them were synthesized with large crown ethers such as 21-crown-7 or dicyclohexano-24-crown-8. These three compounds showed very unusual crystal structures and some interesting features.  $(\text{Cs}^+)_2(21\text{C}7)_2(\text{Na}^-)_2$  has twin cation-anion ion pairs in which the  $\text{Cs}^+-\text{Na}^-$  distances are only 4.44(2)Å and 4.52(3)Å respectively. But optical absorption spectroscopy and  $^{23}\text{Na}$  NMR show no charge transfer between  $\text{Na}^-$  and  $\text{Cs}^+$ . Each  $\text{Cs}^+$  cation in the molecule is bonded to all seven oxygen atoms in one 21-crown-7 and to one of the seven oxygen atoms from another 21-crown-7, giving the  $\text{Cs}^+$  cations a coordination number of eight and connecting the two  $\text{Cs}^+(21\text{C}7)\text{Na}^-$  units together to form  $(\text{Cs}^+)_2(21\text{C}7)_2(\text{Na}^-)_2$ .  $(\text{K}^+)_2(21\text{C}7)_3(\text{MeNH}_2)(\text{Na}^-)_2$  has a third 21-crown-7, which serves as a bridge connecting the two  $\text{K}^+$  cations in the molecule while a solvent molecule,  $\text{MeNH}_2$ , forms a bond to one of the two  $\text{K}^+$  cations. By contrast,  $\text{K}^+(\text{dicyclohexano-24C}8)\text{Na}^-$  has a 1:1 ratio of  $\text{K}^+$  ion to complexant, although dicyclohexano-24-crown-8 is a larger crown ether. The crystal structure of this compound shows that dicyclohexano-24-crown-8 twists around the  $\text{K}^+$  cation in order to have all eight oxygen atoms coordinated to the cation, giving a 'wrap around' complex. These alkalides are stable in spite of the large cavity sizes of the crown ethers compared to the relatively small sizes of the  $\text{Cs}^+$  and  $\text{K}^+$  cations. The stability of these compounds is attributed to their unusual structural feature in which

the cations can be fully coordinated in different ways. Five more new compounds have also been synthesized with dicyclohexano-30-crown-10 and dicyclohexano-24-crown-8. These alkalides appear to be amorphous materials. Attempts to crystallize these compounds failed, probably because they are too 'soft' and disordered as a result of the flexible nature of the large crown ethers. The successful synthesis and crystal structure determination of alkalides that contain large crown ethers showed that large crown ethers could be used as complexants for the synthesis of alkalides. Furthermore, large cryptands such as C322 and C332 may be good candidates for the synthesis of alkalides and even new electrides since they have 3-dimensional cavities which appears to be important for the stability of electrides.

Two new mixed sandwich complexes,  $\text{Rb}^+(18\text{C}6)(12\text{C}4)\text{Na}^-$  and  $\text{Rb}^+(18\text{C}6)(12\text{C}4)\text{Rb}^-$ , have also been synthesized and their crystal structures have been determined. These two compounds show very interesting optical properties and  $\text{Rb}^+(18\text{C}6)(12\text{C}4)\text{Na}^-$  even has a shiny green color while other sodides generally are golden or reddish in color. The optical absorption spectra of  $\text{Rb}^+(18\text{C}6)(12\text{C}4)\text{Na}^-$  and  $\text{Rb}^+(18\text{C}6)(12\text{C}4)\text{Rb}^-$  have two and three absorption peaks while most of alkalides only have one. It is, however, unclear what causes these absorption peaks. One possible explanation is that these unusual optical absorption spectra may result from the effect of the asymmetry of the excited states of  $\text{Na}^-$  and  $\text{Rb}^-$  ions in the compounds. In order to answer this question, polarized single crystal reflectance studies need to be carried out.

$^{133}\text{Cs}$  NMR studies were performed on the concentration dependence of the  $^{133}\text{Cs}$  chemical shifts of  $\text{Cs}^+\text{SCN}^-$ ,  $\text{Cs}^+(\text{18C6})\text{SCN}^-$ , and  $\text{Cs}^+(\text{18C8})_2\text{SCN}^-$  in nitromethane. Studies of  $^{133}\text{Cs}$  chemical shift versus  $[\text{L}]/[\text{Cs}^+]$  mole ratio ( $\text{L} = \text{18-crown-6}$ ,  $\text{15-crown-5}$ ,  $\text{12-crown-4}$ , or  $\text{HMHCY}$ ) were also carried out. These studies showed the formation of stable 2:1 sandwich complexes of  $\text{Cs}^+(\text{18C6})_2$ ,  $\text{Cs}^+(\text{15C5})_2$ , and  $\text{Cs}^+(\text{HMHCY})_2$  in nitromethane. In the case of  $\text{Cs}^+(\text{18C6})_2$ , the formation of an intermediate 'club sandwich',  $(\text{Cs}^+)_2(\text{18C6})_3$ , is possible in nitromethane solvent. By contrast, the  $\text{Cs}^+-\text{12C4}$  system was considered only as a one step complexation. Finally, evidence for the formation of mixed sandwich complexes of  $\text{Cs}^+(\text{18C6})(\text{15C5})$ ,  $\text{Cs}^+(\text{18C6})(\text{12C4})$ ,  $\text{Cs}^+(\text{HMHCY})(\text{15C5})$ , and  $\text{Cs}^+(\text{HMHCY})(\text{12C4})$  were observed in nitromethane solvent.

A single-crystal  $^{133}\text{Cs}$  NMR study of an electride,  $\text{Cs}^+(\text{18C6})_2\text{e}^-$ , was carried out for the first time. The crystal of  $\text{Cs}^+(\text{18C6})_2\text{e}^-$  used for this study was allowed to warm to above  $-50^\circ\text{C}$  and only single-crystal NMR spectra of the high-temperature phase were obtained. It is clear from the results, however, that the original crystalline orientation was preserved rather than the formation of a random powder after the phase transition. This study demonstrated that single-crystal NMR study of an electride is possible although electrides are extremely air- and temperature-sensitive. In order to understand better the NMR properties of  $\text{Cs}^+(\text{18C6})_2\text{e}^-$ , more single-crystal NMR studies need to be carried out, especially for the low-temperature phase of this electride at low temperatures.

## APPENDICES

## APPENDIX A

Crystal Structure Data of  $(\text{Cs}^+)_2(21\text{C7})_2(\text{Na}^-)_2$ ,  
 $(\text{K}^+)_2(21\text{C7})_3(\text{MeNH}_2)(\text{Na}^-)_2$ ,  $\text{K}^+(\text{dicyclohexano-24C8})\text{Na}^-$ ,  
 $\text{Rb}^+(18\text{C6}(12\text{C4})\text{Na}^-$  and  $\text{Rb}^+(18\text{C6}(12\text{C4})\text{Rb}^-$ .

### Table

- A-1. Positional Parameters and Their Estimated Standard Deviations for  $(\text{Cs}^+)_2(21\text{C7})_2(\text{Na}^-)_2$ .
- A-2. Bond Distances (in Angstroms) for  $(\text{Cs}^+)_2(21\text{C7})_2(\text{Na}^-)_2$ .
- A-3. Bond Angles (in Degrees) for  $(\text{Cs}^+)_2(21\text{C7})_2(\text{Na}^-)_2$ .
- A-4. Positional Parameters and Their Estimated Standard Deviations for  $(\text{K}^+)_2(21\text{C7})_3(\text{MeNH}_2)(\text{Na}^-)_2$ .
- A-5. Bond Distances (in Angstroms) for  $(\text{K}^+)_2(21\text{C7})_3(\text{MeNH}_2)(\text{Na}^-)_2$ .
- A-6. Bond Angles (in Degrees) for  $(\text{K}^+)_2(21\text{C7})_3(\text{MeNH}_2)(\text{Na}^-)_2$ .
- A-7. Positional Parameters and Their Estimated Standard Deviations for  $\text{K}^+(\text{dicyclohexano-24C8})\text{Na}^-$ .
- A-8. Bond Distances (in Angstroms) for  $\text{K}^+(\text{dicyclohexano-24C8})\text{Na}^-$ .
- A-9. Bond Angles (in Degrees) for  $\text{K}^+(\text{dicyclohexano-24C8})\text{Na}^-$ .
- A-10. Positional Parameters and Their Estimated Standard Deviations for  $\text{Rb}^+(18\text{C6})(12\text{C4})\text{Na}^-$ .
- A-11. Bond Distances (in Angstroms) for  $\text{Rb}^+(18\text{C6}(12\text{C4})\text{Na}^-$  (I) and  $\text{Rb}^+(18\text{C6}(12\text{C4})\text{Rb}^-$  (II).
- A-12. Bond Angles (in Degrees) for  $\text{Rb}^+(18\text{C6}(12\text{C4})\text{Na}^-$  (I) and

$\text{Rb}^+(18\text{C}6(12\text{C}4)\text{Rb}^-(\text{II}))$ .

A-13. Positional Parameters and Their Estimated Standard  
Deviations for  $\text{Rb}^+(18\text{C}6)(12\text{C}4)\text{Rb}^-$ .

The parameters for hydrogen atoms have not been included, as **they** were constrained in all five structures to ride on the carbon **atoms** to which they belong in all five structures.

Table A-1. Positional Parameters and Their Estimated Standard Deviations for  $(\text{Cs}^+)_2(21\text{C7})_2(\text{Na}^-)_2$

Atom	x	y	z	B( $\text{\AA}^2$ )
Cs1	0.8398	0.5070	0.5043	4.9(3)*
Cs2	0.3975(2)	0.3116(2)	0.8516(2)	4.2(3)*
Na1	1.253(2)	0.836(2)	0.394(2)	7(2)*
Na2	0.975(3)	0.978(3)	0.968(2)	9(2)*
O1	0.266(3)	0.584(3)	0.837(2)	6.9(8)
O4	0.353(3)	0.449(3)	0.634(2)	3.3(7)
O7	0.531(3)	0.276(3)	0.575(2)	7.0(9)
O10	0.524(2)	0.070(2)	0.756(2)	2.9(4)
O13	0.482(2)	0.112(2)	0.984(1)	3.7(4)
O16	0.492(2)	0.373(3)	1.087(2)	6.1(6)
O19	0.351(3)	0.570(3)	1.031(3)	10(1)
O101	0.953(2)	0.245(2)	0.492(2)	2.0(4)
O104	0.918(2)	0.335(2)	0.296(2)	4.8(5)
O107	0.754(2)	0.532(3)	0.256(2)	5.6(6)
O110	0.751(2)	0.773(2)	0.404(2)	4.6(5)
O113	0.712(3)	0.758(3)	0.642(2)	5.9(7)
O116	0.694(3)	0.535(3)	0.783(2)	2.8(7)
O119	0.904(3)	0.370(3)	0.700(2)	3.4(7)
C2	0.224(4)	0.578(4)	0.744(3)	5(1)
C3	0.335(5)	0.601(6)	0.652(5)	7(2)
C5	0.425(3)	0.427(3)	0.527(2)	2.9(8)
C6	0.422(3)	0.284(3)	0.522(3)	7.5(8)
C8	0.568(4)	0.140(4)	0.568(3)	3.5(8)
C9	0.465(4)	0.029(4)	0.661(3)	4.1(8)
C11	0.445(3)	-0.042(3)	0.842(3)	4.7(7)
C12	0.540(4)	-0.019(4)	0.915(3)	7(1)
C14	0.549(4)	0.152(4)	1.071(3)	6(1)
C15	0.442(5)	0.244(6)	1.147(4)	11(2)
C17	0.438(4)	0.472(4)	1.152(3)	5.3(9)
C18	0.459(5)	0.574(5)	1.097(4)	11(1)

**Table A-1. Positional Parameters and Their Estimated Standard Deviations for (Cs<sup>+</sup>)<sub>2</sub>(21C7)<sub>2</sub>(Na<sup>-</sup>)<sub>2</sub> (Continued)**

Atom	x	y	z	B(Å <sup>2</sup> )
C20	0.264(7)	0.621(6)	1.038(5)	11(2)
C21	0.171(4)	0.576(4)	0.944(3)	5(1)
C102	1.044(3)	0.245(3)	0.381(3)	3.4(8)
C103	0.980(6)	0.239(5)	0.311(4)	7(1)
C105	0.841(4)	0.306(4)	0.218(3)	6(1)
C106	0.837(4)	0.446(4)	0.173(3)	6(1)
C108	0.782(4)	0.660(4)	0.225(3)	5.9(9)
C109	0.704(4)	0.741(4)	0.307(3)	7(1)
C111	0.721(5)	0.859(5)	0.480(4)	9(1)
C112	0.771(3)	0.887(3)	0.565(3)	5.4(8)
C114	0.747(4)	0.773(4)	0.737(3)	5(1)
C115	0.658(4)	0.663(4)	0.824(3)	5(1)
C117	0.797(4)	0.511(4)	0.845(3)	1.4(9)
C118	0.802(3)	0.352(3)	0.811(3)	3.5(8)
C120	0.934(3)	0.244(3)	0.700(3)	3.3(6)
C121	1.043(3)	0.251(3)	0.575(3)	3.4(7)

Starred atoms were refined anisotropically.

Table A-2. Bond Distances (in Angstroms) for  $(\text{Cs}^+)_2(21\text{C7})_2(\text{Na}^-)_2$ 

<u>Atom 1</u>	<u>Atom 2</u>	<u>Distance</u>
CS1	O7	3.25(3)
CS1	O101	3.18(2)
CS1	O104	3.18(2)
CS1	O107	3.55(2)
CS1	O110	3.44(2)
CS1	O113	3.43(2)
CS1	O116	3.47(3)
CS1	O119	3.18(3)
CS2	O1	3.44(3)
CS2	O4	3.32(3)
CS2	O7	3.45(3)
CS2	O10	3.16(2)
CS2	O13	3.10(2)
CS2	O16	3.40(2)
CS2	O19	3.48(3)
CS2	O116	3.13(3)
O1	C2	1.38(4)
O1	C21	1.43(4)
O4	C3	1.59(6)
O4	C5	1.41(4)
O7	C6	1.49(4)
O7	C8	1.52(4)
O10	C9	1.50(4)
O10	C11	1.46(3)
O13	C12	1.73(5)
O13	C14	1.46(4)
O16	C15	1.39(6)
O16	C17	1.43(4)
O19	C18	1.59(5)
O19	C20	1.14(6)
O101	C102	1.45(3)

Table A-2. Bond Distances (in Angstroms) for  $(\text{Cs}^+)_2(21\text{C7})_2(\text{Na}^-)_2$   
(Continued)

<u>Atom 1</u>	<u>Atom 2</u>	<u>Distance</u>
O101	C121	1.60(4)
O104	C103	1.35(5)
O104	C105	1.43(4)
O107	C106	1.60(5)
O107	C108	1.27(4)
O110	C109	1.45(4)
O110	C111	1.31(5)
O113	C112	1.49(4)
O113	C114	1.35(4)
O116	C115	1.49(5)
O116	C117	1.58(4)
O119	C118	1.48(4)
O119	C120	1.39(4)
C2	C3	1.36(6)
C5	C6	1.43(5)
C8	C9	1.55(5)
C11	C12	1.52(5)
C14	C15	1.74(6)
C17	C18	1.18(5)
C20	C21	1.73(7)
C102	C103	1.24(6)
C105	C106	1.55(5)
C108	C109	1.51(5)
C111	C112	1.32(5)
C114	C115	1.46(5)
C117	C118	1.66(5)
C120	C121	1.65(4)

**Estimated standard deviations in the least significant figure are given in parentheses.**

Table A-3. Bond Angles (in Degrees) for  $(\text{Cs}^+)_2(21\text{C7})_2(\text{Na}^-)_2$ 

<u>Atom 1</u>	<u>Atom 2</u>	<u>Atom 3</u>	<u>Angle</u>
O7	CS1	O101	85.2(7)
O7	CS1	O104	87.5(7)
O7	CS1	O107	81.5(7)
O7	CS1	O110	97.8(7)
O7	CS1	O113	91.9(7)
O7	CS1	O116	73.9(7)
O7	CS1	O119	88.0(7)
O101	CS1	O104	52.5(5)
O101	CS1	O107	106.5(6)
O101	CS1	O110	156.5(5)
O101	CS1	O113	153.0(5)
O101	CS1	O116	105.7(6)
O101	CS1	O119	54.0(6)
O104	CS1	O107	54.9(6)
O104	CS1	O110	104.1(5)
O104	CS1	O113	154.3(6)
O104	CS1	O116	153.2(6)
O104	CS1	O119	106.5(6)
O107	CS1	O110	51.5(6)
O107	CS1	O113	99.5(6)
O107	CS1	O116	137.2(6)
O107	CS1	O119	158.8(7)
O110	CS1	O113	50.5(5)
O110	CS1	O116	97.5(6)
O110	CS1	O119	149.0(6)
O113	CS1	O116	48.2(6)
O113	CS1	O119	99.2(7)
O116	CS1	O119	54.8(6)
O1	CS2	O4	51.5(7)
O1	CS2	O7	100.1(7)
O1	CS2	O10	154.9(6)
O1	CS2	O13	151.1(6)

Table A-3. Bond Angles (in Degrees) for  $(\text{Cs}^+)_2(21\text{C7})_2(\text{Na}^-)_2$   
(Continued)

<u>Atom 1</u>	<u>Atom 2</u>	<u>Atom 3</u>	<u>Angle</u>
O1	CS2	O16	100.5(6)
O1	CS2	O19	48.8(7)
O1	CS2	O116	86.6(7)
O4	CS2	O7	49.8(7)
O4	CS2	O10	103.5(6)
O4	CS2	O13	157.5(6)
O4	CS2	O16	146.6(6)
O4	CS2	O19	98.8(7)
O4	CS2	O116	85.2(7)
O7	CS2	O10	55.5(7)
O7	CS2	O13	108.2(6)
O7	CS2	O16	142.1(6)
O7	CS2	O19	140.0(8)
O7	CS2	O116	75.7(6)
O10	CS2	O13	54.0(5)
O10	CS2	O16	103.1(5)
O10	CS2	O19	154.4(7)
O10	CS2	O116	91.7(6)
O13	CS2	O16	52.6(6)
O13	CS2	O19	103.1(7)
O13	CS2	O116	94.5(6)
O16	CS2	O19	51.8(7)
O16	CS2	O116	74.1(6)
O19	CS2	O116	77.7(7)
CS2	O1	C2	109(2)
CS2	O1	C21	103(2)
C2	O1	C21	122(3)
CS2	O4	C3	113(2)
CS2	O4	C5	120(2)
C3	O4	C5	116(3)
CS1	O7	CS2	104.2(8)

Table A-3. Bond Angles (in Degrees) for  $(\text{Cs}^+)_2(21\text{C7})_2(\text{Na}^-)_2$   
(Continued)

<u>Atom 1</u>	<u>Atom 2</u>	<u>Atom 3</u>	<u>Angle</u>
CS1	O7	C6	121(2)
CS1	O7	C8	101(2)
CS2	O7	C6	106(2)
CS2	O7	C8	106(2)
C6	O7	C8	117(3)
CS2	O10	C9	103(2)
CS2	O10	C11	101(2)
C9	O10	C11	105(2)
CS2	O13	C12	118(2)
CS2	O13	C14	125(2)
C12	O13	C14	109(2)
CS2	O16	C15	106(2)
CS2	O16	C17	115(2)
C15	O16	C17	109(3)
CS2	O19	C18	102(2)
CS2	O19	C20	122(4)
C18	O19	C20	135(4)
CS1	O101	C102	109(2)
CS1	O101	C121	112(1)
C102	O101	C121	108(2)
CS1	O104	C103	114(3)
CS1	O104	C105	123(2)
C103	O104	105	116(3)
CS1	O107	C106	105(2)
CS1	O107	C108	110(2)
C106	O107	C108	115(3)
CS1	O110	C109	114(2)
CS1	O110	C111	112(3)
C109	O110	C111	129(4)
CS1	O113	C112	107(2)
CS1	O113	C114	108(2)

Table A-3. Bond Angles (in Degrees) for  $(\text{Cs}^+)_2(21\text{C7})_2(\text{Na}^-)_2$   
(Continued)

<u>Atom 1</u>	<u>Atom 2</u>	<u>Atom 3</u>	<u>Angle</u>
C112	O113	C114	115(3)
CS1	O116	CS2	106.2(7)
CS1	O116	C115	122(2)
CS1	O116	C117	107(2)
CS2	O116	C115	101(2)
CS2	O116	C117	114(2)
C115	O116	C117	107(2)
CS1	O119	C118	118(2)
CS1	O119	C120	126(2)
C118	O119	C120	99(2)
O1	C2	C3	111(4)
O4	C3	C2	103(4)
O4	C5	C6	109(3)
O7	C6	C5	104(3)
O7	C8	C9	112(3)
O10	C9	C8	102(3)
O10	C11	C12	102(3)
O13	C12	C11	95(3)
O13	C14	C15	100(3)
O16	C15	C14	103(4)
O16	C17	C18	110(4)
O19	C18	C17	117(4)
O19	C20	C21	116(5)
O1	C21	C20	109(3)
O101	C102	C103	112(4)
O104	C103	C102	124(5)
O104	C105	C106	108(3)
O107	C106	C105	117(3)
O107	C108	C109	114(3)
O110	C109	C108	116(3)
O110	C111	C112	127(5)

Table A-3. Bond Angles (in Degrees) for  $(\text{Cs}^+)_2(21\text{C7})_2(\text{Na}^-)_2$   
(Continued)

<u>Atom 1</u>	<u>Atom 2</u>	<u>Atom 3</u>	<u>Angle</u>
O113	C112	C111	108(3)
O113	C114	C115	114(4)
O116	C115	C114	104(3)
O116	C117	C118	101(2)
O119	C118	C117	106(3)
O119	C120	C121	103(2)
O101	C121	C120	105(2)

Estimated standard deviations in the least significant figure are given in parentheses.

Table A-4. Positional Parameters and Their Estimated Standard Deviations for  $(K^+)_2(21C7)_3(MeNH_2)(Na^-)_2$

Atom	x	y	z	B(Å <sup>2</sup> )
K1	0.9729(5)	0.2507(1)	0.2523(2)	3.2(1)
K2	0.6495(6)	0.5117(2)	0.2490(3)	6.2(2)
Na1	0.536(1)	0.1180(3)	0.4702(5)	6.9(3)
Na2	0.458(1)	0.1169(3)	0.0473(5)	6.3(3)
O1	0.462(1)	0.2376(4)	0.3141(7)	3.9(4)
O4	0.409(2)	0.2991(4)	0.4087(7)	3.7(4)
O7	0.437(2)	0.3783(4)	0.3686(7)	4.2(4)
O10	0.502(2)	0.4424(4)	0.2705(8)	6.2(4)
O13	0.523(2)	0.3883(4)	0.1584(8)	5.6(4)
O16	0.608(2)	0.3131(4)	0.1103(6)	3.7(4)
O19	0.645(1)	0.2433(4)	0.1963(7)	4.0(4)
O101	1.144(2)	0.3172(4)	0.2635(7)	4.1(4)
O104	1.189(2)	0.2697(4)	0.1521(8)	4.9(4)
O107	0.982(1)	0.2139(4)	0.1195(7)	3.5(3)
O110	1.039(2)	0.1745(3)	0.2491(8)	4.4(4)
O113	1.038(2)	0.2078(4)	0.3794(7)	4.0(4)
O116	0.835(1)	0.2662(4)	0.3777(7)	3.6(4)
O119	0.835(2)	0.3195(3)	0.2663(7)	3.6(4)
O201	0.871(4)	0.472(1)	0.167(2)	19(1)*
O204	0.902(3)	0.4681(8)	0.312(2)	18(1)*
O207	0.751(4)	0.512(1)	0.402(2)	21(1)*
O210	0.453(4)	0.550(1)	0.336(2)	18(1)*
O213	0.285(5)	0.536(1)	0.232(3)	20(2)*
O216	0.364(2)	0.5208(6)	0.103(1)	18.2(7)*
O219	0.637(3)	0.5167(8)	0.097(1)	16(1)*
N1	0.828(2)	0.5783(5)	0.244(1)	5.7(5)
C2	0.449(2)	0.2352(5)	0.390(1)	3.4(5)
C3	0.332(2)	0.2645(6)	0.406(1)	3.4(5)
C5	0.306(2)	0.3288(6)	0.424(1)	3.9(6)
C6	0.396(2)	0.3635(5)	0.434(1)	2.9(5)

**Table A-4. Positional Parameters and Their Estimated Standard Deviations for  $(K^+)_2(21C7)_3(MeNH_2)(Na^-)_2$  (Continued)**

Atom	x	y	z	B(Å <sup>2</sup> )
C8	0.543(3)	0.4087(6)	0.378(1)	4.7(6)
C9	0.604(3)	0.4169(6)	0.308(1)	5.3(7)
C11	0.377(3)	0.4276(6)	0.229(1)	5.1(7)
C12	0.414(3)	0.4195(6)	0.154(1)	5.2(6)
C14	0.556(2)	0.3774(6)	0.088(1)	4.1(6)
C15	0.678(3)	0.3485(6)	0.100(1)	4.8(6)
C17	0.721(2)	0.2841(6)	0.107(1)	3.7(5)
C18	0.635(2)	0.2481(6)	0.119(1)	3.4(5)
C20	0.555(2)	0.2115(6)	0.214(1)	3.8(5)
C21	0.569(2)	0.2115(6)	0.295(1)	3.5(5)
C102	1.291(3)	0.3133(6)	0.232(1)	5.1(6)
C103	1.258(3)	0.3054(6)	0.160(1)	5.2(6)
C105	1.130(2)	0.2621(5)	0.083(1)	3.2(5)
C106	1.107(2)	0.2220(5)	0.078(1)	3.3(5)
C108	0.966(2)	0.1741(6)	0.129(1)	3.6(5)
C109	1.083(2)	0.1594(5)	0.183(1)	3.6(6)
C111	1.150(2)	0.1645(6)	0.306(1)	4.6(6)
C112	1.069(2)	0.1696(6)	0.371(1)	4.7(6)
C114	0.951(2)	0.2148(5)	0.438(1)	2.9(5)
C115	0.927(2)	0.2556(6)	0.443(1)	3.2(5)
C117	0.764(2)	0.3028(6)	0.381(1)	3.0(5)
C118	0.710(2)	0.3139(5)	0.309(1)	3.2(5)
C120	0.928(2)	0.3497(6)	0.292(1)	3.7(6)
C121	1.061(2)	0.3502(6)	0.243(1)	4.6(6)
C202	0.928(4)	0.447(1)	0.204(2)	10(1)*
C203	0.997(4)	0.4589(9)	0.272(2)	10(1)*
C205	0.957(4)	0.4796(9)	0.380(2)	10(1)*
C206	0.837(5)	0.489(1)	0.421(2)	17(2)*
C208	0.622(4)	0.524(1)	0.424(2)	12(1)*
C209	0.557(6)	0.555(1)	0.404(3)	18(2)*

Table A-4. Positional Parameters and Their Estimated Standard Deviations for  $(K^+)_2(21C7)_3(MeNH_2)(Na^-)_2$  (Continued)

Atom	x	y	z	B(Å <sup>2</sup> )
C211	0.374(6)	0.534(1)	0.371(3)	18(2)*
C212	0.256(4)	0.546(1)	0.302(2)	15(1)*
C214	0.247(9)	0.551(2)	0.188(4)	40(4)*
C215	0.186(6)	0.515(2)	0.127(3)	29(2)*
C217	0.430(4)	0.555(1)	0.105(2)	16(1)*
C218	0.571(4)	0.541(1)	0.060(2)	14(1)*
C220	0.768(4)	0.504(1)	0.071(2)	10(1)*
C221	0.820(5)	0.476(1)	0.115(2)	13(2)*
C301	0.725(3)	0.6079(7)	0.243(1)	7.3(8)

Starred atoms were refined isotropically.

Table A-5. Bond Distances (in Angstroms) for  
 $(K^+)_2(21C7)_3(MeNH_2)(Na^-)_2$

<u>Atom 1</u>	<u>Atom 2</u>	<u>Distance</u>
K1	O19	3.12(1)
K1	O101	2.89(1)
K1	O104	2.97(2)
K1	O107	2.92(1)
K1	O110	2.85(1)
K1	O113	2.95(1)
K1	O116	2.89(1)
K1	O119	2.84(1)
K2	O10	2.92(2)
K2	O201	3.05(4)
K2	O204	2.99(3)
K2	O207	3.04(3)
K2	O210	2.92(4)
K2	O219	2.95(3)
K2	N1	2.94(2)
O1	C2	1.49(2)
O1	C21	1.44(3)
O4	C3	1.45(3)
O4	C5	1.49(3)
O7	C6	1.46(2)
O7	C8	1.48(3)
O10	C9	1.47(3)
O10	C11	1.45(3)
O13	C12	1.51(3)
O13	C14	1.48(3)
O16	C15	1.46(3)
O16	C17	1.49(3)
O19	C18	1.52(2)
O19	C20	1.48(3)
O101	C102	1.53(3)
O101	C121	1.47(3)

Table A-5. Bond Distances (in Angstroms) for  
 $(K^+)_2(21C7)_3(MeNH_2)(Na^+)_2$  (Continued)

<u>Atom 1</u>	<u>Atom 2</u>	<u>Distance</u>
O104	C103	1.45(3)
O104	C105	1.44(2)
O107	C106	1.48(3)
O107	C108	1.48(3)
O110	C109	1.49(3)
O110	C111	1.49(3)
O113	C112	1.44(3)
O113	C114	1.46(2)
O116	C115	1.51(2)
O116	C117	1.49(2)
O119	C118	1.48(3)
O119	C120	1.46(2)
O201	C202	1.24(5)
O201	C221	1.09(6)
O204	C203	1.26(5)
O204	C205	1.45(5)
O207	C206	1.19(6)
O207	C208	1.37(6)
O210	C209	1.58(6)
O210	C211	1.20(6)
O213	C212	1.46(7)
O213	C214	1.07(9)
O216	C215	1.73(6)
O216	C217	1.39(4)
O219	C218	1.27(5)
O219	C220	1.42(5)
N1	C301	1.43(3)
C2	C3	1.56(3)
C5	C6	1.51(3)
C8	C9	1.54(3)
C11	C12	1.55(3)

Table A-5. Bond Distances (in Angstroms) for  
(K<sup>+</sup>)<sub>2</sub>(21C7)<sub>3</sub>(MeNH<sub>2</sub>)(Na<sup>-</sup>)<sub>2</sub> (Continued)

<u>Atom 1</u>	<u>Atom 2</u>	<u>Distance</u>
C14	C15	1.54(3)
C17	C18	1.56(3)
C20	C21	1.58(3)
C102	C103	1.45(3)
C105	C106	1.49(3)
C108	C109	1.53(3)
C111	C112	1.53(3)
C114	C115	1.51(3)
C117	C118	1.51(3)
C120	C121	1.60(3)
C202	C203	1.48(5)
C205	C206	1.45(6)
C208	C209	1.32(7)
C211	C212	1.71(7)
C214	C215	1.8(1)
C217	C218	1.68(5)
C220	C221	1.40(6)

Estimated standard deviations in the least significant figure are given in parentheses.

Table A-6. Bond Angles (in Degrees) for  $(K^+)_2(21C7)_3(MeNH_2)(Na^-)_2$ 

<u>Atom 1</u>	<u>Atom 2</u>	<u>Atom 3</u>	<u>Angle</u>
O19	K1	O101	126.8(4)
O19	K1	O104	117.5(4)
O19	K1	O107	75.2(4)
O19	K1	O110	96.1(4)
O19	K1	O113	111.8(4)
O19	K1	O116	80.9(4)
O19	K1	O119	71.8(4)
O101	K1	O104	57.8(4)
O101	K1	O107	113.6(4)
O101	K1	O110	135.2(4)
O101	K1	O113	108.2(4)
O101	K1	O116	92.4(4)
O101	K1	O119	59.3(4)
O104	K1	O107	57.2(4)
O104	K1	O110	93.5(4)
O104	K1	O113	125.1(4)
O104	K1	O116	150.1(4)
O104	K1	O119	100.3(4)
O107	K1	O110	60.6(4)
O107	K1	O113	118.6(4)
O107	K1	O116	152.0(4)
O107	K1	O119	122.5(4)
O110	K1	O113	58.0(4)
O110	K1	O116	108.5(4)
O110	K1	O119	164.7(5)
O113	K1	O116	57.9(4)
O113	K1	O119	116.9(4)
O116	K1	O119	61.2(4)
O10	K2	O201	89.6(8)
O10	K2	O204	80.0(7)
O10	K2	O207	88.0(8)
O10	K2	O210	91.3(8)

Table A-6. Bond Angles (in Degrees) for  $(K^+)_2(21C7)_3(MeNH_2)(Na^-)_2$   
(Continued)

<u>Atom 1</u>	<u>Atom 2</u>	<u>Atom 3</u>	<u>Angle</u>
O10	K2	O219	102.6(7)
O10	K2	N1	171.6(5)
O201	K2	O204	55.6(9)
O201	K2	O207	110(1)
O201	K2	O210	176(1)
O201	K2	O219	58.6(9)
O201	K2	N1	89.2(8)
O204	K2	O207	55(1)
O204	K2	O210	121(1)
O204	K2	O219	114.2(9)
O204	K2	N1	92.5(7)
O207	K2	O210	66(1)
O207	K2	O219	164(1)
O207	K2	N1	84.6(8)
O210	K2	O219	124.9(9)
O210	K2	N1	89.4(8)
O219	K2	N1	83.8(7)
C2	O1	C21	109(1)
C3	O4	C5	109(1)
C6	O7	C8	113(1)
K2	O10	C9	110(1)
K2	O10	C11	127(1)
C9	O10	C11	119(2)
C12	O13	C14	110(2)
C15	O16	C17	108(2)
K1	O19	C18	109(1)
K1	O19	C20	121(1)
C18	O19	C20	109(1)
K1	O101	C102	112(1)
K1	O101	C121	114(1)
C102	O101	C121	115(2)

**Table A-6. Bond Angles (in Degrees) for  $(K^+)_2(21C7)_3(MeNH_2)(Na^-)_2$**   
(Continued)

<u>Atom 1</u>	<u>Atom 2</u>	<u>Atom 3</u>	<u>Angle</u>
K1	O104	C103	117(1)
K1	O104	C105	111(1)
C103	O104	C105	113(2)
K1	O107	C106	118(1)
K1	O107	C108	110(1)
C106	O107	C108	111(1)
K1	O110	C109	117(1)
K1	O110	C111	111(1)
C109	O110	C111	110(1)
K1	O113	C112	117(1)
K1	O113	C114	118(1)
C112	O113	C114	112(2)
K1	O116	C115	114(1)
K1	O116	C117	116(1)
C115	O116	C117	114(1)
K1	O119	C118	108(1)
K1	O119	C120	117(1)
C118	O119	C120	111(1)
K2	O201	C202	108(3)
K2	O201	C221	100(3)
C202	O201	C221	140(4)
K2	O204	C203	116(2)
K2	O204	C205	115(2)
C203	O204	C205	116(3)
K2	O207	C206	117(3)
K2	O207	C208	96(2)
C206	O207	C208	134(4)
K2	O210	C209	101(3)
K2	O210	C211	121(3)
C209	O210	C211	85(4)
C212	O213	C214	123(6)

Table A-6. Bond Angles (in Degrees) for  $(K^+)_2(21C7)_3(MeNH_2)(Na^-)_2$   
(Continued)

<u>Atom 1</u>	<u>Atom 2</u>	<u>Atom 3</u>	<u>Angle</u>
C215	O216	C217	121(3)
K2	O219	C218	126(2)
K2	O219	C220	112(2)
C218	O219	C220	114(3)
K2	N1	C301	105(1)
O1	C2	C3	106(1)
O4	C3	C2	106(2)
O4	C5	C6	107(2)
O7	C6	C5	112(2)
O7	C8	C9	108(2)
O10	C9	C8	108(2)
O10	C11	C12	112(2)
O13	C12	C11	106(2)
O13	C14	C15	104(2)
O16	C15	C14	108(2)
O16	C17	C18	103(2)
O19	C18	C17	105(1)
O19	C20	C21	103(2)
O1	C21	C20	105(2)
O101	C102	C103	107(2)
O104	C103	C102	110(2)
O104	C105	C106	107(2)
O107	C106	C105	106(2)
O107	C108	C109	111(2)
O110	C109	C108	104(2)
O110	C111	C112	104(2)
O113	C112	C111	109(2)
O113	C114	C115	108(2)
O116	C115	C114	106(1)
O116	C117	C118	108(2)
O119	C118	C117	111(2)

Table A-6. Bond Angles (in Degrees) for  $(K^+)_2(21C7)_3(MeNH_2)(Na^-)_2$   
(Continued)

<u>Atom 1</u>	<u>Atom 2</u>	<u>Atom 3</u>	<u>Angle</u>
O119	C120	C121	105(2)
O101	C121	C120	103(2)
O201	C202	C203	116(3)
O204	C203	C202	111(3)
O204	C205	C206	110(3)
O207	C206	C205	119(4)
O207	C208	C209	125(4)
O210	C209	C208	113(4)
O210	C211	C212	78(3)
O213	C212	C211	121(4)
O213	C214	C215	102(6)
O216	C215	C214	81(4)
O216	C217	C218	94(3)
O219	C218	C217	106(3)
O219	C220	C221	106(3)
O201	C221	C220	140(5)

Estimated standard deviations in the least significant figure are given in parentheses.

**Table A-7. Positional Parameters and Their Estimated Standard Deviations for  $K^+(dicyclohexano-24C8)Na^-$**

Atom	x	y	z	B(Å <sup>2</sup> )
K1	0.000	0.500	0.1444(4)	2.8(2)
K2	0.000	0.000	0.3562(6)	8.0(4)
Na1	0.500	0.000	0.147(1)	16(1)
Na2	0.000	0.000	0.6479(8)	6.0(6)
O1	-0.040(2)	0.709(2)	0.0895(7)	4.0(6)
O4	0.059(2)	0.736(1)	0.1796(6)	1.4(4)
O7	0.186(2)	0.525(2)	0.2125(7)	3.1(5)
O10	0.266(3)	0.452(2)	0.125(1)	6.8(8)
O21	-0.084(3)	0.205(3)	0.415(1)	10(1)
O24	0.078(3)	0.233(3)	0.313(1)	10(1)
O27	0.189(3)	0.012(3)	0.2848(9)	6.6(7)
O30	0.254(3)	-0.066(2)	0.380(1)	7.4(8)
C2	-0.052(4)	0.836(4)	0.115(2)	9(2)
C3	0.103(3)	0.827(3)	0.136(1)	5(1)
C5	0.182(3)	0.764(3)	0.213(1)	6(1)
C6	0.185(3)	0.635(3)	0.243(1)	5(1)
C8	0.315(3)	0.504(3)	0.202(1)	3.5(7)
C9	0.331(3)	0.402(3)	0.161(1)	4(1)
C11	0.287(4)	0.362(4)	0.087(1)	8(1)
C12	-0.176(3)	0.707(3)	0.065(1)	3.0(7)
C13	-0.279(7)	0.770(6)	0.026(2)	23(3)
C14	-0.134(4)	0.660(4)	-0.006(2)	11(1)
C15	-0.244(5)	0.568(3)	-0.008(2)	9(1)
C16	-0.263(4)	0.505(4)	0.044(1)	11(1)
C22	-0.038(4)	0.319(3)	0.389(1)	5(1)
C23	0.063(3)	0.327(3)	0.353(1)	5(1)
C25	0.168(3)	0.223(3)	0.282(1)	3.5(8)
C26	0.147(3)	0.121(3)	0.254(1)	3.1(8)
C28	0.329(4)	0.028(4)	0.308(1)	8(1)
C29	0.321(4)	-0.088(4)	0.330(2)	8(1)

Table A-7. Positional Parameters and Their Estimated Standard Deviations for  $\text{K}^+(24\text{C8})\text{Na}^-$  (Continued)

Atom	x	y	z	B( $\text{\AA}^2$ )
C31	0.259(3)	-0.206(2)	0.4126(9)	1.9(6)
C32	-0.184(4)	0.261(4)	0.478(1)	10(1)
C33	0.405(4)	-0.160(4)	0.444(1)	10(1)
C34	0.370(3)	-0.068(3)	0.480(1)	7(1)
C35	0.257(4)	-0.112(4)	0.514(2)	8(1)
C36	0.147(3)	-0.079(3)	0.466(1)	8(1)

All atoms were refined isotropically.

Table A-8. Bond Distances (in Angstroms) for  
 $\text{K}^+(\text{dicyclohexano-24C8})\text{Na}^-$

<u>Atom 1</u>	<u>Atom 2</u>	<u>Distance</u>
K1	O1	2.79(2)
K1	O4	2.83(2)
K1	O7	2.71(3)
K1	O10	2.81(3)
K2	O21	2.87(4)
K2	O24	2.92(3)
K2	O27	2.81(3)
K2	O30	2.90(3)
O1	C2	1.55(4)
O1	C12	1.50(4)
O4	C3	1.46(4)
O4	C5	1.63(4)
O7	C6	1.44(4)
O7	C8	1.40(4)
O10	C9	1.43(4)
O10	C11	1.50(5)
O21	C22	1.44(5)
O21	C32	1.62(5)
O24	C23	1.64(5)
O24	C25	1.24(4)
O27	C26	1.53(4)
O27	C28	1.53(5)
O30	C29	1.50(5)
O30	C31	1.67(3)
C2	C3	1.65(5)
C5	C6	1.60(5)
C8	C9	1.63(4)
C11	C12	1.51(4)
C11	C16	1.75(6)
C12	C13	1.71(5)

Table A-8. Bond Distances (in Angstroms) for  
K<sup>+</sup>(dicyclohexano-24C8)Na<sup>-</sup> (Continued)

<u>Atom 1</u>	<u>Atom 2</u>	<u>Distance</u>
C13	C14	1.67(5)
C14	C15	1.67(5)
C15	C16	1.54(6)
C22	C23	1.49(5)
C25	C26	1.36(5)
C28	C29	1.31(5)
C31	C32	1.57(5)
C31	C33	1.77(5)
C32	C36	1.61(5)
C33	C34	1.58(6)
C34	C35	1.62(6)
C35	C36	1.77(5)

Estimated standard deviations in the least significant figure are given in parentheses.

Table A-9. Bond Angles (in Degrees) for  $\text{K}^+(\text{dicyclohexano-24C8})\text{Na}^-$ 

<u>Atom 1</u>	<u>Atom 2</u>	<u>Atom 3</u>	<u>Angle</u>
O1	K1	O1	113(1)
O1	K1	O4	59.0(6)
O1	K1	O4	154.1(6)
O1	K1	O7	114.1(7)
O1	K1	O7	110.9(7)
O1	K1	O10	100.6(7)
O1	K1	O10	66.5(7)
O4	K1	O4	139.4(9)
O4	K1	O7	60.0(6)
O4	K1	O7	91.2(7)
O4	K1	O10	90.1(6)
O4	K1	O10	97.6(6)
O7	K1	O7	93(1)
O7	K1	O10	57.3(7)
O7	K1	O10	143.8(9)
O10	K1	O10	158(1)
O21	K2	O21	115(1)
O21	K2	O24	66.4(9)
O21	K2	O24	147.1(9)
O21	K2	O27	123(1)
O21	K2	O27	102.8(9)
O21	K2	O30	110.7(9)
O21	K2	O30	54.1(8)
O24	K2	O24	132(1)
O24	K2	O27	59.2(9)
O24	K2	O27	86.4(9)
O24	K2	O30	93.7(7)
O24	K2	O30	96.3(8)
O27	K2	O27	90(1)
O27	K2	O30	60.2(7)
O27	K2	O30	143.5(9)

Table A-9. Bond Angles (in Degrees) for  $\text{K}^+(\text{dicyclohexano-24C8})\text{Na}^-$   
(Continued)

<u>Atom 1</u>	<u>Atom 2</u>	<u>Atom 3</u>	<u>Angle</u>
O30	K2	O30	155(1)
K1	O1	C2	121(2)
K1	O1	C12	109(2)
C2	O1	C12	101(3)
K1	O4	C3	117(2)
K1	O4	C5	120(2)
C3	O4	C5	93(2)
K1	O7	C6	119(2)
K1	O7	C8	124(2)
C6	O7	C8	106(3)
K1	O10	C9	115(2)
K1	O10	C11	118(2)
C9	O10	C11	99(3)
K2	O21	C22	111(3)
K2	O21	C32	125(3)
C22	O21	C32	119(4)
K2	O24	C23	102(2)
K2	O24	C25	116(3)
C23	O24	C25	130(3)
K2	O27	C26	101(2)
K2	O27	C28	109(2)
C26	O27	C28	113(3)
K2	O30	C29	105(2)
K2	O30	C31	113(2)
C29	O30	C31	115(3)
O1	C2	C3	104(3)
O4	C3	C2	102(3)
O4	C5	C6	99(3)
O7	C6	C5	111(3)
O7	C8	C9	109(3)

Table A-9. Bond Angles (in Degrees) for  $\text{K}^+(\text{dicyclohexano-24C8})\text{Na}^-$   
(Continued)

<u>Atom 1</u>	<u>Atom 2</u>	<u>Atom 3</u>	<u>Angle</u>
O10	C9	C8	98(3)
O10	C11	C12	111(3)
O10	C11	C16	93(3)
C12	C11	C16	104(3)
O1	C12	C11	132(2)
O1	C12	C13	120(3)
C11	C12	C13	105(3)
C12	C13	C14	85(3)
C13	C14	C15	95(3)
C14	C15	C16	117(4)
C11	C16	C15	107(4)
O21	C22	C23	112(4)
O24	C23	C22	113(3)
O24	C25	C26	111(4)
O27	C26	C25	113(3)
O27	C28	C29	99(4)
O30	C29	C28	111(4)
O30	C31	C32	116(3)
O30	C31	C33	99(2)
C32	C31	C33	95(2)
O21	C32	C31	79(3)
O21	C32	C36	92(3)
C31	C32	C36	102(3)
C31	C33	C34	107(3)
C33	C34	C35	112(4)
C34	C35	C36	86(3)
C32	C36	C35	73(2)

Estimated standard deviations in the least significant figure are given in parentheses.

Table A-10. Positional Parameters and Their Estimated Standard Deviations for  $\text{Rb}^+(18\text{C}6)(12\text{C}4)\text{Na}^-$

Atom	x	y	z	B(Å <sup>2</sup> )
Rb	0.3930(1)	1/4	0.35033(8)	3.00(5)
Na	0.1019(6)	3/4	0.3595(4)	8.3(4)
O1	0.5803(6)	1/4	0.4434(5)	4.4(5)
O4	0.5076(4)	0.0667(5)	0.3872(5)	5.2(4)
O7	0.4262(5)	0.0756(6)	0.2349(5)	6.3(5)
O10	0.3476(6)	1/4	0.1765(6)	6.6(7)
O11	0.2055(4)	0.3545(5)	0.3433(4)	6.0(4)
O14	0.2951(5)	0.3518(6)	0.4968(5)	7.6(5)
C2	0.5781(7)	0.1645(9)	0.4916(6)	6.5(7)
C3	0.5873(7)	0.0769(9)	0.4386(7)	6.2(7)
C5	0.518(1)	-0.0084(9)	0.3293(9)	8.0(9)
C6	0.431(1)	-0.015(1)	0.279(1)	10(1)
C8	0.350(1)	0.075(1)	0.1795(9)	11(1)
C9	0.358(1)	0.162(1)	0.1266(7)	10(1)
C12A	0.151(1)	0.396(1)	0.400(1)	3.3(4)*
C12B	0.215(2)	0.437(2)	0.414(1)	4.4(6)*
C13A	0.222(2)	0.383(2)	0.499(2)	6.4(7)*
C13B	0.228(2)	0.440(2)	0.457(1)	4.0(5)*
C15A	0.302(1)	0.260(6)	0.574(1)	7.6(8)*
C15B	0.246(1)	0.326(1)	0.561(1)	4.6(5)*
C16A	0.136(1)	0.278(1)	0.2907(7)	2.6(4)*
C16B	0.125(1)	0.312(1)	0.344(1)	4.7(5)*

Starred atoms were refined isotropically and the multiplicities are all 0.5.

Table A-11. Bond Distances (in Angstroms) for  
 $\text{Rb}^+(18\text{C}6(12\text{C}4)\text{Na}^-(\text{I}))$  and  $\text{Rb}^+(18\text{C}6(12\text{C}4)\text{Rb}^-(\text{II}))$

Atom 1	Atom 2	Distance	
		I	II
Rb	O1	3.046(8)	3.05(1)
Rb	O4	3.038(7)	3.004(8)
Rb	O7	3.101(8)	3.08(1)
RB	O10	2.969(9)	2.98(2)
Rb	O11	2.988(6)	2.964(7)
RB	O14	3.128(7)	3.155(9)
O1	C2	1.42(1)	1.40(1)
O4	C3	1.41(1)	1.41(2)
O4	C5	1.42(1)	1.43(2)
O7	C6	1.44(2)	1.41(3)
O7	C8	1.41(1)	1.42(3)
O10	C9	1.47(1)	1.44(3)
O11	C12A	1.34(2)	1.27(2)
O11	C12B	1.64(2)	1.55(3)
O11	C16A	1.68(1)	1.78(2)
O11	C16B	1.27(2)	1.26(2)
O14	C13A	1.11(2)	1.12(3)
O14	C13B	1.67(2)	1.70(3)
O14	C15A	1.80(5)	1.67(3)
O14	C15B	1.33(2)	1.29(2)
C2	C3	1.49(1)	1.49(2)
C5	C6	1.48(2)	1.48(3)
C8	C9	1.49(2)	1.52(5)
C12A	C13B*	1.56(3)	1.69(4)
C12B	C13A*	1.60(3)	1.51(4)
C15A	C15B*	1.43(6)	1.60(3)
C16A	C16B*	1.53(2)	1.41(3)

\* Atoms at X, 0.5-Y, Z position. Estimated standard deviations in the least significant figure are given in parentheses.

Table A-12. Bond Angles (in Degrees) for  $\text{Rb}^+(\text{18C6(12C4)Na}^-(\text{I}))$  and  $\text{Rb}^+(\text{18C6(12C4)Rb}^-(\text{II}))$

<u>Atom 1</u>	<u>Atom 2</u>	<u>Atom 3</u>	<u>Angle I</u>	<u>Angle II</u>
O1	Rb	O4	56.1(1)	55.8(2)
O1	Rb	O7	100.8(2)	101.1(3)
O1	RB	O10	133.0(2)	134.2(4)
O1	RB	O11	140.8(2)	140.2(3)
O1	RB	O14	88.8(2)	88.7(3)
O4	RB	O4*	111.2(3)	110.5(4)
O4	RB	O7	54.0(2)	54.7(4)
O4	RB	O10	108.1(2)	108.9(3)
O4	RB	O11	94.4(2)	94.6(3)
O4	RB	O14	72.9(2)	72.2(2)
O7	RB	O7*	100.6(3)	99.8(6)
O7	RB	O10	54.9(2)	54.9(3)
O7	Rb	O11	74.9(2)	75.4(2)
O7	RB	O14	102.0(2)	101.6(4)
O10	RB	O11	76.9(2)	76.6(3)
O10	RB	O14	132.0(2)	130.7(3)
O11	Rb	O11*	57.1(3)	57.1(4)
O11	Rb	O14	55.5(2)	54.6(3)
O14	RB	O14*	52.9(3)	54.5(5)
C2	O1	C2	111(1)	113.2(2)
C3	O4	C5	113.9(9)	112(1)
C6	O7	C8	111(1)	110(3)
C9	O10	C9	110(1)	110(3)
C12A	O11	C16A	108(1)	100(2)
C12B	O11	C16B	112(1)	110(2)
C13A	O14	C15A	107(2)	112(2)
C13B	O14	C15B	103(1)	107(2)
O1	C2	C3	108.9(9)	110(2)
O4	C3	C2	111.7(9)	109(2)
O4	C5	C6	110(1)	109(2)
O7	C6	C5	106(1)	109(2)

Table A-12. Bond Angles (in Degrees) for  $\text{Rb}^+(\text{18C6(12C4)Na}^-(\text{I}))$  and  $\text{Rb}^+(\text{18C6(12C4)Rb}^-(\text{II}))$  (Continued)

<u>Atom 1</u>	<u>Atom 2</u>	<u>Atom 3</u>	<u>Angle I</u>	<u>Angle II</u>
O7	C8	C9	110(1)	108(3)
O10	C9	C8	108.1(9)	108(2)
O11	C12A	C13B	101(1)	90(2)
O11	C12B	C13A	109(2)	116(3)
O14	C13A	C12B	102(2)	110(3)
O14	C13B	C12A	102(2)	106(2)
O14	C15A	C15B*	116(2)	117(2)
O14	C15B	C15A*	93(2)	93(2)
O11	C16A	C16B*	105(1)	105(1)
O11	C16B	C16A*	106(2)	111(2)

\* Atoms at X, 0.5-Y, Z position.

Estimated standard deviations in the least significant figure are given in parentheses.

Table A-13. Positional Parameters and Their Estimated Standard Deviations for  $\text{Rb}^+(18\text{C}6)(12\text{C}4)\text{Rb}^-$

Atom	x	y	z	B(Å <sup>2</sup> )
Rb	0.3921(1)	1/4	0.3540(1)	3.8(1)
Rb <sup>-</sup>	0.1032(2)	3/4	0.3520(1)	8.6(2)
O1	0.5780(8)	1/4	0.4458(7)	6.3(9)
O4	0.5055(6)	0.0757(6)	0.3906(7)	7.1(6)
O7	0.4250(8)	0.0837(9)	0.2407(8)	8.9(8)
O10	0.343(1)	1/4	0.181(1)	10(1)
O11	0.2070(6)	0.3500(6)	0.3489(6)	7.3(6)
O14	0.2941(6)	0.3520(9)	0.4974(6)	10.3(8)
C2	0.575(1)	0.168(1)	0.491(1)	9(1)
C3	0.586(1)	0.083(1)	0.439(1)	12(2)
C5	0.516(1)	0.002(1)	0.334(1)	11(1)
C6	0.430(2)	-0.001(2)	0.284(2)	14(2)
C8	0.346(2)	0.082(3)	0.189(1)	17(3)
C9	0.353(1)	0.167(3)	0.136(1)	19(3)
C12A	0.145(2)	0.378(2)	0.398(2)	4.7(6)*
C12B	0.201(3)	0.423(3)	0.416(2)	8(1)*
C13A	0.223(2)	0.387(2)	0.497(2)	6.3(9)*
C13B	0.231(2)	0.436(2)	0.449(2)	3.8(7)*
C15A	0.302(1)	0.271(3)	0.568(1)	5.4(8)*
C15B	0.242(2)	0.324(2)	0.555(1)	5.2(7)*
C16A	0.137(1)	0.271(2)	0.2918(9)	4.2(7)*
C16B	0.128(2)	0.311(2)	0.339(2)	4.7(7)*

Starred atoms were not refined and the multiplicities are all 0.5.

## APPENDIX B

The Subroutine Program for the Multiple Data Set Fitting

```

C...EQN_2.INC
C...Please enter the equations for CALC and CALCF(i)
C...(i=1,2,...,50)
C...Consider the input format of FORTRAN 77.
      GO TO (1000,1001,1002) JDAT
1000  CONTINUE
      R=DEXP((-3.645d0*SQRT(1.0d0*XX(1)))/
&      (1.0d0+2.88d0*DSQRT(1.0d0*XX(1))))
      A=(-1.0d0+DSQRT(DABS(1.0d0+4.0d0*U(3)*XX(1)*R*R)))/
&      (2.0d0*U(3)*R*R)
      B=U(3)*A*A*R*R
      C=DSQRT(DABS(A/(U(2)*(1.0d0+U(5)*A))))
      D=U(5)*A*C
      CALC=(U(6)*C+U(7)*D+A*U(1)+B*U(4))/XX(1)
      CALCF(1) = CALC
      IF(IMETH.NE.-1) GO TO 35
      RETURN
1001  CONTINUE
      R=DEXP((-3.645d0*SQRT(1.0d0*XX(1)))/
&      (1.0d0+2.88d0*DSQRT(1.0d0*XX(1))))
      A=-1.0d0+SQRT(ABS(1.0d0+4.0d0*U(5)*XX(1)*R*R))
      B=2.0d0*U(5)*XX(1)*R*R
      CALC=(A/B)*(U(6)-U(7))+U(7)
      CALCF(3) = CALC
      IF(IMETH.NE.-1) GO TO 35
      RETURN
1002  CONTINUE
      R=DEXP((-3.645d0*SQRT(1.0d0*XX(1)))/
&      (1.0d0+2.88d0*DSQRT(1.0d0*XX(1))))
      X=ABS(U(11)+XX(1)*U(11)*U(8)*R*R)
      A=(-1.0d0+SQRT(1.0d0+4.0d0*XX(1)*X))/(2.0d0*X)
      B=U(11)*A*A
      C=U(3)*A*(A+B)
      D=U(8)*R*R*B*(A+B)
      CALC=(A*U(1)+B*U(9)+C*U(4)+D*U(10))/XX(1)
      CALCF(4) = CALC
C...XX(1)      = independent variable.
C...CALC      = computer calculated value of Y
C...XX(NOVAR) = refers to an experimental value of Y
C...( X(NOVAR,I) )
C...CALCF(1), CALCF(2), ..... , CALCF(50) are
C...available for functions
C...which can be plotted.
C...constant value are labeled CONST(1), ... CONST(16)

```

## APPENDIX C

### The Subroutine Program for the KINFIT Fitting

```

C...EQN_2.INC
C...Please enter the equations for CALC and CALCF(i)
C...(i=1,2,....,50)
C...=====
C...=====
C...Consider the input format of FORTRAN 77. Do not
C...write before or after
C...the | marks indicated below
C23456789012345678901234567890123456789012345678901234
C567890123456789012345
C----|
C|---
      IF (XX(1).EQ.0.0) GOTO 1007
      A=2.0*XX(1)-CONST(1)+U(3)/U(1)
      B=(1.0+U(3)*XX(1)-CONST(1)*U(3))/U(1)
      C=-CONST(1)/U(1)
      Q=(A*A-3.0*B)/9.0
      Q3=Q**3
      R=(2.0*A**3-9.0*A*B+27.0*C)/54.0
      R2=R*R
      IF (R2.LT.Q3) GOTO 1001
      AA=-(R+SQRT(R2-Q3))**(1/3)
      GOTO 1005
1001  CONTINUE
      AN=R/SQRT(Q3)
      ANG=ACOS(AN)
      X1=-2.0*SQRT(Q)*COS(ANG/3.0)-A/3.0
      IF (X1.GT.0.0) GOTO 2001
1002  CONTINUE
      X2=-2.0*SQRT(Q)*COS((ANG+2.0*3.1415926)/3.0)-
      &      (A/3.0)
      IF (X2.GT.0.0) GOTO 2002
1003  CONTINUE
      X3=-2.0*SQRT(Q)*COS((ANG-2.0*3.1415926)/3.0)-
      &      (A/3.0)
      IF (X3.GT.0.0) GOTO 2003
      GOTO 2004
1005  CONTINUE
      IF (AA.EQ.0.0) GOTO 6001
      BB=Q/AA
      GOTO 6002
6001  CONTINUE
      ROOT=-A/3.0
      GOTO 1008
6002  CONTINUE
      ROOT=AA+BB-A/3.0
      GOTO 1008

```

```

2001  CONTINUE
      ROOT=X1
      IF (ROOT.LT.0.005) GOTO 1008
      GOTO 1002
2002  CONTINUE
      ROOT=X2
      IF (ROOT.LT.0.005) GOTO 1008
      GOTO 1003
2003  CONTINUE
      ROOT=X3
      IF (ROOT.LT.0.005) GOTO 1008
2004  CONTINUE
      WRITE(*,*) 'NO SOLUTION FOUND'
1007  CONTINUE
      ROOT=0.005
1008  CONTINUE
      A1=ROOT
      XY=1.0+U(1)*A1*A1+U(3)*A1
      XYZ=XX(1)/XY
      A2=U(3)*A1*XYZ
      A3=U(1)*XYZ*A1*A1
      CALC=(A1*CONST(2)+A2*CONST(3)+2.0*A3*U(2))/
&      CONST(1)
C      WRITE(LUNOUT,1006)A1,A2,A3
      CALCF(1) = CALC
1006  FORMAT(3F20.16)
C...XX(1)      = independent variable.
C...CALC      = computer calculated value of Y
C...XX(NOVAR) = refers to an experimental value of Y
C...( X(NOVAR,I) )
C...CALCF(1), CALCF(2), ..... , CALCF(50) are
C...available for functions
C...which can be plotted.
C...constant value are labeled CONST(1), ... CONST(16)

```

## LIST OF REFERENCES

## REFERENCES

1. W. Weyl, Ann. Physik., 121, 601(1863)
2. J. L. Dye, J. M. Ceraso, M. T. Lok, B. L. Barnett and F. J. Tehan, J. Am.Chem. Soc., 96, 608(1974).
3. F. J. Tehan, B. L. Barnett and J. L. Dye, J. Am. Chem. Soc., 96, 7203(1974).
4. J. L. Dye, Prog. Inorg. Chem., 32, 327(1984).
5. J. L. Dye and M. G. DeBacker, Ann. Rev. Phys. Chem., 38, 271(1987).
6. S. B. Dawes, D. L. Ward, R. H. Huang and J. L. Dye, J. Am. Chem. Soc., 108, 3534(1986).
7. S. B. Dawes, Ph. D Dissertation, Michigan State University(1986).
8. O. Fussa, Ph. D Dissertation, Michigan State University(1986).
9. J. Kim, Ph. D Dissertation, Michigan State University(1989).
10. L. E. McMills, Ph. D Dissertation, Michigan State University(1989).
11. M. Tinkham, Ph. D Dissertation, Michigan State University(1985).
12. A. Ellaboudy, M. L. Tinkham, B. Van Eck, J. L. Dye and P. B. Smith, J. Phys. Chem., 88, 3852(1984).
13. M. L. Tinkham and J. L. Dye, J. Am. Chem. Soc., 107, 6129(1985).
14. M. L. Tinkham, A. Ellaboudy, J. L. Dye and P. B. Smith, J. Phys. Chem., 90, 14(1986).
15. A. Ellaboudy, Ph. D Dissertation, Michigan State University(1984).

16. A. Ellaboudy, C. J. Bender, J. Kim, D. -H. Shin, M. E. Kuchenmeister, G. T. Babcock and J. L. Dye, J. Am. Chem. Soc., 113, 2347(1991).
17. D. -H. Shin, A. Ellaboudy, J. L. Dye and M. G. DeBacker, J. Phys. Chem., 95, 7087(1991).
18. R. H. Huang, D. L. Ward, M. E. Kuchenmeister and J. L. Dye, J. Am. Chem. Soc., 109, 5561(1987).
19. R. H. Huang, M. K. Faber, K. J. Moeggenborg, D. L. Ward, and J. L. Dye, Nature, 331, 599(1988).
20. D. L. Ward, R. H. Huang and J. L. Dye, Acta Cryst., C44, 1374(1988).
21. M. E. Kuchenmeister and J. L. Dye, J. Am. Chem. Soc., 111, 935 (1989).
22. D. L. Ward, R. H. Huang, M. E. Kuchenmeister and J. L. Dye, Acta Cryst., C46, 1831(1990).
23. R. H. Huang, D. L. Ward and J. L. Dye, Acta Cryst., C46, 1833(1990).
24. D. L. Ward, R. H. Huang and J. L. Dye, Acta Cryst., C44, 1838(1990).
25. K. J. Moeggenborg, Ph. D Dissertation, Michigan State University (1990).
26. K. J. Moeggenborg, J. Papaioannou and J. L. Dye, Chem. Mater., 3, 514(1991).
27. S. Jaenicke and J. L. Dye, J. Solid State Chem., 54, 320(1984).
28. D. Issa, A. Ellaboudy, R. Janakiraman and J. L. Dye, J. Phys. Chem., 88, 3847(1984).
29. S. Doueff, K. -L. Tsai and J. L. Dye, Inorg. Chem., 30, 849(1991).
30. K. -L. Tsai, Ph. D Dissertation, Michigan State University(1991).

31. S. B. Dawes, J. L. Eglin, K. J. Moeggenborg, J. Klm and J. L. Dye, J. Am. Chem. Soc., 113, 1605(1991).
32. R. H. Huang, J. L. Eglin, S. Z. Huang, L. H. McMills and J. L. Dye, J. Am. Chem. Soc., 115, 9542(1993).
33. S. Mooibroek, R. E. Wasylishen, R. Dickson, G. Facey and B. A. Pettitt, J. Magn. Reson., 66, 542(1986).
34. P. J. Chu, B. C. Gerstein, J. Nunan and K. Klier, J. Phys. Chem., 91, 3588(1987).
35. V. Laperche, J. F. Lambert, R. Prost and J. J. Fripiat, J. Phys. Chem., 94, 8821(1990).
36. M. K. Ahn And L. E. Iton, J. Phys. Chem., 95, 4496(1991).
37. Y. Maniwa, K. Mizoguchi, K. Kume, K. Tanigaki, T. W. Ebbesen, S. Saito, J. Mizuki, J. S. Tsai and Y. Kubo, Solid State Commun. 82, 783(1992).
38. A. Samoson and E. Lippmaa, Chem. Phys. Lett., 100, 205(1983).
39. A. Llor and J. Virlet, Chem. Phys. Lett., 152, 248(1988).
40. K. T. Mueller, E. W. Wooten and A. Pines, J. Magn. Reson., 92, 620(1991).
41. A. Samoson and E. Lippmaa and A. Pines, Mol. Phys., 65, 1013(1988).
42. A. Bieleck, D. B. Zax, K. W. Zilm and A. Pines, Rev. Sci. Instrum., 57, 393(1986).
43. D. B. Zax, A. Bieleck, K. W. Zilm, A. Pines and D. P. Weitekamp, J. Chem. Phys., 83, 4877(1985).
44. J. M. Ceraso and J. L. Dye, J. Chem. Phys., 61, 1585(1974).
45. J. L. Dye, C. W. Andrews and J. M. Ceraso, J. Phys. Chem., 79, 3076(1975).
46. J. Kim and J. L. Dye, J. Phys. Chem., 94, 5399(1990).

47. R. H. Huang, D. L. Ward and J. L. Dye, *Acta Cryst.*, C46, 1835(1990).
48. J. L. Dye and R. H. Huang, *Pure & Appl. Chem.*, 65, 435(1993).
49. J. L. Eglin, Ph. D Dissertation, Michigan State University(1990).
50. M. J. Wagner, R. H. Huang, J. L. Eglin and J. L. Dye, *Nature*, 368, 726(1994).
51. R. H. Huang, Ph. D Dissertation, Michigan State University(1987).
52. S. B. Dawes, D. L. Ward, O. Fussa and J. L. Dye, *Abstracts, Am. Cryst. Asso. Proc., Series 2, Vol. 13*, 25(1985).
53. R. D. Shannon and C. T. Prewitt, *Acta Cryst.* B25, 925(1969).
54. F. J. Tehan, B. L. Barnett and J. L. Dye, *J. Am. Chem. Soc.*, 96, 7203(1974).
55. M. E. Kuchenmeister, Ph. D Dissertation, Michigan State University (1989).
56. C. J. Pederson, *J. Am. Chem. Soc.*, 89, 7017(1967).
57. C. J. Pederson, *J. Am. Chem. Soc.*, 90, 3299(1968).
58. J. D. Lamb, R. M. Izatt, C. S. Swain and J. J. Christensen, *J. Am. Chem. Soc.*, 102, 475(1980).
59. K. Reidy-Cederdren and J. McCracken, Unpublished results.
60. P. D. Moras, B. Metz and R. Weiss, *Acta Cryst.*, B29, 383(1973).
61. M. J. Wagner, L. E. H. McMills, A. S. Ellaboudy, J. L. Eglin, J. L. Dye, P. P. Edwards and N. C. Pyper, *J. Phys. Chem.*, 96, 9656(1992).
62. S. Z. Huang, R. H. Huang and J. L. Dye, Unpublished results  
This lab.
63. I. M. Kolthoff, *Anal. Chem.*, 51, 1R(1979).

64. A. I. Popov and J. M. Lehn, Ch. 9, "In Coordination Chemistry of Macrocyclic Compounds". Plenum, New York, (1979).
65. R. M. Izatt, S. J. Bradshaw, S. A. Nielsen, J. D. Lamb, J. J. Christensen and D. Sen, Chem. Rev., 85, 271(1985).
66. R. M. Izatt, K. Pawlak, S. J. Bradshaw and R. L. Bruening, Chem. Rev., 91, 1721(1991).
67. E. Mei, A. I. Popov and J. L. Dye, J. Phys. Chem., 81, 1677(1977).
68. L. -L. Soong, G. E. Leroi and A. I. Popov, Inorg. Chem., 29, 1366(1990).
69. M. K. Amini and M. Shamsipur, J. Solution Chem., 21, 275(1992).
70. M. R. Truter, Struct. Bonding(Berlin), 16, 71(1971).
71. E. Mei, Ph. D Dissertation, Michigan State University (1977).
72. W. J. Dewitte, Ph. D Dissertation, Michigan State University (1974).
73. M. Shamsipur and A. I. Popov, J. Am. Chem. Soc., 101, 4051 (1979).
74. M. K. Amini and M. Shamsipur, J. Phys. Chem., 95, 9601(1991).
75. M. Q. Martin, G. J. Martin, and J. -J. Delpeuch, "Practical NMR Spectroscopy". Heyden and Sons, Ltd., London, (1980).
76. V. A. Nicely and J. L. Dye, J. Chem. Educ., 48, 443(1971).
77. M. Shamsipur, Ph. D Dissertation, Michigan State University (1979).
78. L. -L. Soong, Ph. D Dissertation, Michigan State University (1988).
79. V. Gutmann, "Coordination Chemistry in Nonaqueous Solvents". Springer, Vienna, (1968).
80. E. G. Bloor and R. G. Kidd, Can. J. Chem., 46, 3425(1968).

81. R. D. Shannon, Acta Cryst., 32A, 751(1976).
82. U. Haeberlen, "High Resolution NMR in Solids Selective Averaging". Academic Press., New York, (1976).
83. A. Abragam, "Principles of Nuclear Magnetism". Oxford University Press., London, (1986).
84. C. P. Slichter, "Principles of Magnetic Resonance". Harper & Row, New York, (1963).
85. M. Mehring, "Principles of High Resolution NMR in Solids". Springer-Verlag, Berlin, (1983).
86. W. P. Power, S. Mooibroek, R. E. Wasylshen and T. S. Cameron, J. Phys. Chem., 98, 1552(1994).
87. M. A. Kennedy and P. D. Ellis, Concepts Magn, Res., 1, 109(1989).
88. B. Berglund and J. Tegenfeldt, J. Magn. Reson., 30, 451(1978).
89. M. Irion, N. Weiden and A. Weiss, J. Magn. Reson., 30, 457(1978).
90. M. A. Kennedy and P. D. Ellis, Concepts Magn, Res., 1, 35(1989).
91. S. B. Dawes, A. Ellaboudy and J. L. Dye, J. Am. Chem. Soc., 109, 3508(1987).
92. M. J. Wagner and J. L. Dye, Unpublished results this lab.
93. S. Z. Huang, J. Kim and J. L. Dye, Unpublished results this lab.